UNIVERSITÉ DE LILLE
LABORATOIRE DE GENIE CIVIL ET GEO-ENVIRONNEMENT
ÉCOLE DOCTORALE SCIENCES POUR L'INGÉNIEUR (SPI)

Thèse pour l'obtention du grade de docteur de l'Université de Lille
Spécialité : Bio-mécanique et bio-ingénierie

Présentée et soutenue publiquement par :

Amil DERROUICHE

Le 12 Décembre 2018

Intitulée

REPONSE OSMO-INELASTIQUE DU DISQUE INTERVERTEBRAL: CARACTERISATION EXPERIMENTALE ET MODELISATION CONSTITUTIVE

OSMO-INELASTIC RESPONSE OF INTERVERTEBRAL DISC: EXPERIMENTS AND CONSTITUTIVE MODELING

Composition du jury :

Fahmi ZAÏRI	Professeur des Universités	Université de Lille	Directeur de thèse
Jean-François GANGHOFFER	Professeur des Universités	Université de Lorraine	Rapporteur
Grégory CHAGNON	Maître de conférences	Université de Grenoble Alpes	Rapporteur
Jean-Marc LEFEBVRE	Directeur de recherche émérite	Université de Lille	Président
Caroline FREDERIX	Ingénieure de recherche	Solvay Bruxelles	Examinatrice
Fahed ZAÏRI	Neurochirurgien	Ramsay Générale de Santé	Examinateur

OSMO-INELASTIC RESPONSE OF INTERVERTEBRAL DISC: EXPERIMENTS AND CONSTITUTIVE MODELING

Contents

Remerciements

Merci à Caroline Frederix, Jean-Marc Lefebvre, Jean-François Ganghoffer et Gregory Chagnon pour avoir accepté de jugé mon travail de thèse et pour les discussions passionantes pendant la soutenance.

Cette thèse n'aurait pu s'achever sans mon directeur, Fahmi Zaïri. Tu m'as guidé lorsque je me perdais, tu m'as rassuré lorsque je doutais, tu as toute ma reconnaissance. Merci pour ton soutien et pour les hectolitres de café.

Ces remerciements seraient incomplets sans une pensée pour Ameni, Anouar, Faten, Yan et Li qui m'ont aidé dans mes recherches, cette thèse est aussi la vôtre. Je souhaite également remercier mes collègues Christian, Hamza, Qiang et Karim pour ces moments passés en votre compagnie.

Fahed, merci pour tes encouragements et tes conseils. Ma famille te remercie encore pour t'être occupé de mon grand-père.

Papa, Maman, vous avez toujours souhaité le meilleur pour nous, j'espère vous rendre fiers et être un jour un bon parent comme vous l'avez été.

Mon épouse, mon plus grand soutien, je remercie Dieu pour cet inestimable cadeau. Nous voilà tous les deux docteurs, une nouvelle étape s'ouvre à nous.

Mes frères Jamir, Sliman et Nadir je souhaite que nous soyons toujours proches et que vous soyez heureux, merci pour tout. Anissa et Souad bienvenue et prenez soin de mes frères.

Mes grands-parents, ai-je déjà vu quelqu'un de plus courageux que vous, vous êtes des modèles pour moi, que Dieu vous garde.

Ma grande famille, tantes, oncles, cousins, cousines sachez que je serai toujours là pour vous.

Ma famille de Marseille, vous m'avez accompagné pendant ces années, merci Saïd, Djemy, Yacine mon bof et Kaïna la meilleure des belles sœurs.

Mourad, Ayoub, Naïm, Moustaf, Sofian, Hind, Moh, Sarah, Myriam et tous les autres qui m'ont accompagné le long de ces années merci à vous.

Merci à ceux que j'ai croisé de loin ou de près, pour vos messages, vos sourires et votre aide.

A mes proches, qui nous ont quitté pendant cette thèse, je ne saurai oublier les moments passés avec vous.

Introduction

The life is a complex concept that allows us to move and grow at the macroscopic scale. In the history of mechanics, living body were described with the same mathematical tools than inert body before the consideration of multi-scale organization. A living body is an auto-maintained system requiring a description in relation with the biological, mechanical and chemical features. The first one can explains the microstructural development essential for the second one working, while the third one is strongly coupled with the second. A correct description of the life being is based on these three distinct disciplines which should interact.

From global description of our body towards cellular description, the intermediate scale is essential, in which our organs and soft tissues are studied for the development of more accurate treatments. The word “biomechanics” finds its origin in the beginning of the twentieth century but this discipline is considered millenary with the oldest known prosthesis old by 3000 years.

Biomechanics progresses by the consideration of the specificity of our tissues. That leads to the development of new adapted scientific tools as continuum biomechanics with the capability to describe life. As an application of mechanical concepts on the biology, the biomechanics heads towards mechanobiology with the aim to understand living beings in relation with molecular constitution. The mutual effects are now highlighted especially for the study of biological changes induced by the time or the environment. The study of living being is based on application of mechanics strongly coupled with biology in the aim to understand physiology and development of disease towards enhancement of medical techniques. Nowadays, artificial devices have to be designed in order to interact with living tissues with the required care.

Understand the inevitable alteration is difficult without a correct description of a healthy tissue. It is a way to improve the medical devices with biomimetic materials usable in sport performance, plastic surgery or tissue engineering. Biomechanics is an interdisciplinary domain where biologists, chemists and physicists work with medical doctors for the improvements of our quality of life.

In the context of changes in the lifestyle and the population aging, the aim of the present thesis is to focus on spine, considered as the most complicated join of our body. This fundamental element presents hierarchical organization with hard and soft tissues: vertebrae, intervertebral discs (IVDs) and ligaments. It is subjected to troubles for more and more people while being not well understood in the healthy state. The back pain concerns a growing part of the population with unclear multiple sources. The chronic pain founds often its origin in the IVD disorder. This soft tissue connecting two adjacent vertebrae is a fibrocartilage able to resist at high stresses induced by spine movements. The complex organization of the IVD, with nucleus pulposus in center and annulus fibrosus around, and the strong local heterogeneity make the understanding complicated. IVD malfunction is due to several interacting factors, involving chemical, biological and mechanical effects. This thesis is dedicated to the experimental and theoretical/numerical description of the healthy IVD in relation with the mechanical and the biochemical environment. A two-scale description is employed with a study at the IVD scale and at the AF scale. The thesis dissertation is divided into three Chapters.

Chapter 1 provides the general biomechanical and biochemical considerations on IVD.

Chapter 2 is dedicated to the experimental characterization of the osmo-inelastic coupling in healthy IVD and is divided into two parts. The first part is focused on the experimental study performed on functional units extracted from cervical spine of mature sheep. Multiaxial mechanical experiments provide some insights on the source of inelastic effects in relation with osmolarity by varying mechanical loading path. The second part reports

the experimental observations on the intrinsic response of AF in relation with microstructure, biochemical environment and strain-rate. An interpretation of the osmo-inelastic mechanisms is proposed at the two scales.

Chapter 3 is dedicated to the constitutive modeling and simulation of osmo-inelastic coupling in healthy IVD and is divided into two parts. The first part is devoted to the formulation of a chemo-mechanical constitutive model taking into account the osmo-inelastic couplings in relation with heterogeneous and anisotropic features. This model is a new approach in the description of soft tissues able to reproduce osmo-induced volumetric changes at the AF scale in relation with microstructure, osmolarity and water content. The present formulation is implemented into a finite element program and used to reproduce the AF intrinsic response using the experimental observations reported in Chapter 2. In the second part, the constitutive model is applied to a finite element model of C5-C6 functional unit constructed from computed tomography. Comparisons with experimental data for different neck movements allows us to analyze the local fields in healthy IVD. Some elements towards a better understanding of the mechano-biological coupling in healthy IVD close this chapter.

General conclusions and Research perspectives are presented at the end of the document.

Chapter 1: General considerations

1.1. Public health issue

The spine is composed by vertebrae and soft tissues, including intervertebral discs (IVDs) which provide flexibility and softening, with ligaments avoiding too large displacements. In 16 developed countries, 47% of pains are located to the back and deteriorated IVDs are the second causes of chronic pain (Maetzel and Li, 2002; Breivik et al., 2006; Vos et al., 2016). Direct costs of back pain are estimated around 3 billion euros in France with significant impact on quality of life (Depont et al., 2010). This statistic increases in industrialized western countries (Frymoyer and Cats-Baril, 1991; Schmidt et al., 2007; Raspe, 2008; Hoy et al., 2012) due to changes in lifestyle. Multiple biological and sociological factors are predominant in back pain apparition. There is correlation with physical inactivity and overweight which is increasingly common in our society with time spent on watching TV or on computer (Adams and Hutton, 1985; Skoffer and Foldspang, 2008). Compared to standing posture, sitting posture increases disc pressure which is associated with IVD degeneration and back pain (Makhsous et al., 2009; Aranjan Lione, 2013).This trouble is a public health issue and it justifies public health policies to prevent bad movements or posture which could cause back pain.

1.2. Anatomical aspects

1.2.1. Spine

The spine or vertebral column provides the main support for our body, while protecting spinal cord from injury. The spine is classically separated into three distinct regions, at both functional and anatomical levels: the cervical, thoracic and lumbar regions, see Figure 1.1. There are 23 intervertebral discs placed between each vertebra along the spine, except for the articulation between the first and second cervical vertebrae. Two adjacent vertebrae are interconnected by the IVD and ligaments and constitute the smallest physiological motion segment of the spine.

This segment, well-known as functional spine unit (FSU) is described the elementary element exhibiting the same biomechanical characteristics than the entire spine (White et al., 1990).

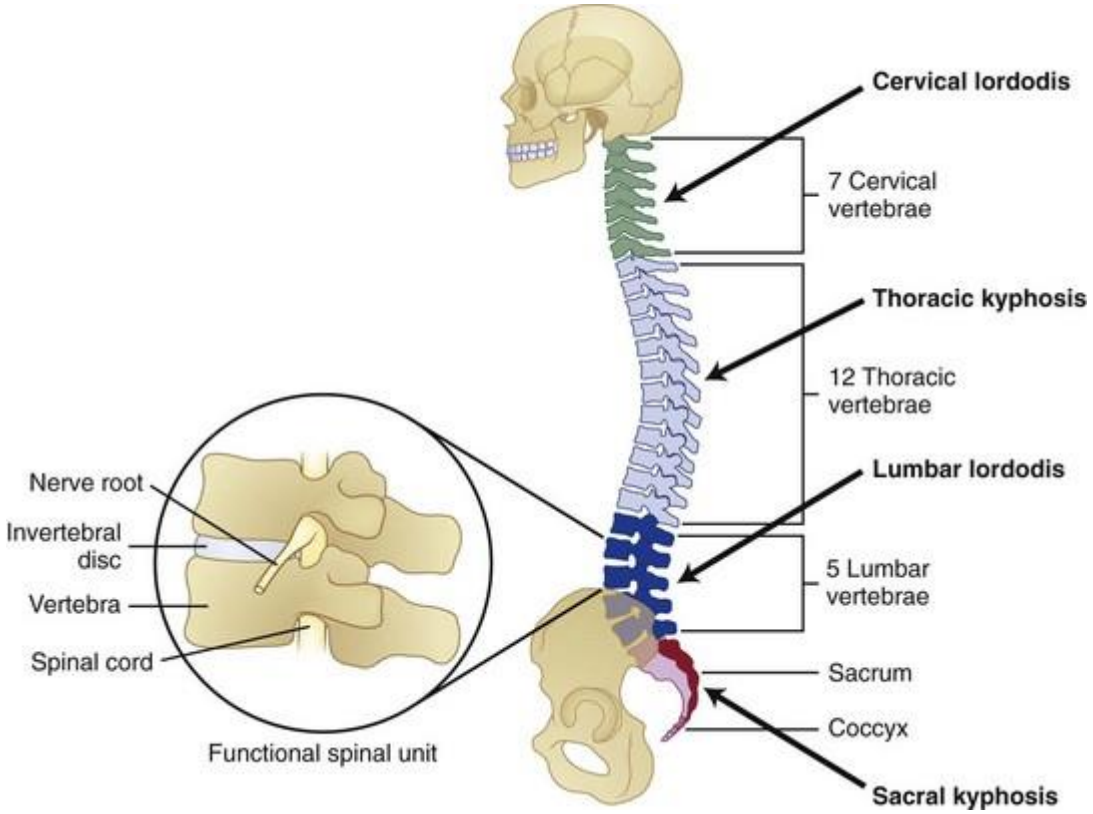

Figure 1.1. Functional spine unit and vertebral column (White et al., 1990).

1.2.2. Intervertebral discs

The IVD is a vascular fibrocartilaginous medium that provides flexibility and softening of the spine thanks to a fibrous ring (annulus fibrosus: AF) and a gelatinous nucleus (nucleus pulposus: NP), see Figure 1.2. At the structural level, IVD is a hydrophilic reinforced medium where the solid phase and the fluid phase interact by osmotic effect with the microstructure (Urban and Roberts, 1995; Bibby et al., 2001; Kramer, 2009). NP is a gelatinous sub-component, which transfers axial loads from the spine towards AF. At the micro-structural scale, the IVD is composed by collagen, proteoglycans (PGs) macromolecules and cellular population, varying in content according to the location.

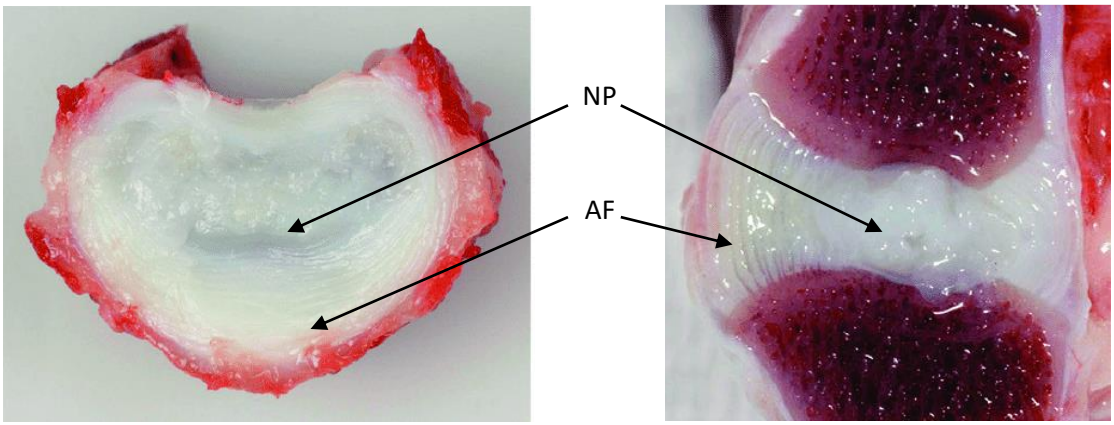

Figure 1.2. Transverse (left) and sagittal (right) section through a L5-L6 IVD of a 2-years old chondrodystrophic dog, showing a fibrocartilaginous NP, a widened transition zone, and a normally structured AF (Smolders et al., 2012).

1.3. Microstructural aspects

1.3.1. Collagen

Collagen is the most abundant protein of the human body. Nineteen types exist with predominance of type one in the AF and two in the NP. With length of 10 to 100 µm and diameters of between 100 and 200 nm (Inoue, 1981; Rannou et al., 2004), they define certain mechanical properties. Collagens that account for 44 to 51% of the dry mass of the IVD (Kraemer, 2009) are distributed differently according to the zones. Indeed, first type of collagen fibers is highly organized with strong tensile modulus that contributes to the AF resistance and help supporting a multiaxial mechanical loading. Second type is tangled with PGs macromolecules mainly in the NP as illustrated in Figure 1.3. The collagen fibers exhibit an increase in content in the AF, generating graded mechanical properties from inner part to outer part. Moreover, they present a variable orientation with approximately 23° in the IVD dorsal part and approximately 43° in the IVD ventral part (Holzapfel et al., 2005).

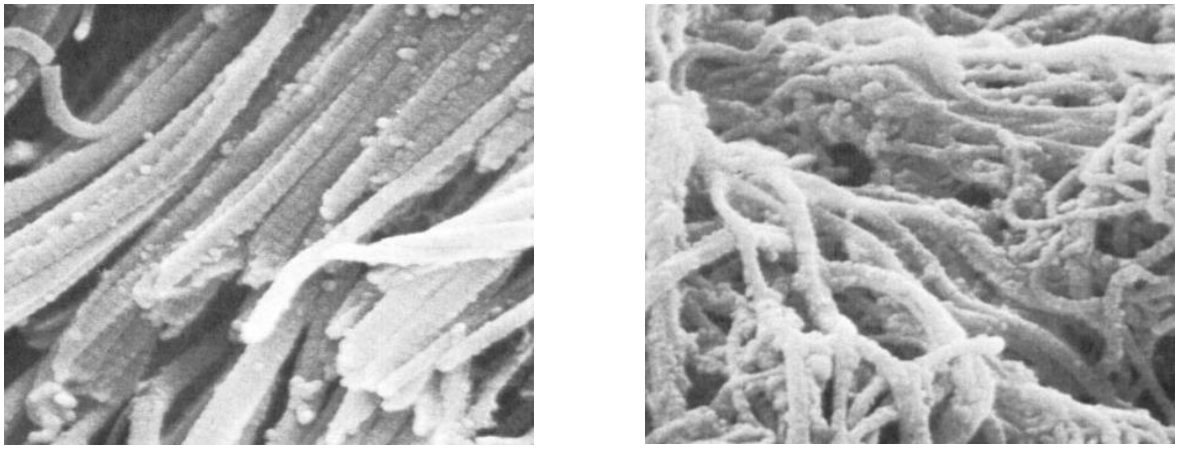

(a) (b)

Figure 1.3. Collagen fiber organization: (a) in AF, (b) in NP (Inoue, 1981).

1.3.2. Proteoglycans

The PGs represent the second major solid element of IVD with 5 to 15% of the weight (Bibby et al., 2001). They are organized as macro-aggregate with the remarkable particularity of being negatively charged. They consist of a core protein filament and glycosaminoglycan (GAG) chains, see Figure 1.4.

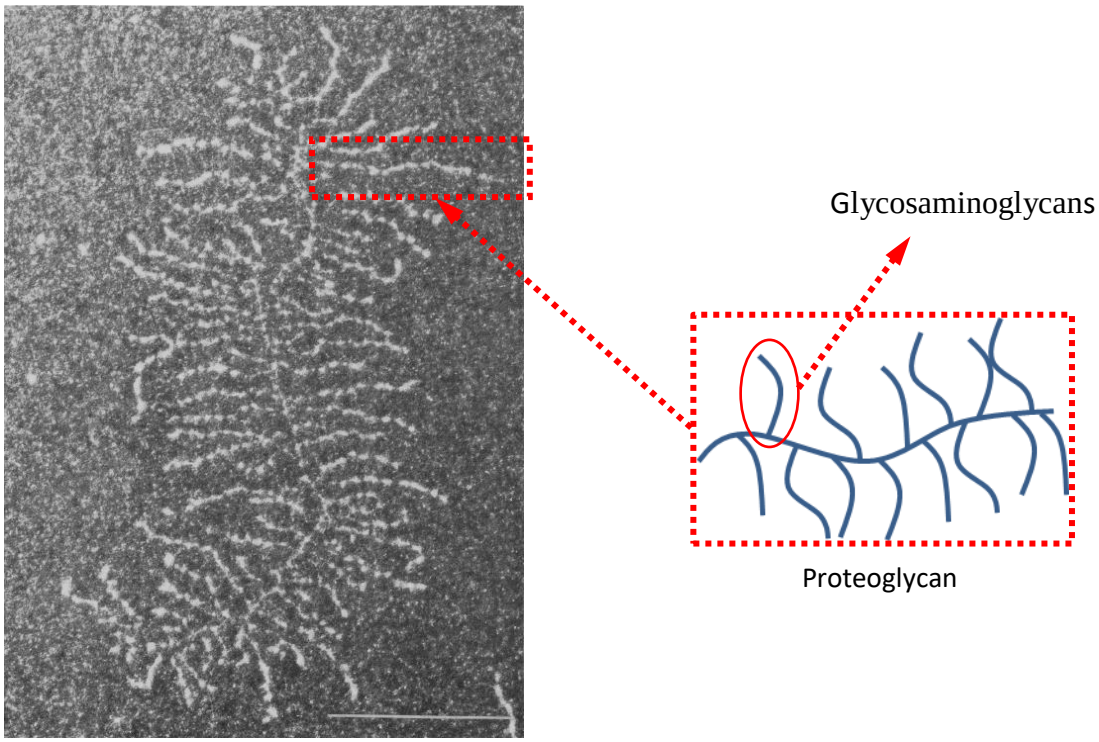

Figure 1.4. Dark field electron micrograph of PGs macromolecules from bovine articular cartilage (×120000) and schematic representation of a PG macromolecule with GAGs chain. The bar at the lower right equals 0.5 µm (Rosenberg et al., 1975).

The high polarity of the GAG gives the hydrophilic property to the PGs by osmotic effect, and then they act as lubricant and shock absorber in the IVD. The IVD hydration remains relatively constant thanks to osmotic effect and water is sucked especially when the disc is compressed. The induced internal osmotic pressure governs the mechanical behavior of the IVD while creating the essential internal fluid flow for the nutrient supply.

1.3.3. Cellular population and nutrients supply

The IVD consists thus in PGs molecules, collagen fibers and internal fluid, which represent 90 to 95% of the disc (Bibby et al., 2001). The rest is minority molecules and cellular population designed for the production of PG and collagen. The IVD contains relatively few cells, compared to other articular cartilages, with approximately 3000 cells/mm3 in the NP, 9000 cells/mm3 in the AF and 15000 cells/mm3 in the vertebral endplates (Maroudas et al., 1975; Rannou et al., 2000; Bibby et al., 2001). Two main types of cells are found in the IVD: fibroblasts, which are responsible for the production of first type of collagen mainly in the outer part of the AF, and chondrocytes, producing PGs and second type of collagen, are found in AF and NP (Bibby et al., 2001). The IVD is vascularized by arterioles during childhood, and then it becomes quickly avascular. The homeostasis depends thus on the nutrients supply and wastes evacuation. These phenomena depend on the internal fluid exchange with the closest vessels in the vertebral bodies and in the periphery of AF.

1.3.4. Degeneration

IVD is a wet tissue mainly composed by water, with 80% at birth and 60% in great age (Gu et al., 1999). Thanks to the fluid phase, IVD thickness decreases during the day and is restored during the night (de Puky, 1935). The age-dependency of fluid content induces changes in mechanical properties leading to degeneration; IVDs lose flexibility and become rigid

(Campana et al., 2011), then IVD diseases can occur as herniation, see Figure 1.5. Fixed charge density of PGs contributes to hydration, nutrition and compressive strength of the tissue (Urban et al., 1979). Alteration in the fixed charge density due to loss of PGs content (Lyons et al., 1981; Urban and Holm, 1986; Antoniou et al., 1996) may explain the degeneration process due to increase in solid matrix stresses, decrease in fluid content, and bad nutrients supply inside tissue (Wills et al., 2016).

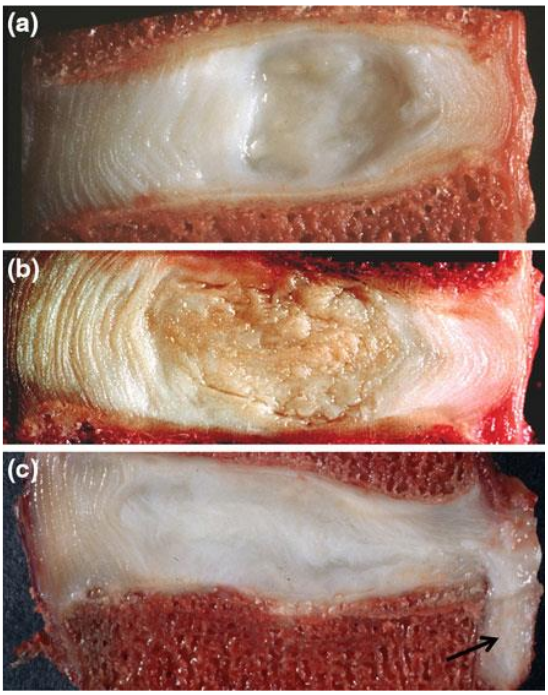

Figure 1.5. Human lumbar IVD: (a) Healthy disc from a young adult, (b) Healthy disc from a middle-aged adult, (c) Herniated disc with signs of aging. A small quantity of NP (arrow) has herniated through the posterior annulus in response to severe mechanical loading.

1.4. Nucleus pulposus

At centrum, with 80% water content, and non-organized collagen fibers network, the NP is an isotropic incompressible gelatinous medium (Rannou et al., 2000). The NP, representing 30 to 60% of the total surface area, absorbs and distributes the loads from the spine. Its cellular population, being mainly composed by chondrocytes, has an active metabolism ensuring a renewal of PGs and second type of collagen. The type of fibers changes gradually in nature by approaching the AF. The extracellular matrix of the nucleus is equivalent to that of cartilage,

with second type of embedded collagen fibers with large PGs macromolecules. Thanks to the water contribution, the NP generates hydrostatic pressure under axial loads (Nachemson and Morris, 1964; Wilke et al., 1999; Goins et al., 2005). The proportion of water is estimated at 90% during childhood and decreases around 80% at 20 years old, to less than 70% after 60 years old (Iatridis et al., 1997). The PGs content can decrease by 30% with aging depending on lifestyle with induced decrease in osmotic pressure. The NP (and inner part of the AF) is connected to the vertebral body via the vertebral endplates. Main contributor to the nutrients supply, the fluid flow is promoted by their porosity and their thickness about 0.6 mm.

1.5. Annulus fibrosus

The second part of IVD, around nucleus is AF. It is composed by PGs macromolecules embedded. However, in annulus, collagen fibers are regularly oriented to form a fiber reinforced deformable solid material (Ghosh et al., 1977). Collagen network gives to annulus mechanical resistance permitting to support high stresses. Indeed, AF has a very specific organization, it is composed by concentric lamellae around the nucleus (Marchand and Ahmed, 1990). Each lamella is reinforced by collagen fibers with angle and content depending on location. There is a regular circumferential evolution between ventro-lateral and dorsal part and an increase in content from inner part to outer part (Holzapfel et al., 2005). Moreover, there is 90° variation of the fiber angle between each lamella (Ghosh et al., 1977). Under compression, NP presses against AF, leading to circumferential tension. The graded property of AF in terms of collagen fibers content, and thus tensile strength, is accompanying with decrease in water content compared with the NP. Non-reinforced interlamellar zones between each lamellae have been recently studied (Tavakoli et al., 2016) especially due to their contribution to shear resistance of AF considered as main mode of damage.

1.6. Experimental pre-requests

Experimental characterization of the biological tissue is a challenge. The variability and representativeness of the specimen mechanical response depends on many factors. The main problem in the human characterization comes from the samples provenance and the low available samples. The age of donators exceed 70 years old for the in-vitro studies (Panjabi et al., 1991; McBride et al., 1995; Weis et al., 1996). Therefore, the results are not representative of population and cannot provide correct behavior of the healthy IVD. In-vivo studies allow to include more young population but mechanical parameters are uncertain. The passage to the animal model was the solution of some authors against the lack of human samples. The ovine spine is close to human IVDs (see Figure 1.6). So, this is a good way to describe biomechanical behavior of IVDs (Wilke et al., 1997; Alini et al., 2008). The bovine spine is a good alternative, permitting extraction of biggest samples. Animal models are useful to have better understanding of healthy IVD behavior, however experiments need to be validated with human tissues and results have to be discussed.

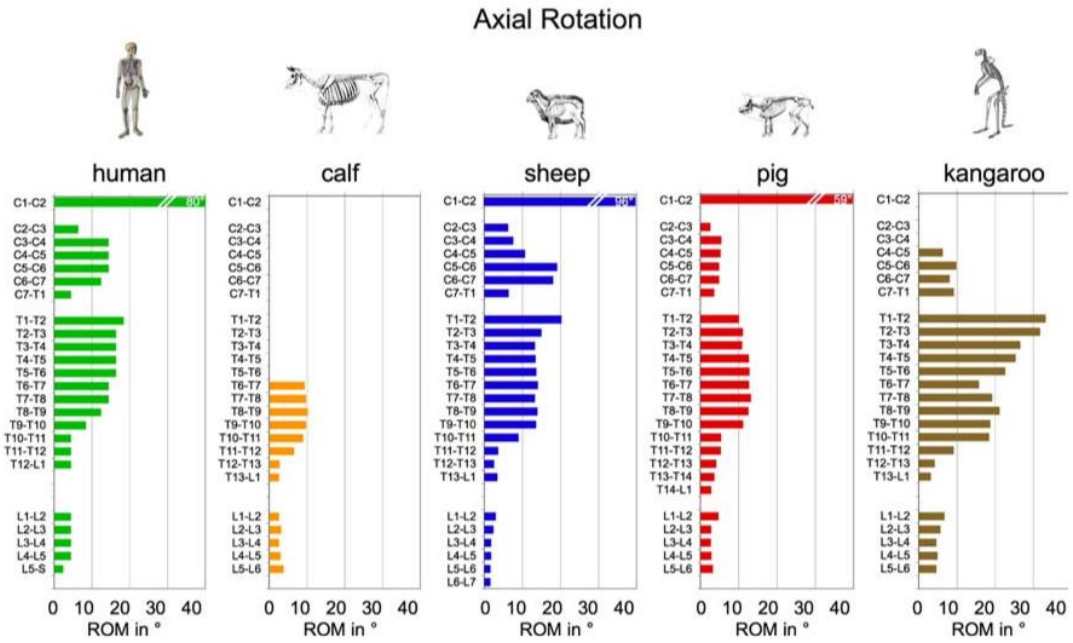

Figure 1.6. Motion range of different species (Alini et al., 2008).

Another requirement comes from the samples storage. Properties of biological tissues are altered ex-vivo within hours (Fung, 1981; Brown et al., 2003). Freezing implies microstructure damages (Bass et al., 1997) and decrease in PGs content resulting on chemical disorders. The osmotic pressure is thus altered as the mechanical behavior. Yet, some studies show freezing influence is negligible in compression, flexion or torsion (Smeathers and Joanes, 1988; Gleizes et al., 1998). The fresh tissues with short storage appear as good compromise.

1.7. Thesis organization

The complex behavior of healthy spine is studied since several years but a lot of features are not completely understood yet. This PhD thesis is focused on the structural and intrinsic response of the healthy IVD. Experimental characterization in relation with chemical environment and mechanical loading conditions are performed in *Chapter 2*. In *Chapter 3*, the observed chemo-mechanical couplings are then used to create a constitutive model able to reproduce the intrinsic response and to simulate the healthy IVD biomechanics.

1.8. References

Adams, M.A., Hutton, W.C., 1985. The effect of posture on the lumbar spine. The Journal of Bone and Joint Surgery 67, 625-629.

Alini, M., Eisenstein, S.M., Ito, K., Little, C., Kettler, A.A., Masuda, K., Melrose, J., Ralphs, J., Stokes, I., Wilke, H.J., 2008. Are animal models useful for studying human disc disorders/degeneration? European Spine Journal 17, 2-19.

Antoniou, J., Steffen, T., Nelson, F., Winterbottom, N., Hollander, A.P., Poole, R.A., Aebi, M., Alini, M., 1996. The human lumbar intervertebral disc: evidence for changes in the biosynthesis and denaturation of the extracellular matrix with growth, maturation, ageing, and degeneration. Journal of Clinical Investigation 98, 996-1003.

Aranjan Lione, K., 2013. Risk factors forchronic low back pain. Journal of Community Medicine and Health Education 4, 1000271.

Bass, E.C., Duncan, N.A., Hariharan, J.S., Dusick, J., Bueff, H.U., Lotz, J.C., 1997. Frozen storage affects the compressive creep behavior of the porcine intervertebral disc. Spine 22, 2867-2876.

Bibby, S.R., Jones, D.A., Lee, R.B., Yu, J., Urban, J.P., 2001. The pathophysiology of the intervertebral disc. Joint Bone Spine 68, 537-542.

Breivik, H., Collett, B., Ventafridda, V., Cohen, R., Gallacher, D., 2006. Survey of chronic pain in Europe: Prevalence, impact on daily life, and treatment. European Journal of Pain 10, 287-333.

Brown, J.D., Rosen, J., Kim, Y.S., Chang, L., Sinanan, M.N., Hannaford, B., 2003. In-vivo and in-situ compressive properties of porcine abdominal soft tissues. Studies in Health Technology and Informatics94, 26-32.

Campana, S., Charpail, E., de Guise, J.A., Rillardon, L., Skalli, W., Mitton, D., 2011. Relationships between viscoelastic properties of lumbar intervertebral disc and degeneration grade assessed by MRI. Journal of the Mechanical Behavior of Biomedical Materials 4, 593-599.

Depont, F., Hunsche, E., Abouelfath, A., Diatta, T., Addra, I., Grelaud, A., Lagnaoui, R., Molimard, M., Moore, N., 2010. Medical and non-medical direct costs of chronic low back pain in patients consulting primary care physicians in France. Fundamental and Clinical Pharmacology 24, 101-108.

de Puky, P., 1935. The physiological oscillation of the length of the body. Acta Orthopaedica Scandinavica 6, 338-347.

Frymoyer, J.W., Cats-Baril, W.L., 1991. An overview of the incidences and costs of low back pain. The Orthopedic Clinics of North America 22, 263-271.

Fung, Y.C., 1981. Biomechanics: mechanical properties of living tissues. New York: Springer-Verlag.

Ghosh, P., Bushell, G.R., Taylor, T.F., Akeson, W.H., 1977. Collagens, elastin and noncollagenous protein of the intervertebral disk. Clinical Orthopaedics and Related Research 129, 124-132.

Gleizes, V., Viguier, E., Feron, J.M., Canivet, S., Lavaste, F., 1998. Effects of freezing on the biomechanics of the intervertebral disc. Surgical and Radiologic Anatomy 20, 403-407.

Goins, M.L., Wimberley, D.W., Yuan, P.S., Fitzhenry, L.N., Vaccaro, A.R., 2005. Nucleus pulposus replacement: an emerging technology. The Spine Journal 5, 317S-324S.

Gu, W.Y., Mao, X.G., Foster, R.J., Weidenbaum, M., Mow, V.C., Rawlins, B.A., 1999. The anisotropic hydraulic permeability of human lumbar anulus fibrosus. Influence of age, degeneration, direction, and water content. Spine 24, 2449-2455.

Holzapfel, G.A., Schulze-Bauer, C.A.J., Feigl, G., Regitnig, P., 2005. Single lamellar mechanics of the human lumbar anulus fibrosus. Biomechanics and Modeling in Mechanobiology 3, 125-140.

Hoy, D., Bain, C., Williams, G., March, L., Brooks, P., Blyth, F., Woolf, A., Vos, T., Buchbinder, R., 2012. A systematic review of the global prevalence of low back pain. Arthritis and Rheumatism 64, 2028-2037.

Iatridis, J.C., Setton, L.A., Weidenbaum, M., Mow, V.C., 1997. Alterations in the mechanical behavior of the human lumbar nucleus pulposus with degeneration and aging. Journal of Orthopaedic Research 15, 318-322.

Inoue, H., 1981. Three-dimensional architecture of lumbar intervertebral discs. Spine 6, 139-146.

Kramer, J., 2009. Intervertebral disk diseases: causes, diagnosis, treatment, and prophylaxis. New York: Thieme.

Lyons, G., Eisenstein, S.M., Sweet, M.B., 1981. Biochemical changes in intervertebral disc degeneration. Biochimica et Biophysica Acta 673, 443-453.

Maetzel, A., Li, L., 2002. The economic burden of low back pain: a review of studies published between 1996 and 2001. Best Practice and Research Clinical Rheumatology16, 23-30.

Makhsous, M., Lin, F., Bankard, J., Hendrix, R.W., Hepler, M., Press, J., 2009. Biomechanical effects of sitting with adjustable ischial and lumbar support on occupational low back pain: evaluation of sitting load and back muscle activity. BMC Musculoskeletal Disorders 10, 1-11.

Marchand, F., Ahmed, A.M., 1990. Investigation of the laminate structure of lumbar disc anulus fibrosus. Spine 15, 402-410.

Maroudas, A., Stockwell, R.A., Nachemson, A., Urban, J., 1975. Factors involved in the nutrition of the human lumbar intervertebral disc: Cellularity and diffusion of glucose in vitro. Journal of Anatomy 120, 113-130.

McBride, A.D., Mukherjee, D.P., Kruse, R.N., Albright, J.A.,1995. Anterior screw fixation of type II odontoid fractures. A biomechanical study. Spine 20, 1855-1860.

Nachemson, A., Morris, J.M., 1964. In vivo measurements of intradiscal pressure. Discometry, a method for the determination of pressure in the lower lumbar discs. The Journal of Bone and Joint Surgery46, 1077-1092.

Panjabi, M., Dvorak, J., Crisco, J., Oda, T., Hilibrand, A., Grob, D.,1991. Flexion, extension, and lateral bending of the upper cervical spine in response to alar ligament transections. Journal of Spinal Disorders 4, 157-167.

Rannou, F., Poiraudeau, S., Corvol, M., Revel, M., 2000. Biochimie et biologie du disque intervertébral. Revue du Rhumatisme67, 214-218.

Rannou, F., Mayoux-Benhamou, M.A., Poiraudeau, S., Revel, M., 2004. Disque intervertébral et structures voisines de la colonne lombaire : anatomie, biologie, physiologie et biomécanique. EMC - Rhumatologie-Orthopédie 1, 487-507.

Raspe, H., 2008. Management of chronic low back pain in 2007-2008. Current Opinion in Rheumatology 20, 276-281.

Rosenberg, L., Hellmann, W., Kleinschmidt, A.K., 1975. Electron microscopic studies of proteoglycan aggregates from bovine articular cartilage. The Journal of Biological Chemistry 250, 1877-1883.

Schmidt, C.O., Raspe, H., Pfingsten, M., Hasenbring, M., Basler, H.D., Eich, W., Kohlmann, T., 2007. Back pain in the German adult population: Prevalence, severity, and sociodemographic correlates in a multiregional survey. Spine 32, 2005-2011.

Skoffer, B., Foldspang, A., 2008. Physical activity and low-back pain in schoolchildren. European Spine Journal 17, 373-379.

Smeathers, J. E., Joanes, D. N., 1988. Dynamic Compressive Properties of Human Lumbar Intervertebral Joints: A Comparison between Fresh and Thawed Specimens. Journal of Biomechanics 21, 425-33.

Smolders, L.A., Bergknut, N., Grinwis, G.C., Hagman, R., Lagerstedt, A.S.., Hazewinkel, H.A., Tryfonidou, M.A., Meij, B.P., 2012. Intervertebral disc degeneration in the dog. Part 2: Chondrodystrophic and non-chondrodystrophic breeds. The Veterinary Journal 195, 292-299.

Tavakoli, J., Elliott, D.M., Costi, J.J., 2016. Structure and mechanical function of the inter-lamellar matrix of the annulus fibrosus in the disc: inter-lamellar matrix of the inter-vertebral disc. Journal of Orthopaedic Research 34, 1307-1315.

Urban, J.P., Maroudas, A., Bayliss, M.T., Dillon, J., 1979. Swelling pressures of proteoglycans at the concentrations found in cartilaginous tissues. Biorheology 16, 447-464.

Urban, J.P.G., Holm, S.H., 1986. Intervertebral disc nutrition as related to spinal movements and fusion. Tissue Nutrition and Viability, 101-119. New York: Springer.

Urban, J.P.G., Roberts, S., 1995. Development and degeneration of the intervertebral discs. Molecular Medicine Today 1, 329-335.

Vos, T., Allen, C., Arora, M., et al. 2016. Global, regional, and national incidence, prevalence, and years lived with disability for 310 diseases and injuries, 1990-2015: a systematic analysis for the Global Burden of Disease Study 2015. Lancet 388, 1545-1602.

Weis, J.C., Cunningham, B.W., Kanayama, M., Parker, L., McAfee, P.C., 1996. In vitro biomechanical comparison of multistrand cables with conventional cervical stabilization. Spine 21, 2108-2114.

White, A.A., Panjabi, M.M., 1990. Clinical Biomechanics of the Spine. JB Lippincott Company.

Wilke, H.J., Kettler, A., Claes, L.E., 1997. Are sheep spines a valid biomechanical model for human spines? Spine 22, 2365-2374.

Wilke, H.J., Neef, P., Caimi, M., Hoogland, T., Claes, L.E., 1999. New in vivo measurements of pressures in the intervertebral disc in daily life. Spine24, 755-762.

Wills, C.R., Malandrino, A., van Rijsbergen, M.M., Lacroix, D., Ito, K., Noailly, J., 2016. Simulating the sensitivity of cell nutritive environment to composition changes within the intervertebral disc. Journal of the Mechanics and Physics of Solids 90, 108-123.

Chapter 2: Experimental characterization

Part 1: Osmo-inelastic response of the intervertebral disc[1]

Abstract

The intervertebral disc (IVD) exhibits a complex inelastic response characterized by relaxation, hysteresis during cyclic loading and rate-dependency. All these inelastic phenomena are dependent on the surrounding chemical environment in which the physiological fluid reacts with the soft tissue by osmotic effect. The coupling between osmotic and inelastic effects which usually appears together is far from being fully established. The research design adopted in the present part of the Chapter 2 is to study the behavior changes of the IVD in different mechanical and chemical conditions in the aim to highlight the existence of the osmo-inelastic couplings. Eighteen non-frozen specimens, extracted from cervical spines of mature sheep, were tested under different loading paths (tension, compression and torsion) at various loading rates and saline concentrations. Analysis of variance shows that the osmotic and inelastic effects are statistically significant ($p<0.05$) in tension and in compression. The osmo-inelastic features are found higher in compression than in tension, and almost imperceptible in torsion. An inverse chemical effect is observed between tension and compression due to modulation of the intradiscal pressure and the interactions between annulus fibrosus and nucleus pulposus. An interpretation of the underlying osmo-inelastic mechanisms is proposed in which two sources of inelastic effects are identified, i.e. extracellular matrix rearrangements and fluid exchange created by osmotic effect.

Keywords: Intervertebral disc; Chemo-mechanical coupling; Inelastic effects; Mechanical loading state; Osmo-inelastic mechanisms.

[1] This Part of this chapter is based on the following paper: Amil Derrouiche, Fahmi Zaïri, Fahed Zaïri, Osmo-inelastic response of the intervertebral disc, *Journal of Engineering in Medicine*, *in press*.

2.1.1. Partial introduction

Chronic low back pain or neck pain is increasingly affecting people worldwide; it becomes the main reason for long-term disabilities in developed countries with a major socio-economic impact (Vos et al., 2016). Although the exact origin of the chronic back pain remains unclear, its correlation with the intervertebral disc (IVD) degeneration is commonly accepted (Cheung et al., 2009). The IVD degeneration is due to several interacting factors including biological and biomechanical malfunctions (Vergroesen et al., 2015). The natural effect of aging has, for consequence, to disturb the delicate homeostasis of the IVD, entering with the time in a vicious loop in which mechanical and biological phenomena are indeed interconnected. The IVD mechanical response at the macroscopic scale is entirely governed by the rearrangement of the collagen fibers and proteoglycans (PGs) that interact with a liquid phase composed of water, mobile charges and small proteins. In the healthy IVD, the negatively charged PGs generate an osmotic pressure through the liquid phase attraction. The decrease in PGs content with degeneration is accompanied by a water loss with age (Vergroesen et al., 2015): 70% water in healthy IVD and 61% water in Thompson grade III (Thompson et al.,1990; Gu et al.,1999). The IVD mechanical response is directly related to chemical disorders (Iatridis et al., 2005). Indeed, every change in osmolarity has a direct effect on the IVD mechanical behavior with variations in fluid content inside extracellular matrix and modifications in chemical equilibrium. The osmolarity variations are naturally present in the IVD via the internal fluid flow (Ferguson et al., 2004) due to the disc movement. The connection of the IVD degeneration with sustainable chemical changes and the related changes in mechanical properties may be also understood as a chemo-mechanical coupling.

As a mechanical dashpot organ in the spine, the IVD exhibits a complex history-dependent response characterized by relaxation, hysteresis during cyclic loading and rate-dependency (Asano et al., 1992 ; Yingling et al., 1997; Smeathers and Joanes, 1998; Race et al., 2000;

Holzapfel et al., 2005; Kemper et al., 2007; Costi et al., 2008; Newell et al., 2016, 2017; Tavakoli and Costi, 2018).

The inelastic behavior, that assures a more even distribution of local stresses, is a fundamental characteristic of the healthy IVD provided by its two main subcomponents, i.e. inner nucleus pulposus (NP) and outer annulus fibrosus (AF). The respective role of NP and AF during motion of the functional spine unit (FSU) has to be understood through their interactions and their specificities, e.g. NP migration (Seroussi et al., 1989; Osti and Fraser, 1992; Balkovec and McGill , 2012; Kim et al., 2017) and AF micro-structure (Cassidy et al., 1989; Marchand and Ahmed , 1990; Newell et al., 2017). Cyclically loaded FSUs exhibit a hysteretic response manifested by a difference between loading and unloading paths. This phenomenon highlights the dissipative capability of the IVD and its dashpot role. The deviation from a purely elastic response is due to the presence of a viscous stress in the extracellular matrix which is strongly dependent on the level of microstructural interactions between the constituents, i.e. PGs and collagen fibers. The hysteresis also depends on the fluid content in the IVD which is altered by osmolarity (Adams et al., 1996; McMillan et al., 1996; Iatridis et al., 1997), driving fluid outward during loading and inward during unloading (Drost et al., 1995). The loading-unloading process contributes to provide nutrients under normal circumstance. However, at high rate magnitudes, it generates high local stresses which may affect cell metabolism (Chan et al., 2011). Under usual loads and without degeneration, the IVD response is totally recovered without any effect of previous imposed chemo-mechanical loadings. This total recovery phenomenon excludes micro-alterations; It depends on PG macromolecules rearrangement, collagen fibers-PGs interactions, fluid-PGs interactions and chemo-mechanical coupling. The loading rate affects the osmotic gradient between the NP and the surrounding fluid, and then the chemo-mechanical coupling. The latter is responsible for the time-dependent behavior of the IVD. Although the coupling between inelastic phenomena and chemical effects have been

very recently investigated (Emanuel et al., 2018; Vergroesen et al., 2018), the inherent chemo-mechanical mechanisms are far from being fully established, especially regarding the mechanical loading path. Establishing the relationship between the osmo-inelastic response and the mechanical loading path would allow highlighting the origin of the coupling.

The present part of the Chapter 2 is focused on the chemical sensitivity of the FSU inelastic response in relation with the mechanical loading path. In-vitro experiments were performed for different osmolarity and loading rate conditions in order to provide insights on the time-dependent chemo-mechanical response of the FSU. The response was examined in tension, compression and torsion. A plausible explanation of the inherent chemo-mechanical coupling is discussed under the guidance of our experimental observations.

2.1.2. Materials and methods

2.1.2.1. Specimen preparation

Nineteen FSUs from cervical spines were harvested from mature sheep cadavers (8-10 months) obtained from a local abattoir. Sheepwas selected in reason of the vertebrae size that facilitates cutting operations and easily fits our testing machine. The selected specimens were stored at 4°C at maximum two days before testing. Note that although the responses of fresh and frozen FSUs are expected to be different (Callaghan and McGill, 1995; Bass and al., 1997), the storage effects in terms of temperature and duration are still unknown (Newell et al., 2017). That is why fresh specimens were used in this study. The entire cervical spines extracted within two days after animal death were first separated from muscles and ligaments by hand using a surgical tool, and then separated into nineteen FSUs with a band saw, consisting in « bone-disc-bone » segment without neural arches. The cutting was carefully performed in order to assure a sufficient bone segment size. External cracks in bone segment due to cutting operation were carefully examined, and after a visual inspection, only eighteen intact FSUs were chosen for

mechanical testing. Immediately after extraction, the FSU was cleaned and then immerged in 9 g/L saline solution at room temperature during 100 minutes. Since the storage condition after animal death in dry cold room decreases the water content, immerging specimens in that solution increases its hydration content to reach the chemical equilibrium (Costi et al., 2002) when IVD height remains constant. Note that ex-vivo conditions increase the equilibrated water content compared to in-vivo conditions. Due to the irregular shape of the vertebra, the bone segment was embedded in polyurethane resin Axson F180 to obtain two parallel plans. The specimen preparation procedure is illustrated in Figure 2.1.1. The superior and inferior parts of the FSU were glued to metal plates in order to be gripped between clamps of the testing machine. The applied loadings were lower than the maximal physiological movements in order to keep normal working conditions and to avoid any damage in IVDs or in both bone-resin interface and resin-metal plate gluing.

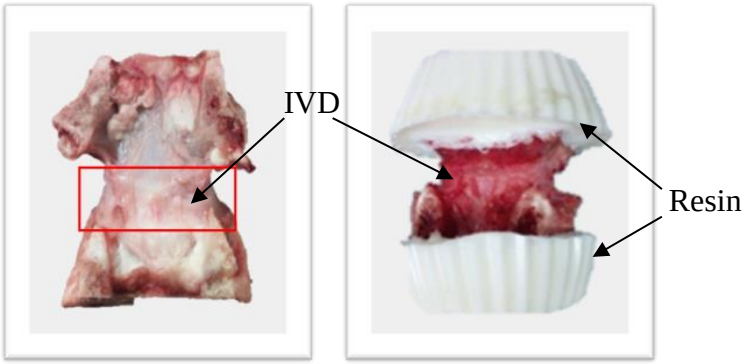

Figure 2.1.1. Preparation of FSU specimen (dorsal view): (a) extraction of IVD and two adjacent bone segments, (b) bone segments embedded in resin.

2.1.2.2. Methods

In-vitro experiments were performed under controlled-environment using a displacement-controlled universal-axial testing machine Instron-5500 equipped with a 5 kN load cell and an angle-controlled universal-torsion testing machine Instron-8874 equipped with a 100 Nm load

cell. Throughout the mechanical loading, the FSUs were immerged in a saline solution. The osmolarity was controlled by varying the NaCl content in water from 0 g/L hypo-osmotic solution to 36 g/L hyper-osmotic solution. The temperature influence is not considered in the present work, and all measurements were performed at room temperature.

The results reported in this investigation follow the experimental procedure illustrated in Figure 2.1.2.

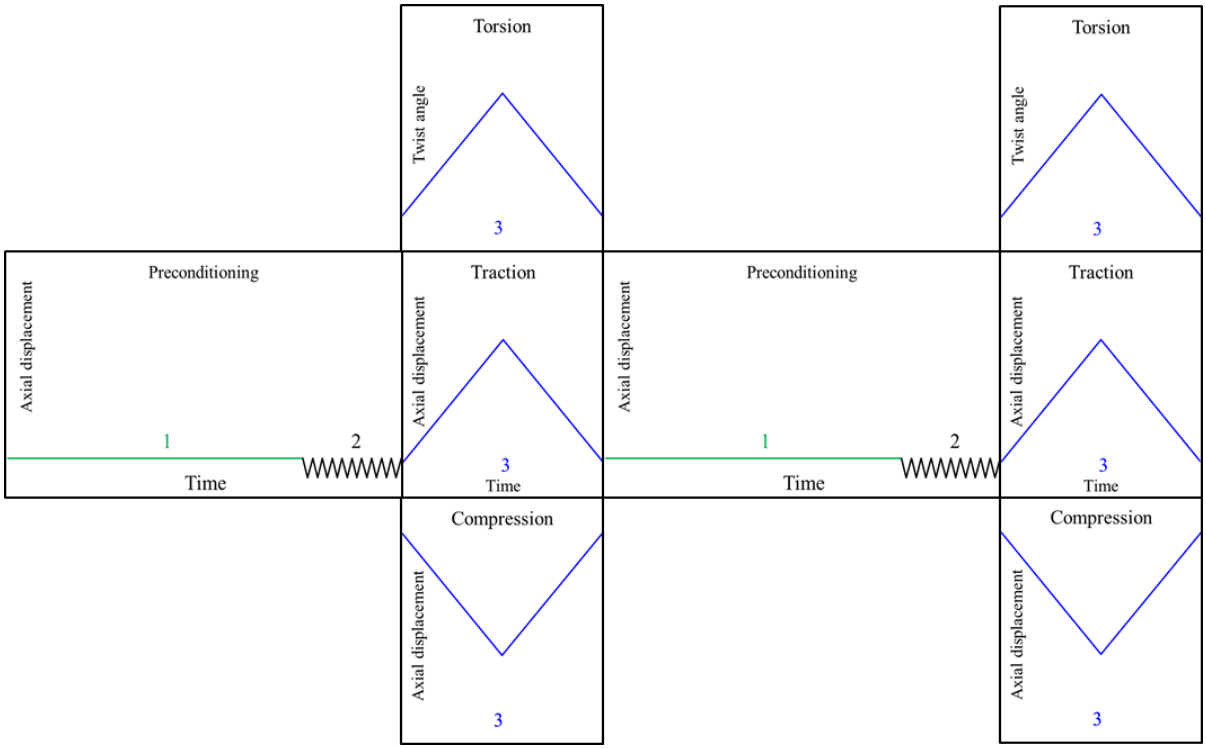

Figure 2.1.2. Experimental design for two successives loading-unloading tests (1: mechanical rest, 2: successive low-strain compressions, 3: loading-unloading test).

A two-step preconditioning was applied in the aim to adapt the IVD tissue to its new environment after changes in NaCl content and to ensure reproducibility of the mechanical response. The two-step preconditioning consists in a period of 30 minutes of mechanical rest without load and successive low-strain compressions which generate inter-vertebral pressure and promote a fluid exchange with the environment (Urban and McMullin, 1985; Adams et al., 1987; Ferguson et al., 2004). In particular, the fluid exchange during this preconditioning avoids

internal imbalances due to changes in solution osmolarity and allows penetration of NaCl inside IVD. The reliability of the preconditioning can be verified by performing two successive relaxation tests. In the test, a compressive displacement was progressively increased until reaching a prescribed value and then maintained constant during 1 hour.

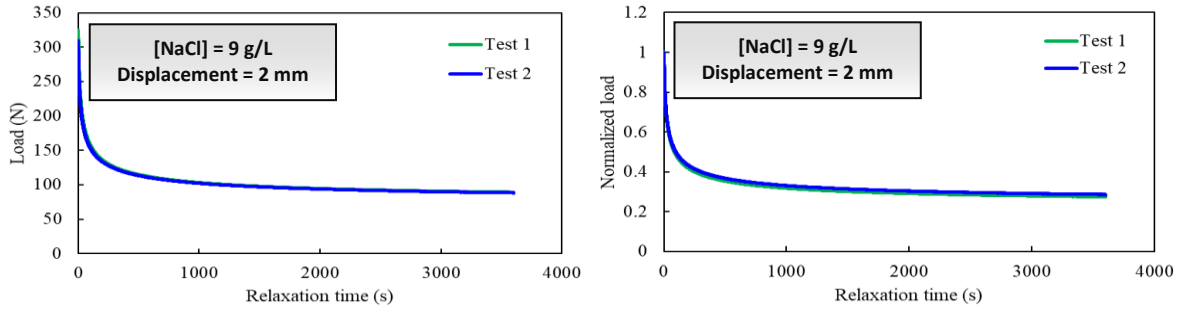

(a)

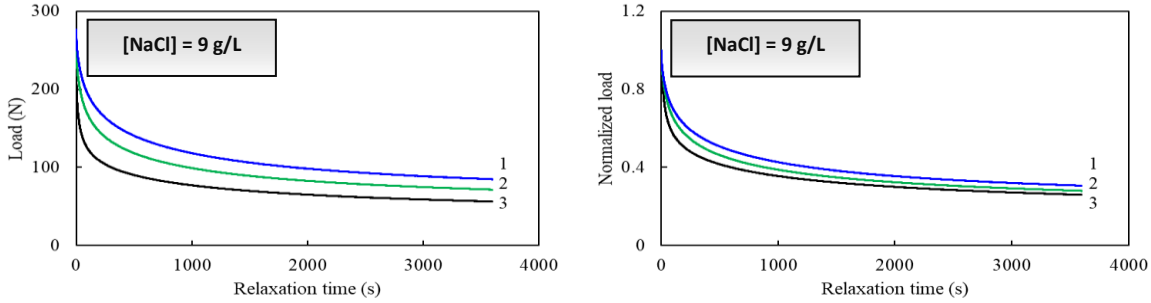

(b)

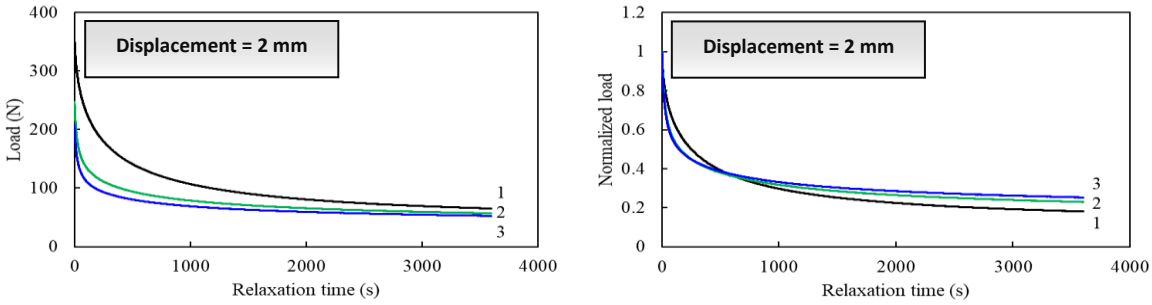

(c)

Figure 2.1.3. Relaxation response: (a) two successive relaxation tests performed on the same FSU, (b) displacement level effect (1: 3 mm, 2: 2 mm, 3: 1 mm) and (c) osmolarity effect (1: 0 g/L, 2: 9 g/L, 3: 18 g/L).

The results of two successive relaxation tests are reported in Figure 2.1.3a for a reference saline concentration of 9 g/L and a compressive displacement of 2 mm. The load begins to substantially decrease in the first relaxation period and then evolves towards an end corresponding to an obvious stabilized state. Since the two relaxation curves are superimposed, a total recovery is obtained between the repeated tests. This result assesses our test method in which the mechanical and structural features of the FSU specimen remain intact. As an inelastic feature that depends on the chemical state of the IVD, the stabilized response is function of the compressive displacement level (Figure 2.1.3b) and the NaCl concentration (Figure 2.1.3c). Although the applied displacements seem substantial, no failure was reported.

The preconditioning allows the chemo-mechanical equilibrium of the FSU before experiments. Experiments on FSU specimens are, however, repeatable only if the loading is within the physiological range in order to avoid all damage phenomena in the unit. Even after 10,000 cycles, a total recovery of the FSU response was observed by Johannessen et al. (2004). Although in some studies thousands of preconditioning cycles are applied, the reproducibility of the mechanical response is generally reached upon only first three cycles (Newell et al., 2017). In the present study, the FSUs were preconditioned by 10 cycles with low amplitude of 0.1 mm (at a rate of 5×10^{-2} mm s^{-1}) in order to adapt the IVD tissue to its new environment. This step is particularly important due to the storage conditions in dry cold room, in terms of relative humidity and temperature, which decrease the water content in IVD and its thickness. Experiments were sufficiently slow to ensure fluid circulation, chemical equilibrium and to avoid dynamic effects. A recovery period of 30 minutes was imposed between two successive experiments in order to restore both mechanical and chemical equilibrium. The measurements on the same FSU were repeated after each preconditioning and the total recovery was observed. The FSU chemo-mechanical response was studied in tension, compression and torsion. These loading types provide fundamental information about physiological motions of the FSU such

as lateral bending, flexion-extension and axial rotation. Experiments were performed by successively increasing the loading rates: 5×10^{-4} mm s^{-1}, 5×10^{-3} mm s^{-1}, 5×10^{-2} mm s^{-1} for axial experiments and 0.01 deg s^{-1}, 0.05 deg s^{-1}, 0.1 deg s^{-1} for twisting experiments. The axial displacement and the twist were limited to a maximum value of 0.25 mm and 2 deg, respectively. The maximum twist angle value of 2 deg corresponds to a neck movement of 50 deg (Anderst et al., 2015). The osmolarity effect was studied by varying the NaCl content in solution: 0 g/L, 9 g/L, 18 g/L and 36 g/L in order to change the environment from hypo-osmotic condition to hyper-osmotic condition and the respective mechanical response. During the physiological movements, the ionic repartition in IVD is inhomogeneous due to water exchange. These experiments permit a better understanding of changes in mechanical response as a result of chemical changes.

2.1.2.3. Statistical analysis

Statistical analysis was carried out to determine standard deviation and error bars on the load and torque values at a 95% confidence. The data presented in the next section represent the mechanical response on one IVD. A p-value < 0.05 was considered to be statisticallysignificant. For both the compression (n=5) and the torsion (n=7), at the same loading rate and the same NaCl concentration, one-way analysis of variance (ANOVA) indicates a p-value < 0.05. A two-way ANOVA without replication is then performed to other FSUs (n=6) in order to indicate the statistical significance of the loading rate and osmolarity effects. Although the present study is based on a relatively small number of specimens (n=18), the goal is to provide qualitative trends allowing to highlight the existence of the osmo-inelastic coupling with our validated protocol.

2.1.3. Results

2.1.3.1. Tension

The load-displacement curves under tension are plotted in Figure 2.1.4 for different NaCl concentrations and loading rates. The two latter effects are both statistically significant, with a p-value of 0.015 and 0.002, respectively.

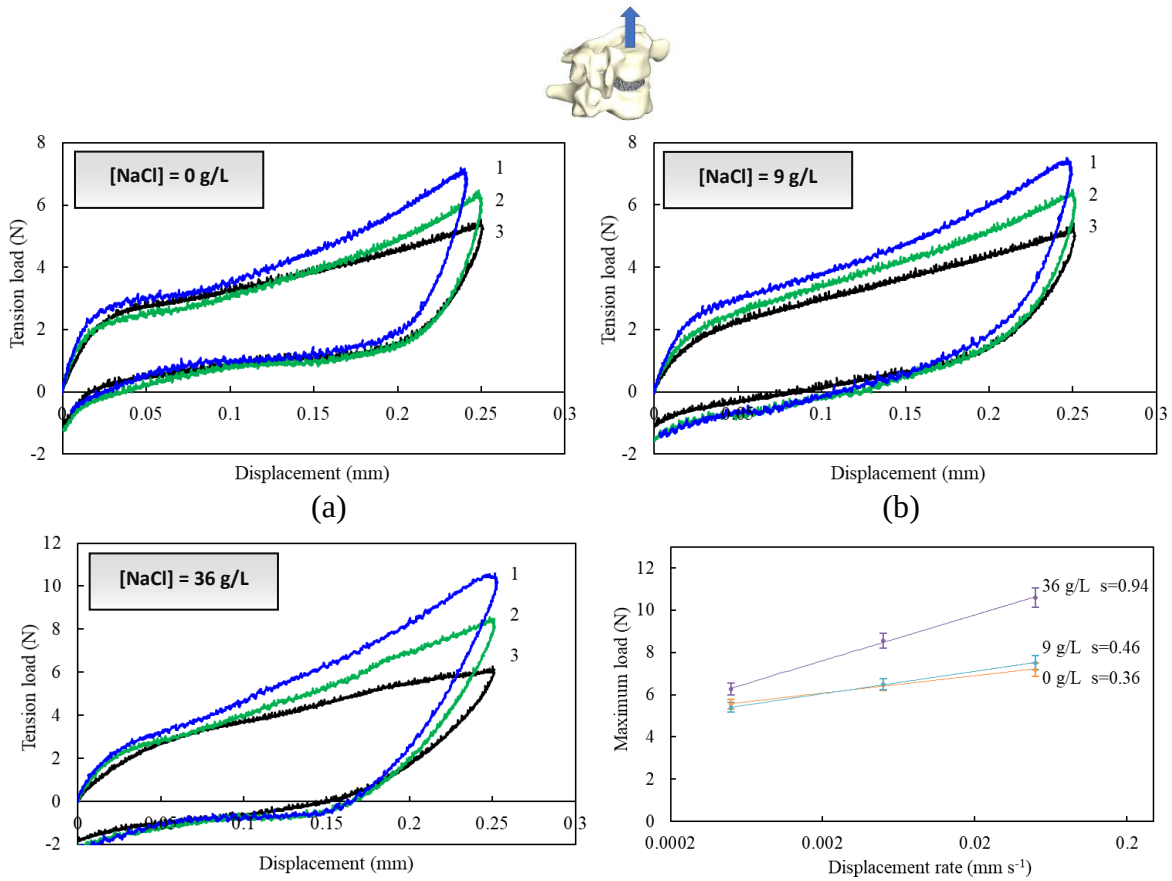

Figure 2.1.4. Tension load-displacement responses at three different rates (1: 5×10^{-2} mm s^{-1}, 2: 5×10^{-3} mm s^{-1}, 3: 5×10^{-4} mm s^{-1}) for (a) 0 g/L, (b) 9 g/L, (c) 36 g/L NaCl concentration, and (d) maximum load-rate response.

The FSU tension response exhibits different stages including an initial stiff response followed by a gradual rollover to hardening. The response depends markedly on the applied loading rate. Higher the loading rate, stiffer the response. The unloading path is different from the loading one, and a residual set appears upon complete unloading, i.e. zero load. The osmolarity affects

the residual set. Due to its effect on the water content and the microstructure, the increase in NaCl concentration induces a decrease in IVD height. Higher axial strains are then applied on the tissue when the NaCl concentration is increased. The maximum tension load is reported in Figure 2.1.4d as a function of the loading rate, such that a straight-line fit adequately describes the results. The slope, characterizing the rate sensitivity, increases with the NaCl concentration. The osmolarity effect is more important at high loading rate. The rate sensitivity is two time higher between hypo-osmotic and hyper-osmotic conditions.

2.1.3.2. Compression

The compression is a more common mechanical loading applied to IVDs, resulting from the head weight, muscles tension or loads carried by the individual. The FSU load-displacement curves under compression are plotted in Figure 2.1.5. The loading rate effect and the osmolarity effect on the FSU response in compression are obviously statistically significant ($p<0.001$ for both effects). Chemo-mechanical couplings are then highlighted especially in compression. The FSU compressive response exhibits important energy dissipation, indicating again the dashpot role of the IVD. The osmolarity modifies the compressive response in shape and in magnitude. In particular, the observed inflexion point is delayed with the increasing osmolarity. Also, the residual set increases when the osmolarity increases. More interestingly, the osmolarity effects are inversed in compression and in tension. Indeed, higher the NaCl concentration, softer the response. As reported in Figure 2.1.5d, the rate sensitivity decreases with the NaCl concentration. Moreover, the impact of the loading rate on the FSU response is more important in compression than in tension. At the end of the unloading path, the load, for which the displacement is zero, is the same whatever the conditions.

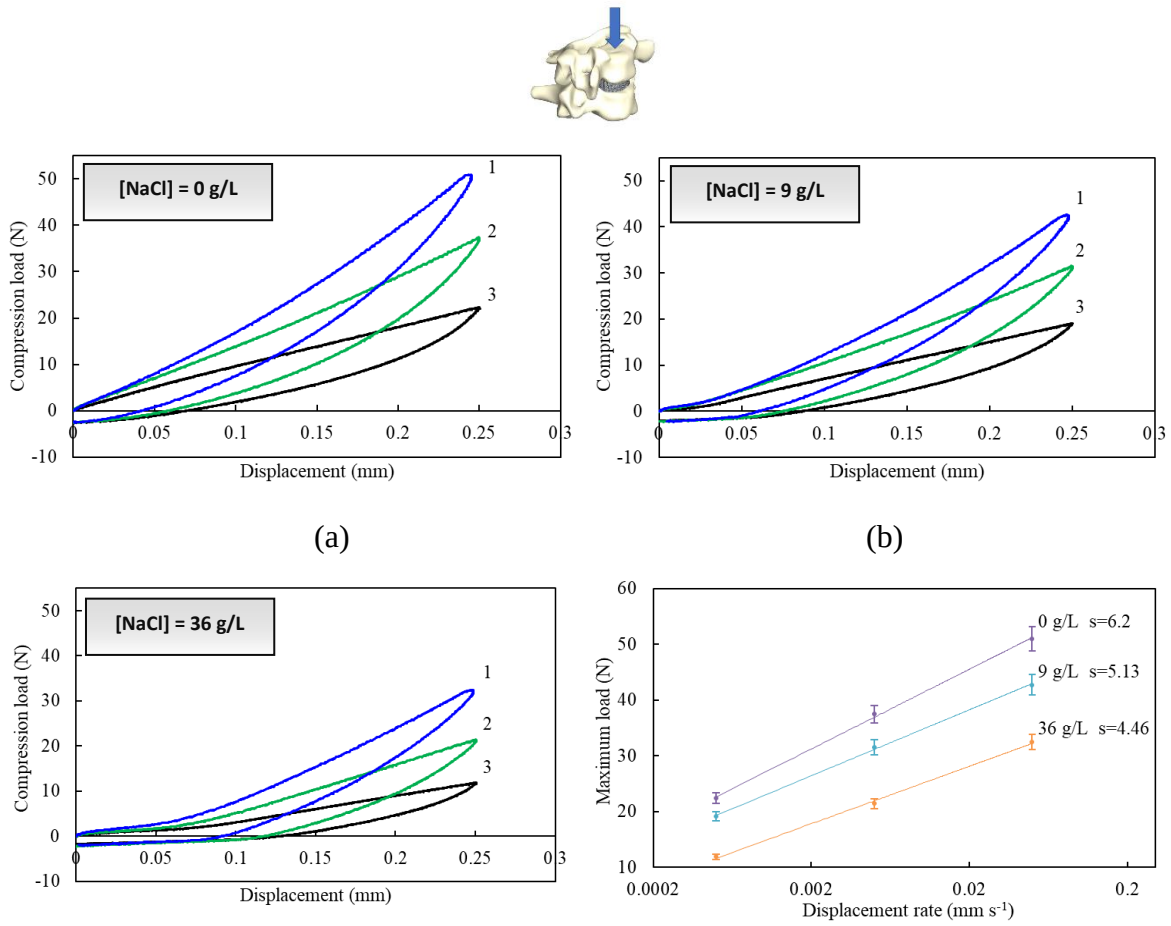

Figure 2.1.5. Compression load-displacement responses at three different rates (1: 5×10^{-2} mm s^{-1}, 2: 5×10^{-3} mm s^{-1}, 3: 5×10^{-4} mm s^{-1}) for (a) 0 g/L, (b) 9 g/L, (c) 36 g/L NaCl concentration, and (d) maximum load-rate response.

2.1.3.3. Torsion

The spine twisting is also a very common physiological loading mode. The loading rate effect on the FSU torsion response is reported in Figure 2.1.6 for different NaCl concentrations. A p-value > 0.05 is found for both effects in torsion. At low twist angle no appreciable effect of the loading rate can be observed on the torsional stiffness. The FSU response became rate sensitive only athigh twist angle. The chemical sensitivity is not dependent on the loading rate, as illustrated by Figure 2.1.6d in which the rate sensitivity is almost unchanged with the concentration.

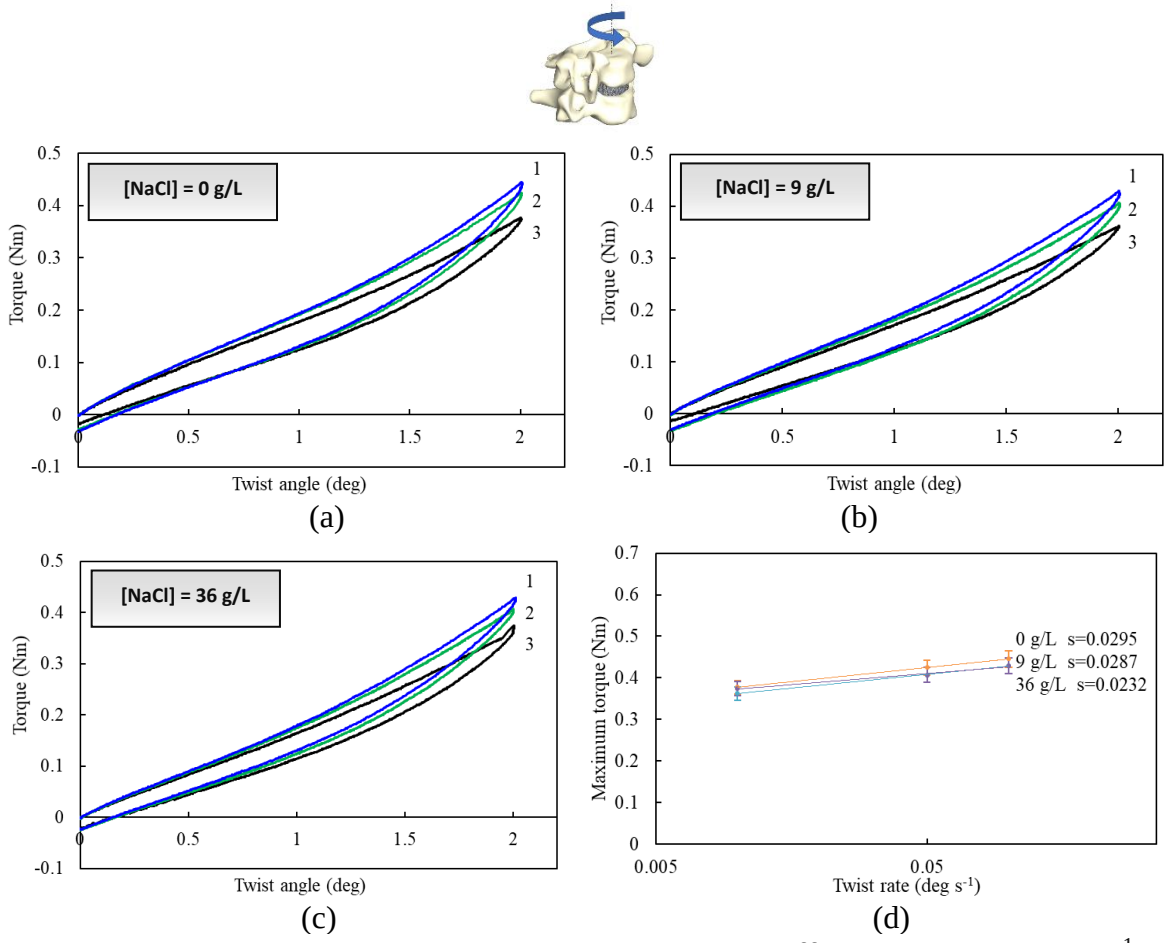

Figure 2.1.6. Torsion load-displacement responses at three different rates (1: 0.1 deg s^{-1}, 2: 0.05 deg s^{-1}, 3: 0.01 deg s^{-1}) for (a) 0 g/L, (b) 9 g/L, (c) 36 g/L NaCl concentration, and (d) maximum torque-rate response.

2.3.4. Discussion

Our results show a significant effect of the osmolarity on the axial inelastic response and an almost imperceptible effect on the torsional inelastic response. Figure 2.1.7 provides our interpretation of the inherent osmo-inelastic mechanisms by means of a schematic representation in which inelastic and osmolarity effects are separated.

The IVD consists of randomly distributed PG macromolecules and organized collagen fibers. The chemical reaction between negatively charged PG macromolecules and mobile ions of the saline solution governs the fluid exchange with the environment. The fluid flow, induced by external ionic imbalance, is dependent on the mechanical loading path, i.e. tension, compression or torsion, and implies osmotic force and IVD swelling (Lanir, 1987).

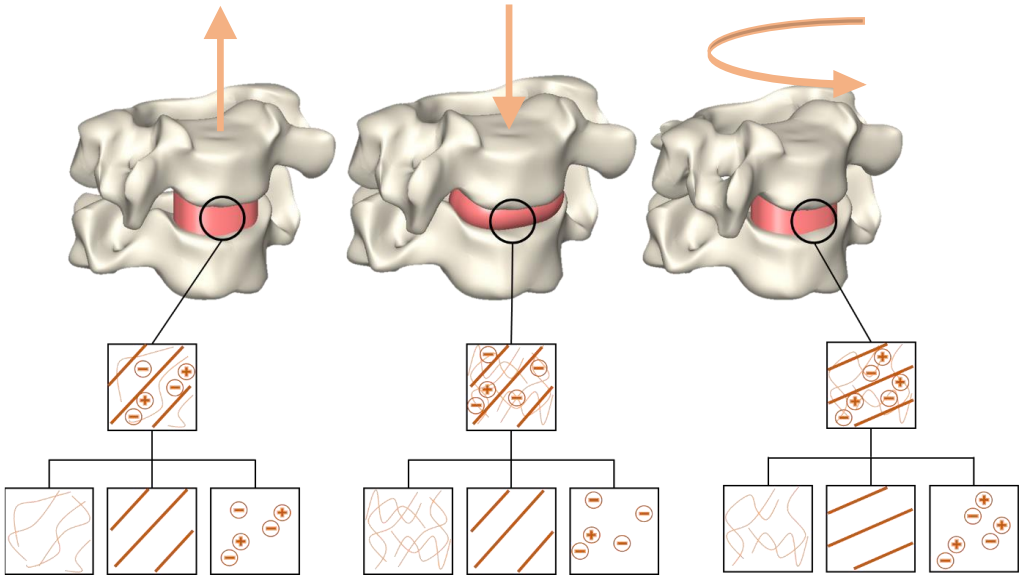

(a) (b) (c)

Figure 2.1.7. Osmo-inelastic mechanisms in (a) tension, (b) compression and (c) torsion.

The FSU time-dependent response is intrinsically linked with the variation of fluid content in the IVD and with the PG macromolecules rearrangement. The inherent chemo-mechanical coupling is strongly dependent on the water and NaCl content, and is shown in our experiments for the FSU under various mechanical loading types. The water content in the IVD is reduced with increasing NaCl concentration leading to reduced chemical exchanges. The rate sensitivity is found higher in compression than in tension, and almost imperceptible in torsion. The NaCl content has a strong impact on the FSU compression rate-dependency (Figure 2.1.5d). By contrast, the rate-dependency in tension (Figure 2.1.4d) is slightly affected by the saline concentration and nearly not affected in torsion (Figure 2.1.6d). In torsion, the overall response is mainly due to collagen fibers reorientation. In hyper-osmotic environment, although the fluid flow is limited (Lai et al., 1991; Ateshian et al., 2004; Vergroesen et al., 2018), our results show a time-dependence of the chemo-mechanical response. The higher chemical sensitivity in compression than in tension is directly linked to the solely increase in fixed charge, i.e. chemical imbalances. The response in Figure 2.1.3 of an IVD compressed and stimulated by a chemical loading gives some insights on the fluid flow contribution. Increasing the compression level

(Figure 2.1.3b) or the NaCl concentration (Figure 2.1.3c) decreases the fluid content and leads to an increasing omostic pressure attempting to neutralize the mechanical loading. With the applied compressive displacement, the fluid content in IVD decreases and the chemical unbalance increases. In reaction, the IVD swells in proportion to the applied compression to reach the chemo-mechanical equilibrium. The swelling implies higher chemical stresses in IVD which opposite to the applied compressive displacement. That results in the increase of the relaxed-load with the displacement as observed in Figure 3b. As shown in Figure 3c, the same effect is reported with the increase in NaCl concentration since the osmolarity increases the internal chemical stresses. By increasing the NaCl concentration, the IVD contracts to eject superfluous ionic component and the equilibrium response is quickly reached since there is more ionic component in solution. Under hypo-osmotic condition, for which the solution is poor in ionic component, the relaxation time increases. In hyper-osmotic environment, the extracellular matrix is saturated and the time necessary to achieve ionic equilibrium is shorter. The apparent viscosity seems to be thus related to the PG macromolecules rearrangement. This statement indicates that the macroscopic inelastic features are due to both microstructural rearrangements and fluid flow. The viscoelastic properties of the soft tissue are predominant at high rates whereas the fluid exchange requires longer times (Vogel and Pioletti, 2012; Vergroesen et al., 2018). As observed in Figure 2.1.3c, the equilibrium response is delayed by decreasing the osmolarity, and then by increasing the chemical exchanges.

Our results bring some insights on the FSU chemo-mechanical response, and a better understanding of interactions between NP and AF is highlighted. The macro-dissipative response is generally attributed to the gelatinous NP but also the AF plays a major role in it (Liu et al., 2014; Emanuel et al., 2018). The NP is an essential element in the FSU behavior, its main role being to generate a hydrostatic pressure on the AF (Nachemson and Morris, 1964; Iatridis et al., 1997; Wilke et al., 1999; Goins et al., 2005). Tensile and compressive FSUs

exhibit opposite responses concerning the environment dependency since the internal pressure generated by the NP is reduced in tension. This observation is not common and must be associated to the fluid flow in the IVD (Ferguson et al., 2004; Schmidt et al., 2016). Indeed, the chemical-dependence is due to the difference in fluid mobility between tensile and compressive states. Under a compressive load the fluid is pushed out of the IVD leading to a chemical unbalance and the negative charge of the PGs generates an osmotic pressure through the attraction of water. By contrast, the tensile state decreases the PGs density and leads to a lesser chemical sensitivity. With the increase in osmolarity the IVD constrains to push out excess mobile ions contained in the fluid which results in a force opposing the tensile load and matching the compressive load. Upon the complete unloading, the amount of fluid loss in the IVD governs the extent of residual set. The latter is found lesser in compression than in tension due to higher fluid exchange in compression than in tension. With the increase in osmolarity, the PGs density increases, the IVD constrains and the residual set increases. Due to their concentric organization with ventral and dorsal parts that strain in opposing directions, the AF collagen fibers have a preponderant role under twisting. As a consequence, the fluid flow effect on the torsional inelastic response is reduced.

2.1.5. Partial conclusion

This study has been conducted to determine the chemical sensitivity of the FSU inelastic response under different mechanical loading paths. The osmotic and time-dependent properties have been considered at the same time to better understand the osmo-inelastic mechanisms and the biomechanical behavior.

The torsional stiffness and rate-dependency were found chemically insensitive whereas an inverse chemical sensitivity was found between tension and compression. Although it is difficult to know to what extent the time-dependent behavior can be attributed to the PGs

rearrangement and the fluid flow, an interpretation of the inherent chemo-mechanical coupling was proposed.

The chemo-mechanical coupling is strong. Indeed, the PGs density depends on the chemical environment affecting the fluid content, and in the meantime, the mechanical loading modulates the PGs density which changes the chemical sensitivity and the level of microstructural interactions. Due to the body weight and muscles tension, the FSU is constantly submitted to a compressive loading stimulating the fluid exchanges with the increase in PGs density which increases the chemical exchanges and the nutrient supply in vivo.

2.1.6. References

Adams, M.A., Dolan, P., Hutton, W.C., 1987. Diurnal variations in the stresses on the lumbar spine. Spine 12, 130-137.

Adams, M.A., McNally, D.S., Dolan, P., 1996. “Stress” distributions inside intervertebral discs. The effects of age and degeneration. Journal of Bone and Joint Surgery 78, 965-972.

Anderst, W.J., Donaldson, W.F., Lee, J.Y., Kang, J.D., 2015. Cervical motion segment contributions to head motion during flexion\extension, lateral bending, and axial rotation. The Spine Journal 15, 2538-2543.

Asano, S., Kaneda, K., Umehara, S., Tadano, S., 1992. The mechanical properties of the human L4-5 functional spinal unit during cyclic loading: the structural effects of the posterior elements. Spine 17, 1343-1352.

Ateshian, G.A., Chahine, N.O., Basalo, I.M., Hung, C.T., 2004. The correspondence between equilibrium biphasic and triphasic material properties in mixture models of articular cartilage. Journal of Biomechanics 37, 391-400.

Balkovec, C., McGill, S., 2012. Extent of nucleus pulposus migration in the annulus of porcine intervertebral discs exposed to cyclic flexion only versus cyclic flexion and extension. Clinical Biomechanics 27, 766-770.

Bass, E., Duncan, N., Hariharan, J., 1997. Frozen storage affects the compression creep behavior of the porcine intervertebral disc. Spine 22, 2867-2876.

Callaghan, J.P., McGill, S.M., 1995. Frozen storage increases the ultimate compression load of porcine vertebrae. Journal of Orthopaedic Research 13, 809-812.

Cassidy, J.J., Hiltner, A., Baer, E., 1989. Hierarchical structure of the intervertebral disc. Journal Connective Tissue Research 23, 75-88.

Chan, S.C.W., Ferguson, S.J., Gantenbein-Ritter, B., 2011. The effects of dynamic loading on the intervertebral disc. European Spine Journal 20, 1796‑1812.

Costi, J.J., Hearn, T.C., Fazzalari, N.L., 2002. The effect of hydration on the stiffness of intervertebral discs in an ovine model. Clinical Biomechanics 17, 446-455.

Costi, J.J., Stokes, I.A., Gardner-Morse, M.G., Iatridis, J.C., 2008. Frequency-dependent behavior of the intervertebral disc in response to each of six degree of freedom dynamic loading: solid phase and fluid phase contributions. Spine 33, 1731-1738.

Drost, M.R., Willems, P., Snijders, H., Huyghe, J.M., Janssen, J.D., Huson, A., 1995. Confined compression of canine annulus fibrosus under chemical and mechanical loading. Journal of Biomechanical Engineering 117, 390-396.

Emanuel, K.S., van der Veen, A.J., Rustenburg, C.M.E., Smit, T.H., Kingma, I., 2018. Osmosis and viscoelasticity both contribute to time-dependent behaviour of the intervertebral disc under compressive load: A caprine in vitro study. Journal of Biomechanics 70, 10-15.

Ferguson, S.J., Ito, K., Nolte, L.P., 2004. Fluid flow and convective transport of solutes within the intervertebral disc. Journal of Biomechanics 37, 213-221.

Goins, M.L., Wimberley, D.W., Yuan, P.S., Fitzhenry, L.N., Vaccaro, A.R., 2005. Nucleus pulposus replacement: an emerging technology. The Spine Journal 5, 317-324.

Gu, W.Y., Mao, X.G., Foster, R.J., Weidenbaum, M., Mow, V.C., Rawlins, B.A., 1999. The anisotropic hydraulic permeability of human lumbar anulus fibrosus: influence of age, degeneration, direction, and water content. Spine 24, 2449-2455.

Holzapfel, G.A., Schulze-Bauer, C.A.J., Feigl, G., Regitnig, P., 2005. Single lamellar mechanics of the human lumbar anulus fibrosus. Biomechanics and Modeling in Mechanobiology 3, 125-140.

Iatridis, J.C., Setton, L.A., Weidenbaum, M., Mow, V.C., 1997. Alterations in the mechanical behavior of the human lumbar nucleus pulposus with degeneration and aging. Journal of Orthopaedic Research 15,318-322.

Iatridis, J.C., MaClean, J.J., Ryan, D.A., 2005. Mechanical damage to the intervertebral disc annulus fibrosus subjected to tensile loading. Journal of Biomechanics 38, 557-565.

Johannessen, W., Vresilovic, E.J., Wright, A.C., Elliott, D.M., 2004. Intervertebral disc mechanics are restored following cyclic loading and unloaded recovery. Annals of Biomedical Engineering 32, 70-76.

Johnson, Z.I., Shapiro, I.M., Risbud, M.V., 2014. Extracellular osmolarity regulates matrix homeostasis in the intervertebral disc and articular cartilage: evolving role of TonEBP. Matrix Biology 40, 10-16.

Kemper, A.R., McNally, C., Duma, S.M., 2007. The influence of strain rate on the compressive stiffness properties of human lumbar intervertebral discs. Biomedical Sciences Instrumentation 43, 176-181.

Kim, Y.H., Kim S.I., Park, S., Hong, S.H., Chung, S.G., 2017. Effects of cervical extension on deformation of intervertebral disk and migration of nucleus pulposus. Physical Medicine and Rehabilitation 9, 329-338.

Lai, W.M., Hou, J.S., Mow, V.C., 1991. A triphasic theory for the swelling and deformation behaviors of articular cartilage. Journal of Biomechanical Engineering 113, 245-258.

Lanir, Y., 1987. Biorheology and fluid flux in swelling tissues. I. bicomponent theory for small deformations, including concentration effects. Biorheology 24, 173-187.

Marchand, F., Ahmed, A.M., 1990. Investigation of the laminate structure of lumbar disc anulus fibrosus. Spine 15, 402-410.

McMillan, D.W., Garbutt, G., Adams, M.A., 1996. Effect of sustained loading on the water content of intervertebral discs: implications for disc metabolism. Annals of Rheumatic Diseases 55, 880-887.

Nachemson, A., Morris, J.M., 1964. In vivo measurements of intradiscal pressure: discometry, a method for the determination of pressure in the lower lumbar discs. The Journal of Bone and Joint Surgery 46, 1077-1092.

Newell, N., Grigoriadis, G., Christou, A., Carpanen, D., Masouros, S.D., 2016. Material properties of bovine intervertebral discs across strain rates. Journal of the Mechanical Behavior of Biomedical Materials 65, 824-830.

Newell, N., Little, J.P., Christou, A., Adams, M.A., Adam, C.J., Masouros, S.D., 2017. Biomechanics of the human intervertebral disc: a review of testing techniques and results. Journal of the Mechanical Behavior of Biomedical Materials 69, 420-434.

Osti, O.L., Fraser, R.D., 1992. MRI and discography of annular tears and intervertebral disc degeneration: a prospective clinical comparison. The Journal of Bone and Joint Surgery 74, 431-435.

Race, A., Broom, N.D., Robertson, P., 2000. Effect of loading rate and hydration on the mechanical properties of the disc. Spine 25, 662-669.

Schmidt, H., Schilling, C., Reyna, A.L.P., Shirazi-Adl, A., Dreischarf, M., 2016. Fluid-flow dependent response of intervertebral discs under cyclic loading: on the role of specimen preparation and preconditioning. Journal of Biomechanics 49, 846-856.

Seroussi, R.E., Krag, M.H., Muller, D.L., Pope, M.H., 1989. Internal deformations of intact and denucleated human lumbar discs subjected to compression, flexion, and extension loads. Journal of Orthopaedic Research 7, 122-131.

Smeathers, J.E., Joanes, D.N., 1988. Dynamic compression properties of human lumbar intervertebral joints: a comparison between fresh and thawed specimens. Journal of Biomechanics 21, 425-433.

Tavakoli, J., Costi, J.J., 2018. New findings confirm the viscoelastic behaviour of the inter-lamellar matrix of the disc annulus fibrosus in radial and circumferential directions of loading. Acta Biomaterialia 71, 411-419.

Thompson, J.P., Pearce, R.H., Schechter, M.T., Adams, M.E., Tsang, I.K., Bishop, P.B., 1990. Preliminary evaluation of a scheme for grading the gross morphology of the human intervertebral disc. Spine 15, 411-415.

Urban, J.P., McMullin, J.F., 1985. Swelling pressure of the intervertebral disc: influence of proteoglycan and collagen contents. Biorheology 22, 145-157.

Vergroesen, P.P.A., Kingma, I., Emanuel, K.S., Hoogendoorn, R.J.W., Welting, T.J., van Royen, B.J., van Dieen, J.H., Smit, T.H., 2015. Mechanics and biology in intervertebral disc degeneration: a vicious circle. Osteoarthritis and Cartilage 23, 1057-1070.

Vergroesen, P.P.A., Emanuel, K.S., Peeters, M., Kingma, I., 2018. Are axial intervertebral disc biomechanics determined by osmosis? Journal of Biomechanics 70, 4-9.

Vogel, A., Pioletti, D.P., 2012. Damping properties of the nucleus pulposus. Clinical Biomechanics 27, 861-865.

Vos, T., Allen, C., Arora, M., Barber, R.M., Bhutta, Z.A., Brown, A., et al., 2016. Global, regional, and national incidence, prevalence, and years lived with disability for 310 diseases and injuries, 1990-2015: a systematic analysis for the Global Burden of Disease Study 2015. Lancet 388, 1545-1602.

Wilke, H. J., Neef, P., Caimi, M., Hoogland, T., Claes, L.E., 1999. New in vivo measurements of pressures in the intervertebral disc in daily life. Spine 24, 755-762.

Yingling, V.R., Callaghan, J.P., McGill, S.M., 1997. Dynamic loading affects the mechanical properties and failure site of porcine spines. Clinical Biomechanics 12, 301-305.

Chapter 2: Experimental characterization

Part 2: Pre-strain effect on the chemo-torsional response of the intervertebral disc[2]

Abstract

The role of an axial pre-strain on the torsional response of the intervertebral disc (IVD) remains largely undefined. Besides, the chemo-mechanical interactions in IVD remain yet unclear. The present paper emphasizes the pre-strain effect on the chemical sensitivity of the IVD torsional response. The in-vitro response of fifteen non-frozen specimens, extracted from cervical spines of mature sheeps, was meticulously investigated for various compressive/tensile pre-strain levels in different saline solutions ranging from hypo-osmotic to hyper-osmotic conditions. Analysis of variance shows that the osmotic effect is statistically significant ($p<0.05$) only when the IVD is pre-compressed. The pre-strain type leads to a significant variation of the IVD chemo-torsional response with a chemical sensitivity significantly higher in compression than in tension. The pre-strain level does not affect the torsional response. However, the chemical sensitivity of the torsional stiffness is much more important under a compressive pre-strain than under a tensile pre-strain. An inverse effect of the compressive pre-strain is found under hypo-osmotic and hyper-osmotic conditions illustrating the role of the chemo-mechanical coupling. A plausible interpretation of the inherent chemo-torsional coupling with the pre-strain dependency is proposed according to our experimental observations. The combination of a compressive pre-strain with the twisting amplifies the tension of the annulus collagen fibers thanks to nucleus hydrostatic pressure, and leads to an increase in torsional stiffness. The negatively charged proteoglycans (PGs) density increases with the compressive pre-strain and leads to higher chemical imbalances, which explains the increase in chemical sensitivity.

Keywords: Intervertebral disc; Pre-strain; Torsion; Chemical sensitivity; Chemo-mechanical mechanisms.

[2] This Part of this chapter is based on the following paper: Amil Derrouiche, Fahmi Zaïri, Fahed Zaïri, Pre-strain effect on the chemo-torsional response of the intervertebral disc, *submitted*.

2.2.1. Partial introduction

The intervertebral disc (IVD) is a fundamental spinal component made to sustain and transmit loads between each two adjacent vertebrae. The functional spine unit (FSU) is basicallyconsisting of a vertebra-IVD-vertebra segment and is subjected, in-vivo, to a complex combination of tension, compression and torsion. Organs motions during daily activities, muscular tension and body weight permanently apply a compressive pre-strain on the FSU prior to every further loading type (Janevic et al., 1991; Gardner-Morse and Stokes, 2003; Newell et al., 2017; Bezci et al., 2018). In the meantime, the spine twisting is a very common physiological loading type in various activities and its study allows understanding the possible causes of IVD injuries (Adams and Hutton, 1981; Farfan, 1984; Barbir et al., 2011; Orias et al., 2016). Many reports about activity sectors, such as on factory workers (Lotters et al., 2003), on militaries (Ulaska et al., 2001) and on athletes (Mortazavi et al., 2015), conclude that spine twisting, while carrying heavy objects, leads to an increase in pain. Indeed, twisting induces a local shear stress state considered as a precursor of the IVD failures (Adams and Hutton, 1981; Farfan, 1984; Costi et al., 2007) which cause chronic low back pain or neck pain (Adams et al., 2012). The latter, by severely curtailing quality of life, became the main origin of long-term disability worldwide (Vos et al., 2016).

Accurate mechanical characterization of the FSU under in-vitro conditions can simulate in-vivo ones, without interaction with the surrounding tissues (Newell et al., 2017). A literature survey shows that most of studies on the FSU mechanics have been limited to simple mechanical load type such as compression or bending and a relatively little attention has been so far paid to the interaction between different mechanical loadings (Janevic et al., 1991; Gardner-Morse and Stokes, 2003; Garges et al., 2008; Orias et al., 2009; Veres et al., 2010; Newell et al., 2017; Bezci et al., 2018). Up to now, the coupling between the FSU mechanics and the bio-chemical

state of the IVD is far from being fully established. The IVD response depends on the macromolecular composition with negatively charged proteoglycans (PGs) and on the physiological fluid sucked by osmotic effect (Drost et al., 1995; Bezci et al., 2015). This fluid exchange through the IVD governs its chemo-mechanical behavior by stimulating ionic transport. At the bone-disc interface, the latter contributes to the management of the nutrient supply. Indeed, due to the avascular nature of the tissue, nutrients penetrate from interosseous arteries into the IVD by diffusion under pressure gradients. Apart from too high level of mechanical loading conditions which may potentially decrease solutes diffusivity, the compressive pre-strain, resulting from muscular tension and body weight, improves nutrient supply (Grunhagen et al., 2006). The IVD has a core-shell structure composed of a core, i.e. the nucleus pulposus (NP), and a shell, i.e. the annulus fibrosus (AF), arranged to form a number of adjoining concentric stratified layers (Cassidy et al., 1989; Marchand and Ahmed, 1990).The active interaction between NP and AF during the FSU physiological motions, such as lateral bending and flexion-extension, is relatively well understood. The induced local compression state generates a NP hydrostatic pressure on AF (Nachemson and Morris, 1964; Wilke et al., 1999; Goins et al., 2005; Schmidt et al., 2016). By contrast, the respective role of NP and AF is yet unclear in torsional mode (Adams and Hutton, 1981; Barbir et al., 2011; Newell et al., 2017). As a biological soft tissue, the IVD is highly dependent on its physiological environment and an increase in osmolarity of the fluid surrounding the IVD limits the chemical exchanges (Emanuel et al., 2015). The relationship between chemical exchanges and mechanical behavior is not yet established, especially regarding the interaction between different mechanical loadings (Janevic et al., 1991; Gardner-Morse and Stokes, 2003; Garges et al., 2008; Orias et al., 2009; Veres et al., 2010; Newell et al., 2017; Bezci et al., 2018).

The aim of this part is to present our understanding of the pre-strain dependency of the IVD chemo-torsional response. Tensile and compressive pre-strains with different levels are

considered in order to modulate the intradiscal pressure under different osmolarity conditions as a result of the change in the solution salinity. Finally, a plausible explanation of the inherent chemo-mechanicalcoupling is discussed under the guidance of our experimental observations.

2.2.2. Materials and methods

2.2.2.1. Specimen preparation

Cervical spines of mature sheeps were obtained from a local abattoir and inspected visually to exclude possible spinal damages. The choice of sheep spinal to make specimens is mainly due to the appropriate size of the vertebrae whichfacilitates cutting operations to fit the testing machine. Note that sheep FSUs provide similar mechanical responses to human FSUs in terms of level and range of motion (Alini et al., 2008). Due to their huge difference in water content, fresh and frozen FSUs are expected to exhibit different mechanical responses (Callaghan and McGill, 1995; Bass et al., 1997). The effect of freezing conditions in terms of temperature and duration is unknown to date (Newell et al., 2017), so the specimens used in this study were fresh and held at maximum two days in a dry cold room of 4°C before testing. The cutting was carefully performed in order to assure a sufficient bone segment size. The specimen preparation procedure is illustrated in Figure 2.2.1. The FSUs were immerged immediately after extraction in a 9 g/L saline solution (reference concentration) at room temperature during 100 minutes. Since the storage condition after animal death in a dry cold room decreases its water content, the immersion in liquid allows to increase the specimen hydration and to reach the chemical equilibrium (Costi et al., 2002) when the IVD height remains constant. After the removal of all soft tissues, and surrounding muscles using a dissecting scissor, fifteen usable FSUs were embedded at each end in parallel deep polyurethane resin Axson F180 wells to provide two

parallel flat resin surfaces. The superior and inferior parts of the FSU were glued to two metal plates in order to be gripped between clamps of the testing machine as shown in Figure 1.

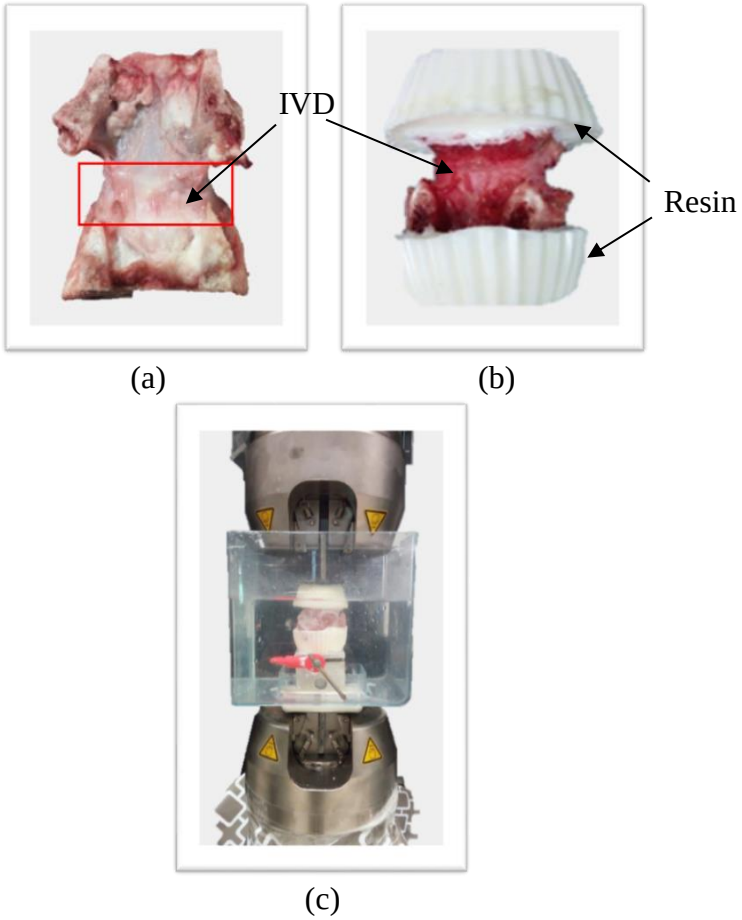

Figure 2.2.1. Preparation of FSU specimen (dorsal view): (a) extraction of IVD and two adjacent bone segments, (b) bone segments embedded in resin, (c) FSU specimen glued to two metal plates and placed in the testing machine.

2.2.2.2. Mechanical experiments

Mechanical experiments were carried out on a universal testing machine Instron-8874 equipped with a cell of 25 kN axial load and 100 Nm torsional load. Throughout the mechanical loading, the FSUs were immersed in various NaCl solutions: 0 g/L hypo-osmotic solution, 9 g/L iso-osmotic solution (closes to human physiological solution) and 18 g/L hyper-osmotic solution.

The temperature influence was disregarded in the present work, and all measurements were performed at room temperature.

Figure 2.2.2 provides a scheme of our protocol with two successive loading-unloading tests as an example. A two-step preconditioning was applied in the aim to alleviate the effects of specimen preparation, to ensure reproducibility of the mechanical response and to adapt the IVD tissue to its new environment after changes in NaCl content.

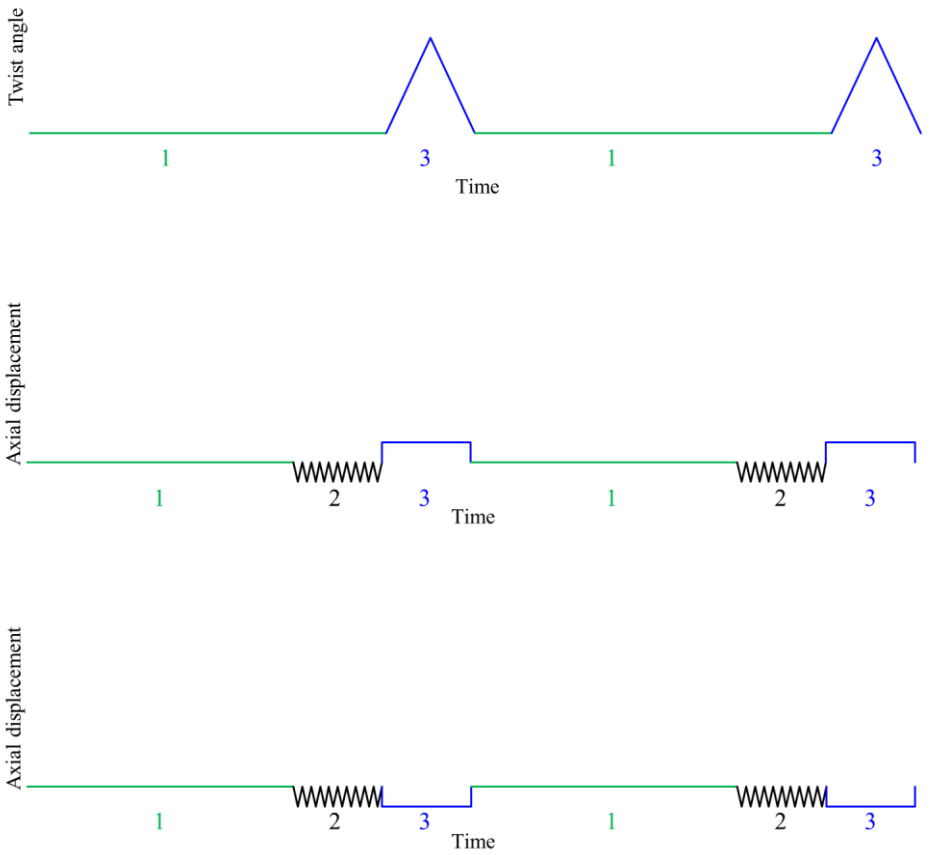

Figure 2.2.2. Experimental design for two successives loading-unloading tests (1: mechanical rest, 2: successive low-strain compressions, 3: loading-unloading test in torsion with a tensile pre-strain or a compressive pre-strain).

The two-step preconditioning consists in a period of 30 minutes of mechanical rest without load and successive low-strain compressions which promote fluid exchange with the environment by generating inter-vertebral pressure (Urban and McMullin, 1985; Adams et al., 1987; Ferguson et al., 2004). Although in some studies authors have applied thousands of preconditioning cycles, the chemical equilibrium is generally reached upon applying only three cycles (Newell et al., 2017). In the present study, 10 preconditioning cycles were adopted with low amplitude of 0.1 mm, corresponding to about 2.5% of the IVD height. The preconditioning cycles were performed under a sufficiently low rate (5×10^{-2} mm s^{-1}) to ensure fluid circulation and to avoid dynamic effects. The circulation of fluid during the preconditioning prevents the internal imbalances due to changes in solution osmolarity. This step is particularly important since during the storage in dry cold room the IVD becomes thinner due to its lack of hydration. After preconditioning, different tests were performed.

The axial (compression/tension) and torsional responses of three different FSUs were examined under loading-unloading with increasing maximum (displacement/angle) levels between two successive cycles. In these experiments, no pre-strain was executed, and a reference saline concentration was selected.

The effect of an axial pre-strain (in compression or in tension) on the chemical sensitivity of the FSU torsional response was studied. Loading-unloading torsion experiments were performed under a twist angle-rate of 5×10^{-2} deg s^{-1} on three different FSUs immerged in various saline solutions. The FSUs were pre-strained by imposing a constant axial displacement during torsion as illustrated in Figure 2.2.2. The ultimate twist angle was limited to 2 deg which corresponds to a neck rotation of 50 deg (Anderst et al., 2015). The applied loadings were lower than the maximal physiological motions in order to keep normal working conditions and to avoid any damage in the IVDs, the bone-resin interface and the resin-metal plate gluing.

The active role of the NP was observed on two hemi-spine units extracted from the same FSU loaded in compression at a rate of 3.5×10^{-3} mm s^{-1}. The cervical FSU was frozen at -18°C (Smeathers and Joanes, 1988) in order to prevent nucleus expanding during cutting due to internal pressure. The NP of one hemi-spine unit was removed using dissecting scissors. A Plexiglas window was screwed on the other hemi-spine unit before defrosting in order to keep the NP in the IVD. Images were recorded during experiments by means of a CCD camera Imager E-lite 2M (LaVision GmbH) at a frequency of 3 Hz with resolution of 290 pixels/mm and size of 1628 × 1236 pixels. Images were analyzed with Davis Software 8.0 (StrainMaster, LaVision GmbH).

2.2.2.3. Histological experiments

A histological study was carried out to evaluate the influence of the chemical effect on the gross morphology of the IVD subcomponents. Dissecting scissors were used to delicately separate each specimen from one IVD by cutting through the vertebrae. Sixteen specimens from AF and NP were isolated and immersed for 48 hours in a saline solution ranging from 0 g/L hypo-osmotic solution to 36 g/L hyper-osmotic solution. All samples were held in 10% neutral buffered formalin to immobilize cells for subsequent histological studies. The samples were then placed in paraffin blocks. Sections of 4 µm thick of both NP and AF from each sample were debited along a transverse plane using a sliding microtome (Leica RM 2235) and were stained using two commonly used stains: Hematoxylin/Eosin (H&E) and Safranin-O (Saf-O) (Walter et al., 2015). Once colored, the section was mounted between slide and slip cover. The colored sections were observed through a binocular microscope (Nikon Eclipse E200) and the observations were captured using a digital camera.

2.2.2.4. Statistical analysis

Statistical analysiswas carried out to determine standard deviation and error bars on the torsional response at the same loading rate and the same NaCl concentration. A p-value < 0.05 was considered to be statistically significant. By using one-way analysis of variance (ANOVA), at a 95% confidence, on different FSUs (n=7), standard deviation is evaluated at about 4.4% on the torque value with a p-value of 0.039. A two-way ANOVA without replication is then performed on other FSUs (n=7) in order to indicate the statistical significance of the pre-strain and osmolarity effects. Although the present study is based on a relatively small number of specimens (n=14), the goal is to provide qualitative trends allowing to highlight the role of the pre-strain in the osmo-torsional coupling with our validated protocol.

2.2.3. Results

2.2.3.1. Inelastic effects

The FSU behavior under loading-unloading with increasing maximum (displacement or angle) levels is presented in Figure 2.2.3 for different mechanical loading types, i.e. compression, tension and torsion. A global view at these plots shows that the FSU response exhibits a hysteresis (manifested by a difference between the unloading and reloading paths), a residual set (for which the load/torque is zero upon unloading) and a load/torque softening (observed when the displacement/angle level exceeds the maximum one previously applied). These main inelastic effects are strongly dependent on the mechanical load type and, are more important in compression, lesser in tension and almost unseen in torsion.

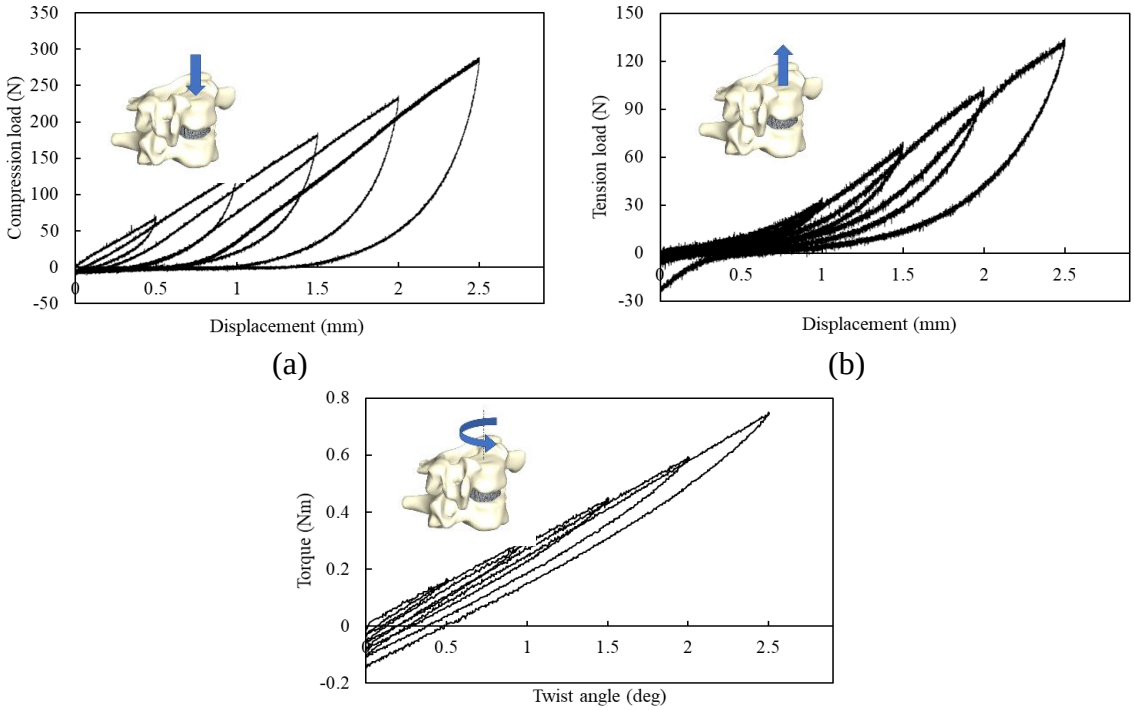

Figure 2.2.3. Inelastic response under different loading types: (a) compression, (b) tension, (c) torsion.

2.2.3.2. Pre-strain type dependency

Figure 2.2.4 presents the osmolarity effect on the torsional response obtained on one FSU under a tensile pre-strain, a compressive pre-strain and without pre-strain. The osmolarity and pre-strain type effects are both statistically significant, with a p-value of 0.02 and 0.033, respectively. The residual set is insensitive both to the environment and the pre-strain type. By contrast, the torsional stiffness and the hysteresis area are strongly dependent on the pre-strain type, increasing with a compressive pre-strain and decreasing with a tensile pre-strain. The chemical sensitivity is dependent on the kind of pre-strain. Indeed, the osmolarity effect is much more important under a compressive pre-strain than under a tensile pre-strain, as illustrated in Figure 2.2.4d in terms of maximum torque. Furthermore, the results of a pre-strain in tension are very similar to those obtained without pre-strain.

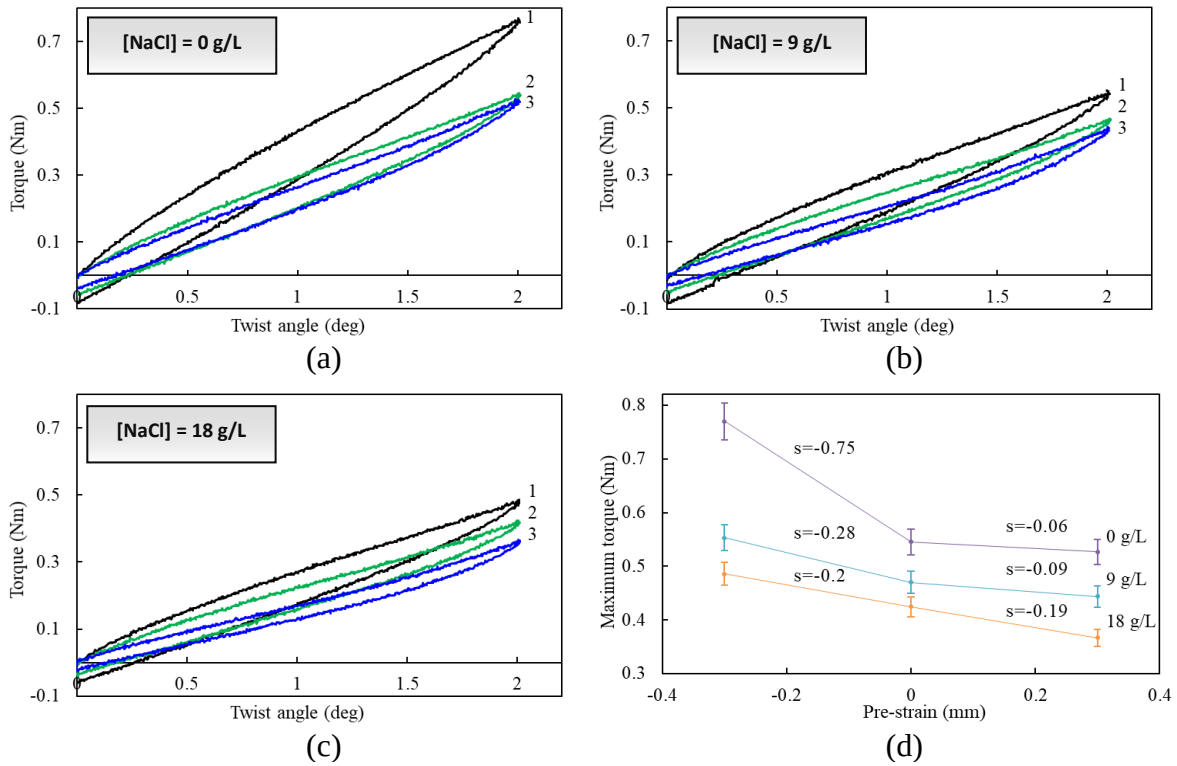

Figure 2.2.4. Pre-strain type effect (1: 0.3 mm compression, 2: 0 mm, 3: 0.3 mm tension) on the torque-twist response for (a) 0 g/L, (b) 9 g/L, (c) 18 g/L NaCl concentration and (d) on the maximum torque.

2.2.3.3. Pre-strain level dependency

Figures 2.2.5 and 2.2.6 show the effect of the pre-strain level on the chemical sensitivity of the torsional response of two FSUs with a tensile pre-strain and a compressive pre-strain, respectively. A global view at these results shows that the pre-strain level has nearly no effect on the inelastic features. No significant effect of the pre-strain level is observed on the torsional stiffness when a tensile pre-strain is applied. Indeed, it can be observed in Figure 2.2.5d that the pre-strain level has no appreciable effect on the maximum torque. Moreover, the hysteretic response is not affected by the pre-strain level. The tensile pre-strain level and osmolarity effects are not statistically significant, with a p-value of 0.212 and 0.213, respectively. These p-values and the very close mechanical responses indicate that the pre-strain level and the osmolarity have no effect on the torsional response when the pre-strain is in tension. For a pre-

strain in compression, the level effect is not statistically significant, with a p-value of 0.8, whereas theosmolarity effect is statistically significant, with a p-value of 0.002. The compressive pre-strain level has a relative effect on the maximum torque as observed in Figure 2.2.6d in which an inverse effect is found under hypo-osmotic and hyper-osmotic conditions. This observation points out the active role of the compression on the chemo-mechanical coupling.

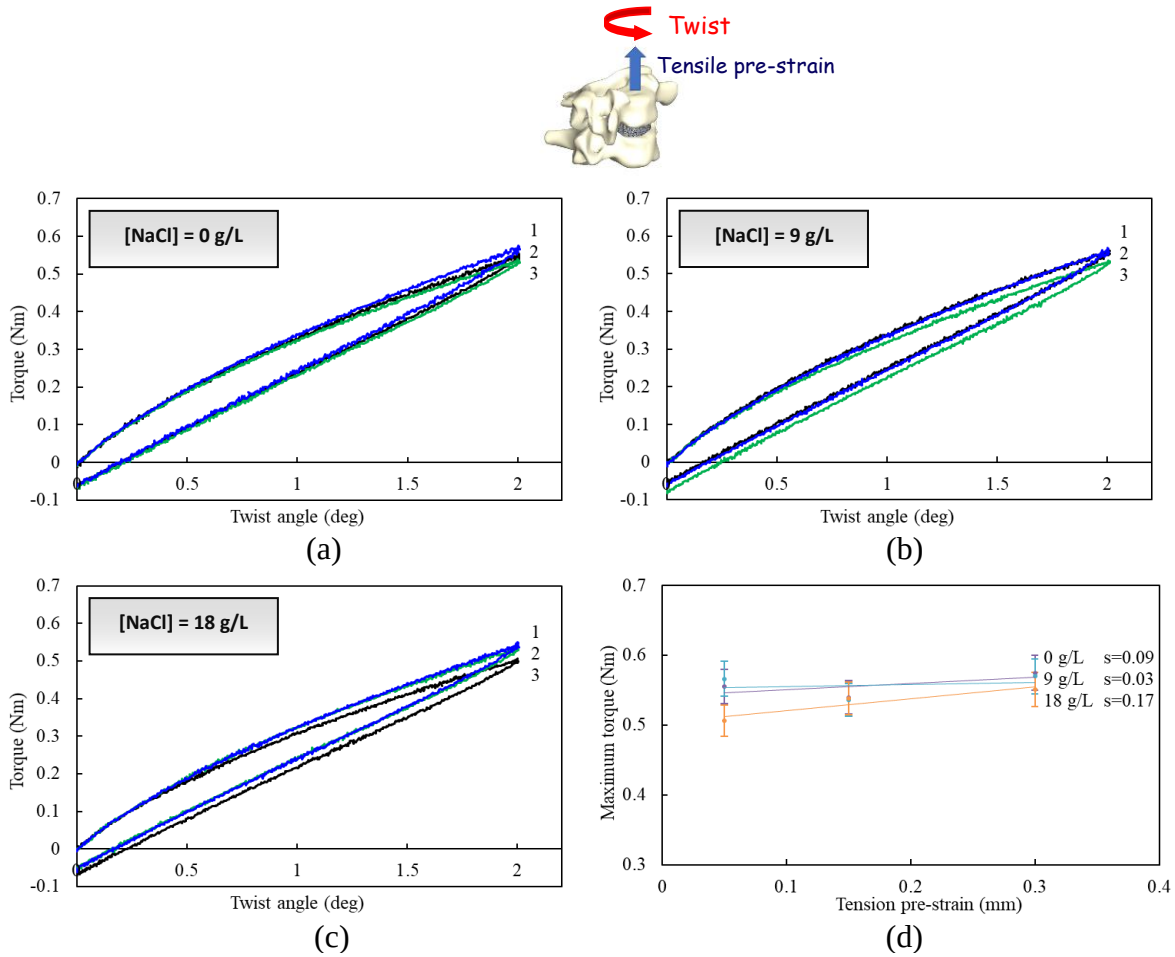

Figure 2.2.5. Tensile pre-strain level effect (1: 0.05 mm tension, 2: 0.15 mm tension, 3: 0.3 mm tension) on the torque-twist response for (a) 0 g/L, (b) 9 g/L, (c) 18 g/L NaCl concentration and (d) on the maximum torque.

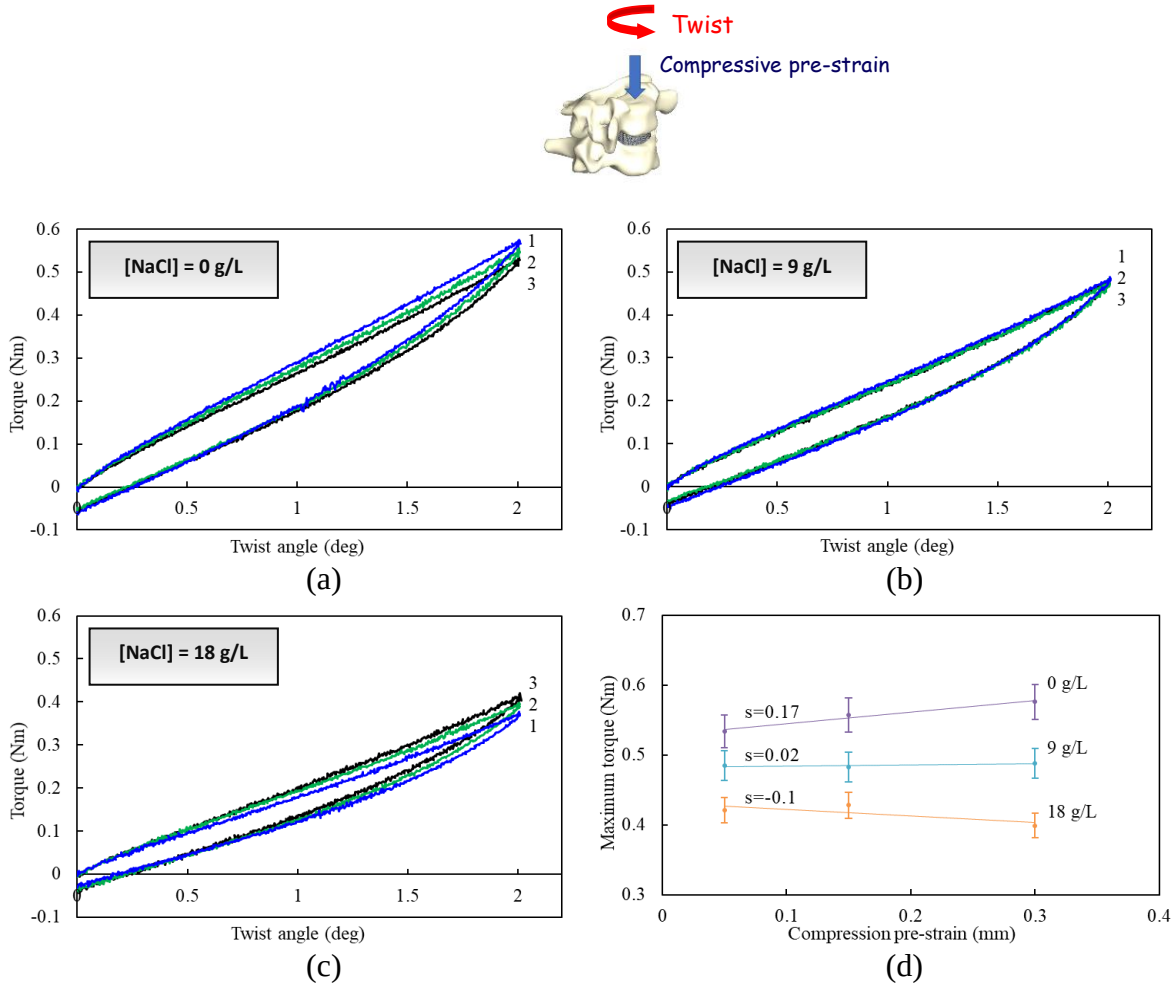

Figure 2.2.6. Compressive pre-strain level effect (1: 0.05 mm compression, 2: 0.15 mm compression, 3: 0.3 mm compression) on the torque-twist response for (a) 0 g/L, (b) 9 g/L, (c) 18 g/L NaCl concentration and (d) on the maximum torque.

In order to basically illustrate the fundamental role of the NP under compression, Figure 2.2.7 presents the kinematic fields obtained by digital image correlation of healthy and denucleated hemi-spine units of a same FSU, cutted in half and loaded in compression. The presence or not of the NP has no effect on the full-field axial displacement. By contrast, the full-field transversal displacement in specimen without NP is dramatically lower than that in specimen with NP. For the intact disc, the boundaries of the AF exhibit a radial movement away from the disc center. This configuration stimulates the AF role by stretching the collagen fibers. The removal of the NP changes the AF behavior under compression, and the transversal displacement tends to vanish.

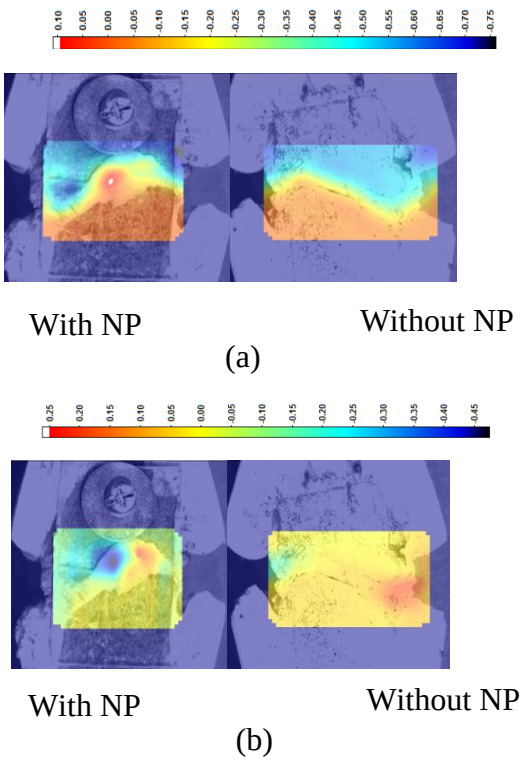

Figure 2.2.7. Full-field displacements in IVD with and without NP: (a) axial, (b) transversal.

2.2.3.4. Histological study

Figure 2.2.8 illustrates representative images of the NP and AF microstructure at different saline concentrations. A global view at these images shows that the concentration effect within the NP is better assessed using Saf-O staining whereas the concentration effect within the AF is better evaluated using H&E staining. Indeed, within the NP, the Saf-O staining shows differences in the staining intensity according to different concentrations. The staining intensity of specimens at 0 g/L and 36 g/L NaCl concentrations is, clearly, less explicit than that observed for the reference concentration. H&E stain gives a poor differentiation between the NP images at different concentrations. H&E stain exhibits a regular orientation of the annular lamella at the reference concentration. But, an evident irregular network of the AF collagen fibers at 0 g/L

can be noticed. By contrast, there is no evident disorganization of the AF collagen fibers at 36 g/L.

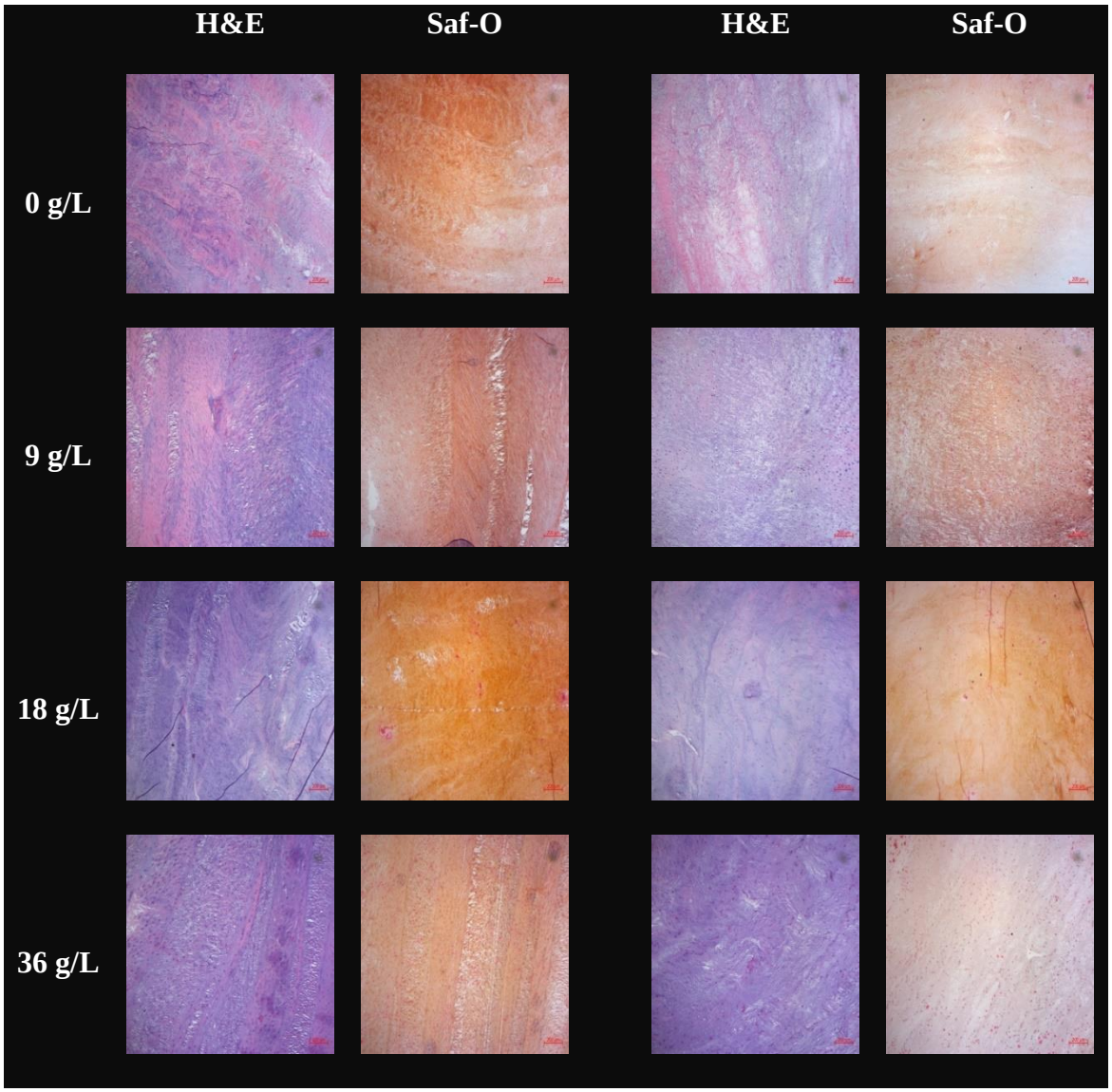

(a) (b)

Figure 2.2.8. Chemical sensitivity of the IVD microstructure: (a) AF, (b) NP.

2.2.4. Discussion

This study has been conducted to determine the effect of a tensile/compressive pre-strain on the chemical sensitivity of the FSU torsional response.

The inelastic effects are found much more preponderant under an axial loading than under a torsion loading indicating that the fluid-like behavior of the IVD is imperceptible in torsion.

With the addition of a compressive pre-strain, the torsional response becomes chemically sensitive in contrast to the application of a tensile pre-strain. The present results show qualitative trends about osmolarity effect promoted in pre-compressed FSUs illustrating the chemo-mechanical mechanisms. The reported experimental observations highlight very different FSU torsional responses vis-à-vis the chemical dependency under a tensile pre-strain and a compressive pre-strain. Figure 2.2.9 illustrates our interpretation of the inherent chemo-mechanical coupling by means of a schematic representation at different scales, i.e. FSU, IVD and microstructure. The negative fixed charge density increases with the pre-strain in compression. The flowed-out fluid leads to higher chemical imbalances, which explains the increase in chemical sensitivity.

The FSU chemo-mechanical response may be basically understood as a NP/AF interaction. The NP generates hydrostatic pressure on the AF under axial loading which is basically illustrated by our kinematic fields measurements in Figure 2.2.7. The respective role of the NP and AF depends on the pre-strain type and the pre-strain level. The NP has a higher active role at low pre-strain level. When the pre-strain level increases, the load is transferred radially from the NP to the AF which results in stiffening (Figures 2.2.5 and 2.2.6). The combination of a compressive pre-strain with the twisting (Figure 2.2.6) amplifies the tension of the AF collagen fibers, and leads to an increase in torsional stiffness and hysteresis area (Gardner-Morse and Stokes, 2003; Orias et al., 2009; Bezci et al., 2018). The compressive pre-strain diminishes the shear stress in the AF and gives more importance to the local tension due to the hydrostatic pressure in the NP. Figure 2.2.4d shows a change in the FSU mechanical response between a compressive pre-strain and a tensile pre-strain, which illustrates a change in the stress distribution shifting from a hydrostatic to a shear state. Changes in IVD height during small in-vivo vertebral rotations have been reported by Orias et al. (2016). They found that the twisting leads to a compression in the NP induced by the IVD morphology whereas the height changes

in AF are heterogeneous with a decrease in ventral part and an increase in dorsal part. These opposite changes may locally modulate the applied pre-strain.

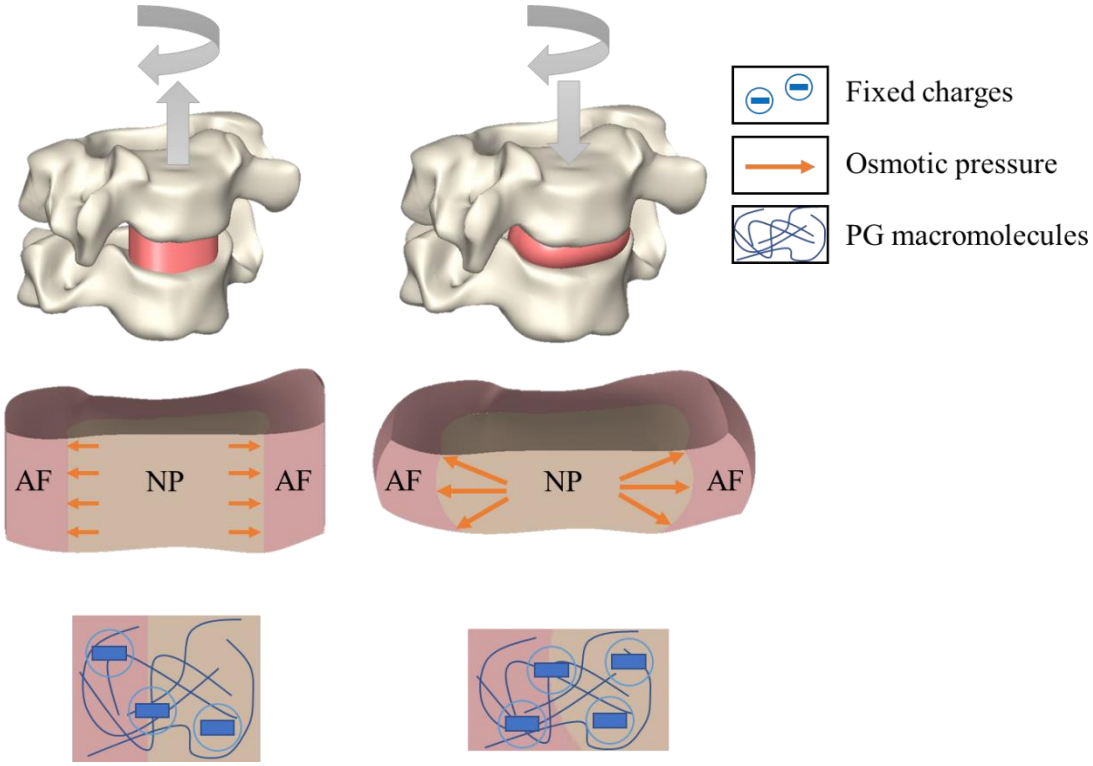

(a) (b)

Figure 2.2.9. Chemo-mechanical coupling in torsion with: (a) tensile pre-strain, (b) compressive pre-strain.

The staining intensity in Figure 2.2.8 is directly related to the PGs density contained in the biological tissue. Indeed, the PGs density, as indicated by the orange-red color intensity of the extracellular matrix, can be clearly assessed by the staining, especially at 0 g/L and 36 g/LNaCl concentrations. The decreased staining highlights significant structural changes in IVD with the chemical concentrations. The decline in PGs density in NP and AF is an indicator of degeneration and reduction in osmosis within the NP and AF leading to a change in the FSU mechanical response due to a reduction in fluid. In fact, biology and mechanics interact with each other in vivo. The mechanical stimulation of cells plays an important role on cellular

function and PGs biosynthesis. In the physiological range of stimuli, the collagen fibers and PGs biosynthesis is promoted. The compression level has a key role in biosynthesis and thus in the regulation of the amount of collagen fibers and the PGs density. Moderate compression levels increase the biosynthesis whereas high levels give rise to a catabolic response (Hee et al., 2010).

The NaCl concentration has a strong effect on the FSU chemo-mechanical response under compression loading. Indeed, the hydrostatic pressure applied by the NP on the AF is dependent on the chemical environment and the pre-strain type. The NP role is weak under pure torsion. By contrast, the AF collagen fibers have a preponderant role in the FSU torsional response due to their concentric organization with a ventral part and a dorsal part strained in reverse directions. As a consequence, the fluid flow contribution, due to the chemical coupling, on the inelastic phenomena is reduced. The contribution of the AF collagen fibers being preponderant under torsion, the osmolarity has thus no significant effect on the response. In hypo-osmotic conditions, both NP and AF swell in the aim to catch more ionic components in the environment. That results in an increase of the torsional stiffness. By contrast, the IVD area decreases in hyper-osmotic conditions which may explain the decrease in torque. The compressive pre-strain stimulates ionic transport by increasing the osmotic pressure leading to a stronger chemical effect on the mechanical response. Although its role in the literature is limited to a stress distributor during the physiological movements, the experimental observations reported in the present study point out that the NP contributes also to the management of the chemo-mechanical behavior by stimulating ionic transport. The change in fluid content is mainly observed in the NP under compression. That indicates that the chemo-mechanical coupling is mainly governed by the hydrostatic pressure in the NP. The dashpot role of the NP is mainly observed under compression. Indeed, the hysteresis loop exhibited by the FSU cyclic response under a compression loading is significantly higher than that observed

under a tension or a torsion loading (Figure 2.2.3). The NP/AF interaction depends on a minimal internal pressure thanks to the NP swelling. In-vivo, this effect exists for each physiological motion via the head and body weight. This natural compressive pre-strain on spine stimulates the AF role by stretching the collagen fibers thanks to the NP swelling. Indeed, our in-vitro experiments show that the NP, by opposing to the loading, amplifies the chemo-mechanical coupling under compression. In addition, the migration of the NP during the mechanical loading enhances the AF contribution by stretching the collagen fibers (Seroussi et al., 1989; Osti and Fraser, 1992; Balkovec and McGill, 2012; Kim et al., 2017).

The AF and its complex stratified composite structure is a misunderstanding issue for the complex physiological motions. As expected, our in-vitro experiments show that the AF concentric structure is preponderant in the FSU pure torsional response. The circumferential mechanical contribution of the AF collagen fibers minimizes the chemo-mechanical coupling. Combined with a compressive pre-strain, the ionic transport is stimulated resulting in a stronger chemical effect on the FSU torsional response. Indeed, the internal pressure governs the IVD chemo-mechanical response by favoring the chemical exchanges. The osmotic gradient between the NP and the fluid surrounding the IVD is due to the PGs negative charges which attract positive ions into the NP, the so-called Gibbs-Donnan effect (Urban et al., 1979). Under compression, the fluid is pushed out of the IVD which increases the PGs density, and thereby the osmotic pressure in the IVD. The changes in mechanical behavior, induced by the fluid content variation, are a consequence of the chemo-mechanical interaction. The active function of the NP in the chemo-mechanical coupling is pointed out by increasing the osmolarity with a compressive pre-strain. Ionic transport is stimulated by the osmotic pressure leading to a stronger chemical effect on the mechanical response. With a compression within physiological range, the fluid content in IVD decreases and the chemical unbalance increases. In reaction, the IVD swells to reach the chemo-mechanical equilibrium and the fluid content in IVD increases.

In vivo, the reduction in fluid content in the IVD decreases the PGs synthesis, and thereby the osmotic pressure, which leads to a higher reduction in fluid content in the IVD; that is the vicious loop of the IVD degeneration (Vergroesen et al., 2015).

2.2.5. References

Adams, M.A., Bogduk, N., Burton, A.K., Dolan, P., 2012. The Biomechanics of Back Pain. Churchill Livingstone.

Adams, M.A., Dolan, P., Hutton, W.C., 1987. Diurnal variations in the stresses on the lumbar spine. Spine 12, 130-137.

Adams, M.A., Hutton, W.C., 1981. The relevance of torsion to the mechanical derangement of the lumbar spine. Spine 6, 241-248.

Alini, M., Eisenstein, S.M., Ito, K., Little, C., Kettler, A.A., Masuda, K., Melrose, J., Ralphs J., Stokes, I., Wilke, H.J., 2008. Are animal models useful for studying human disc disorders/degeneration? European Spine Journal 17, 2-19.

Anderst, W.J., Donaldson, W.F., Lee, J.Y., Kang, J.D., 2015. Cervical motion segment contributions to head motion during flexion\extension, lateral bending, and axial rotation. The Spine Journal 15, 2538-2543.

Balkovec, C., McGill, S., 2012. Extent of nucleus pulposus migration in the annulus of porcine intervertebral discs exposed to cyclic flexion only versus cyclic flexion and extension. Clinical Biomechanics 27, 766-770.

Barbir, A., Godburn, K.E., Michalek, A.J., Lai, A., Monsey, R.D., Iatridis, J.C., 2011. Effects of torsion on intervertebral disc gene expression and biomechanics, using a rat tail model. Spine 36, 607-614.

Bass, E., Duncan, N., Hariharan, J., 1997. Frozen storage affects the compression creep behavior of the porcine intervertebral disc. Spine 22, 2867-2876.

Bezci, S.E., Klineberg, E.O., O'Connell, G.D., 2018. Effects of axial compression and rotation angle on torsional mechanical properties of bovine caudal discs," Journal of the Mechanical Behavior of Biomedical Materials 77, 353-359.

Bezci, S.E., Nandy, A., O'Connell, G.D., 2015. Effect of hydration on healthy intervertebral disk mechanical stiffness. Journal of Biomechanical Engineering 137, 101007.

Callaghan, J.P., McGill, S.M., 1995. Frozen storage increases the ultimate compression load of porcine vertebrae. Journal of Orthopaedic Research 13, 809-812.

Cassidy, J.J., Hiltner, A., Baer, E., 1989. Hierarchical structure of the intervertebral disc. Journal Connective Tissue Research 23, 75-88.

Costi, J.J., Stokes, I.A., Gardner-Morse, M., Laible, J.P., Scoffone, H.M., Iatridis, J.C., 2007. Direct measurement of intervertebral disc maximum shear strain in six degrees of freedom: motions that place disc tissue at risk injury. Journal of Biomechanics 40, 2457-2466.

Costi, J.J., Hearn, T.C., Fazzalari, N.L., 2002. The effect of hydration on the stiffness of intervertebral discs in an ovine model. Clinical Biomechanics 17, 446-455.

Drost, M.R., Willems, P., Snijders, H., Huyghe, J.M., Janssen, J.D., Huson, A., 1995. Confined compression of canine annulus fibrosus under chemical and mechanical loading. Journal of Biomechanical Engineering 117, 390-396.

Emanuel, K., Vergroesen, P.P.A., Peeters, M., Holewijn, R.M., Kingma, I., Smit, T.H., 2015. Poroelastic behaviour of the degenerating human intervertebral disc: a ten-day study in a loaded disc culture system. European Cells and Materials 29, 330-341.
Farfan, H.F., 1984. The torsional injury of the lumbar spine. Spine 9, 53-53.
Ferguson, S.J., Ito, K., Nolte, L.P., 2004. Fluid flow and convective transport of solutes within the intervertebral disc. Journal of Biomechanics 37, 213-221.
Gardner-Morse, M.G., Stokes, I.A., 2003. Physiological axial compression preloads increase motion segment stiffness, linearity and hysteresis in all six degrees of freedom for small displacements about the neutral posture. Journal of Orthopaedic Research 21, 547-552.
Garges, K.J., Nourbakhsh, A., Morris, R., Yang, J., Mody, M., Patterson, R., 2008. A comparison of the torsional stiffness of the lumbar spine in flexion and extension. Journal of Manipulative and Physiological Therapeutics 31, 563-569.
Goins, M.L., Wimberley, D.W., Yuan, P.S., Fitzhenry, L.N., Vaccaro, A.R., 2005. Nucleus pulposus replacement: an emerging technology. The Spine Journal 5, 317-324.
Grunhagen, T. Wilde, G., Soukane, D.M., Shirazi-Adl, S.A., Urban, J.P., 2006. Nutrient supply and intervertebral disc metabolism. The Journal of Bone and Joint Surgery 88, 30-35.
Hee, H.T., Zhang, J., Wong, H.K., 2010. An in vitro study of dynamic cyclic compression stress on human inner annulus fibrosus and nucleus pulposus cells. The Spine Journal 10, 795-801.
Janevic, J., Ashton-Miller, J.A., Schultz, A.B., 1991. Large compression preloads decrease lumbar motion segment flexibility. Journal of Orthopaedic Research 9, 228-236.
Kim, Y.H., Kim S.I., Park, S., Hong, S.H., Chung, S.G., 2017. Effects of cervical extension on deformation of intervertebral disk and migration of nucleus pulposus. Physical Medicine and Rehabilitation 9, 329-338.
Lotters, F., Burdorf, A., Kuiper, J., Miedema, H., 2003. Model for the work-relatedness of low-back pain. Scandinavian Journal of Work, Environment and Health 29, 431-440.
Marchand, F., Ahmed, A.M., 1990. Investigation of the laminate structure of lumbar disc anulus fibrosus. Spine 15, 402-410.
Mortazavi, J., Zebardast, J., Mirzashahi, B., 2015. Low back pain in athletes. Asian Journal of Sports Medicine 6, e24718.
Nachemson, A., Morris, J.M., 1964. In vivo measurements of intradiscal pressure: discometry, a method for the determination of pressure in the lower lumbar discs. The Journal of Bone and Joint Surgery 46, 1077-1092.
Newell, N., Little, J.P., Christou, A., Adams, M.A., Adam, C.J., Masouros, S.D., 2017. Biomechanics of the human intervertebral disc: a review of testing techniques and results. Journal of the Mechanical Behavior of Biomedical Materials 69, 420-434.
Orias, A.E.E., Mammoser, N.M., Triano, J.J., An, H.S., Andersson, G.B.J., Inoue, N., 2016. Effects of axial torsion on disc height distribution: an in vivo study. Journal of Manipulative and Physiological Therapeutics 39, 294-303.
Orias, A.E.E., Malhotra, N.R., Elliott, D.M., 2009. Rat disc torsional mechanics: effect of lumbar and caudal levels and axial compression load. The Spine Journal 9, 204-209.
Osti, O.L., Fraser, R.D., 1992. MRI and discography of annular tears and intervertebral disc degeneration: a prospective clinical comparison. The Journal of Bone and Joint Surgery 74, 431-435.
Schmidt, H., Shirazi-Adl, A., Schilling, C., Dreischarf, M., 2016. Preload substantially influences the intervertebral disc stiffness in loading-unloading cycles of compression. Journal of Biomechanics 49, 1926-1932.
Seroussi, R.E., Krag, M.H., Muller, D.L., Pope, M.H., 1989. Internal deformations of intact and denucleated human lumbar discs subjected to compression, flexion, and extension loads. Journal of Orthopaedic Research 7, 122-131.

Smeathers, J.E., Joanes, D.N., 1988. Dynamic compression properties of human lumbar intervertebral joints: a comparison between fresh and thawed specimens. Journal of Biomechanics 21, 425-433.

Ulaska, J., Visuri, T., Pulkkinen, P., Pekkarinen, H., 2001. Impact of chronic low back pain on military service. Military Medicine 166, 607-611.

Urban, J.P., McMullin, J.F., 1985. Swelling pressure of the intervertebral disc: influence of proteoglycan and collagen contents. Biorheology 22, 145-157.

Urban, J.P.G., Maroudas, A., Bayliss, M.T., Dillon, J., 1979. Swelling pressures of proteoglycans at the concentrations found in cartilaginous tissues. Biorheology 16, 447-464.

Vos, T., Allen, C., Arora, M., Barber, R.M., Bhutta, Z.A., Brown, A., et al., 2016. Global, regional, and national incidence, prevalence, and years lived with disability for 310 diseases and injuries, 1990-2015: a systematic analysis for the Global Burden of Disease Study 2015. Lancet 388, 1545-1602.

Veres, S.P., Robertson, P.A., Broom, N.D., 2010. The influence of torsion on disc herniation when combined with flexion. European Spine Journal 19, 1468-1478.

Vergroesen, P.P.A., Kingma, I., Emanuel, K.S., Hoogendoorn, R.J.W., Welting, T.J., van Royen, B.J., van Dieen, J.H., Smit, T.H., 2015. Mechanics and biology in intervertebral disc degeneration: a vicious circle. Osteoarthritis and Cartilage 23, 1057-1070.

Walter, B.A., Torre, O.M., Laudier, D., Naidich, T.P., Hecht, A.C., Iatridis, J.C., 2015. Form and function of the intervertebral disc in health and disease: a morphological and stain comparison study. Journal of Anatomy 227, 707-716.

Wilke, H. J., Neef, P., Caimi, M., Hoogland, T., Claes, L.E., 1999. New in vivo measurements of pressures in the intervertebral disc in daily life. Spine 24, 755-762.

Chapter 2: Experimental characterization

Part 3: Osmo-inelastic response of the annulus fibrosus[3]

Abstract

The aim of this part of the Chapter 2 is to provide some insights on the osmo-inelastic response of annulus fibrosus (AF) under stretching. AF specimens of rectangular cross-section, extracted from different regions of bovine cervical discs, were tested under different strain-rates and saline concentrations within the normal range of strains. An accurate optical strain measuring technique, based upon digital image correlation, was developed in order to determine the full-field displacements in the lamellae and fibers planes of the layered reinforced soft tissue. The AF mechanical response is found hysteretic, rate-dependent and osmolarity-dependent with a Poisson's ratio higher than 0.5 in the fibers plan and negative (auxeticity) in the lamellae plan. Analysis of variance shows that the strain-rate, osmolarity and regional effects are statistically significant ($p<0.05$). While the stiffness presents a regional-dependency due to variations in collagen fibers content/orientation, the rate-sensitivity of the response is found independent on the region. A significant osmotic effect is found on both the auxetic response and the rate-sensitivity. These local observations allowed identifying the extracellular matrix rearrangements and the inter-lamellae fluid exchanges as the main sources of the osmo-inelastic coupling.

Keywords: Annulus fibrosus; Digital image correlation; Osmo-inelastic coupling; Poisson's ratio; Auxetic.

[3] This Part of this chapter is based on the following paper: Amil Derrouiche, Fahmi Zaïri, Fahed Zaïri, Osmo-inelastic response of the annulus fibrosus, *submitted*.

2.3.1. Partial introduction

As an essential element of the intervertebral disc (IVD), the annulus fibrosus (AF) is a very complex medium, able to resist at high stresses induced by the spine movements. This capacity was studied since several years but it is still largely misunderstood (Newell et al., 2017). The AF is a fiber-reinforced tissue organized by concentric lamellae around nucleus pulposus. Its mechanical response exhibits complex inelastic effects manifested by a hysteresis during cyclic loading and a rate-dependency (Race et al., 2000; Holzapfel et al., 2005; Kemper et al., 2007; Ambard and Cherblanc, 2009; Newell et al., 2016, 2017; Tavakoli and Costi, 2018). Both anisotropy and regional-dependency of the mechanical response (Skaggs et al., 1994; Ebara et al., 1996; Holzapfel et al., 2005; Michalek et al., 2009) are essentially due to the circumferential and radial variation in content and orientation of collagen fibers (Inoue and Takeda, 1975; Eyre, 1979; Guerin and Elliott, 2006). The collagen has a high tensile stiffness compared to the extracellular matrix and constitutes the reinforcement of the soft tissue; its layered graded repartition in AF permits to contain the nucleus swelling which in turn exposes AF to tensile stresses in the circumferential direction under flexion/extension or lateral bending movements (Nachemson and Morris, 1964).

Understanding the AF mechanical response is of prime importance in the aim to bring a more accurate multi-scale understanding of the IVD function. Due to its complex microstructure organization, the size of the AF specimen (i.e. single or multiple lamellae) and the zone of interest inside IVD are important issues for the determination of the AF mechanical response. Some authors examined the mechanical response of a single lamella with circumferential cut inside IVD (Ebara et al., 1996; Holzapfel et al., 2005; Michalek et al., 2009) whereas others considered AF as a stratified medium with transversal cut inside IVD (Michalek et al., 2009; Adam et al., 2015; Mengoni et al., 2015; Tavakoli and Costi, 2018). Although the information brought by the mechanical response of a single lamella is fruitful to understand the mechanics

of IVD, the dependence on the surrounding chemical environment may be only understood at the stratified scale, essentially due to the active role of inter-lamellae interactions in the fluid transfers. The extracellular matrix rearrangements and the collagen fibers-matrix interactions have certainly a strong impact on the inelastic effects due to the active role of proteoglycans (PGs) and fibers via the viscous sliding. Although remaining imprecisely understood to date, the fluid-matrix interactions have also a strong impact on the inelastic effects. Indeed, the negatively charged extracellular matrix interacts by osmotic effect with the liquid phase composed of water, mobile charges and small proteins (Newell et al., 2017). The underlying coupling depends on the chemical state of the IVD (Emanuel et al., 2018) with variations in fluid content inside extracellular matrix and modifications in chemical equilibrium (Drost et al., 1995; Costi et al., 2002; Huyghe and Drost, 2004; Bezci et al., 2015). Although inelastic and osmotic effects in IVD usually appear together, the coupling between both effects is rarely studied (Newell et al., 2017; Emanuel et al., 2018; Vergroesen et al., 2018). The evaluation of the intrinsic mechanics of AF multiple lamellae in relation with the surrounding chemical environment should bring precious information on the implication of PGs/collagen fibers as well as inter-lamellae interactions on the coupling between osmotic and inelastic effects.

The main purpose of this part of the Chapter 2 is to bring a better understanding of the osmo-inelastic coupling in the AF tensile response. The full-field displacements are determined simultaneously in the lamellae plane (LP) and in the fibers plane (FP) using an optical strain measuring technique based upon digital image correlation (DIC) on AF specimens of rectangular cross-section. The response is carefully evaluated only in relation to the microstructure, the biochemical environment and the mechanical loading conditions by considering, respectively, different locations in AF, osmolarity conditions and strain-rates. By this way, the "intrinsic" osmo-inelastic response of AF is obtained. The experimental

observations, related to both the intrinsic response and the local transversal strains, provide valuable insights into the underlying physical mechanisms of the osmo-inelastic coupling.

2.3.2. Materials and methods

2.3.2.1. Specimen preparation

Cervical hemi-spines were harvested from three bovine cadavers obtained from a local abattoir. Bovine was selected in reason of its size that facilitates specimen preparation and local strain measurements. The fifteen IVDs extracted within two days after death were first separated from the adjacent vertebral bodies by hand using a surgical tool. Immediately after excision, IVDs were immerged in a distilled water bath with a saline concentration closes to physiological fluid of 9 g/L during 100 minutes. This time was necessary to re-establish chemical and hydration equilibrium (Costi et al., 2002).

The specimen preparation procedure is illustrated in Figure 2.3.1. The regional variation was examined according to well-documented variations of content and orientation in collagen fibers (Inoue and Takeda, 1975; Eyre, 1979; Guerin and Elliott, 2006). Rectangular circumferentially-oriented specimens with a regular cross-section were isolated from ventro-lateral and dorso-lateral regions of AF. The specimens were circumferentially extracted in the aim to stretch them in this direction and to reproduce the compression mechanics of IVD. The tissue blocks of approximately $25 \times 10 \times 10$ mm^3 were divided into two parts: inner and outer. According to the location in the IVD, the AF specimens are designated as VI (ventro-inner), VO (ventro-outer) and DI (dorso-inner). The outer part of the dorsal region did not allow extracting usable specimens. The extracted specimens were stored at 4°C at maximum two days before testing. Fresh specimens were used to avoid any storage effects in terms of temperature and duration.

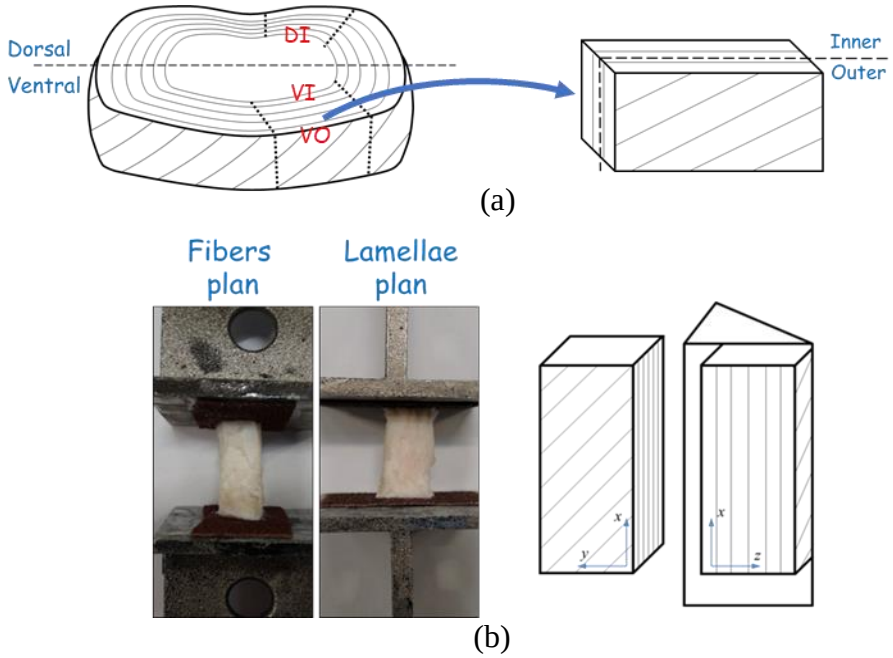

Figure 2.3.1. Preparation of AF specimens: (a) extraction from different locations in IVD, VO: Ventro-Outer,VI: Ventro-Inner, DI: Dorso-Inner, (b)specimen glued to two metal plates for the placement in the testing machine with simultaneous local displacement measurements in fibers plan (xy) and in lamellae plan (xz) using a right angle prism.

The softness of AF specimens leads to gripping difficulties. Keeping bone is a solution (Holzapfel et al., 2005) but limited by bone brittleness and potential bone failure during cutting and grips pressure. The AF specimens may be also glued with cyanoacrylate to grips (Bruehlmann et al., 2004; O'Connell et al., 2011; Baldit et al., 2013), the cyanoacrylate stiffness being much higher than the AF stiffness (15-25 MPa) and its influence may be neglected. Here, the AF specimens were glued at metal plates using cyanoacrylate and then immerged in a 9 g/L saline solution during 100 minutes to reach equilibrium swelling and to cancel all residual stresses due to specimen preparation.

2.3.2.2. Methods

2.3.2.2.1. Mechanical tests

The mechanical tests were carried out on an electro-pulse mechanical machine (Instron-5500) equipped with 1 kN load cell. A displacement-control function was imposed, load and cross-

head displacement versus time being recorded during the tests. The displacement imposed to the specimen is related to a given axial strain, i.e. circumferential strain imposed to the IVD part (Figure 2.3.1). Loading-unloading tensile tests were performed at different axial strain-rates and at room temperature. The AF specimens were stretched up to a prescribed stretch at a certain axial strain-rate and unloaded down to its initial position at the same absolute strain-rate.

The results reported in this investigation follow the experimental procedure illustrated in Figure 2.3.2. Before testing, the AF specimens were preconditioned by 10 cycles of 1% axial strain at a rate of $10^{-3}\,s^{-1}$ in order to chemically equilibrate the tissue by favoring fluid transfers. In order to remove the Mullins effect and to verify the specimen adherence with the metal plates, the specimens were stretched to a 7% axial strain at a rate of $10^{-3}\,s^{-1}$. Preliminary tests have showed the importance of the preload and the specimens were carefully preloaded at 0.1 N before testing.

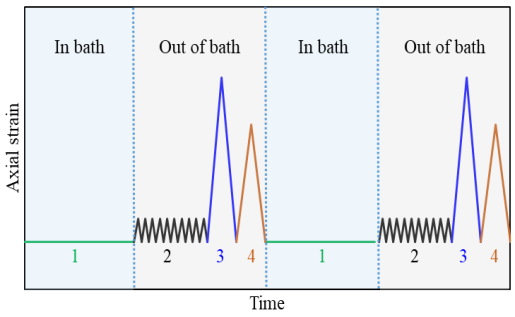

Figure 2.3.2. Experimental design for two successives loading-unloading tensile tests (1: mechanical rest, 2: succesive low-strain tensions, 3: Mullins effect removing, 4: loading-unloading test).

In order to examine the location effect, the experiments were performed on VI, VO and DI specimens extracted from the same IVD. The axial strain was limited to a maximum value of 5%. This value is consistent with physiological loads (Stokes and Greenapple, 1985) and micro-alteration risks are limited. For severe conditions in terms of either strain level or cyclic number,the recovery is not ensured (Green et al., 1993; Iatridis et al., 2005; Andarawis-Puri et

al., 2012; Qasim et al., 2014), but only recoverable mechanisms are expected at this strain level (Johannessen et al., 2004). The strain-rate sensibility was investigated by applying successively the following axial strain-rates: 10^{-4} s^{-1}, 10^{-3} s^{-1} and 10^{-2} s^{-1}. After each constant strain-rate test, the same AF specimen was removed from the test device and immerged on a NaCl solution during 100 minutes to dissipate residual stresses and to get back chemical equilibrium. The osmolarity was controlled by varying the NaCl content in water from 9 g/L iso-osmotic solution to 36 g/L hyper-osmotic solution. These variations in osmolarity permit to simulate the inhomogeneous repartition of mobile ions in IVD during the spine movements.

2.3.2.2.2. Statistical analysis

Statistical analysis was carried out to determine standard deviation and error bars on the load value at a 95% confidence. The data presented in each figure in the results section represent the mechanical response of one AF specimen. A p-value < 0.05 was considered to be statistically significant. One-way analysis of variance (ANOVA), performed on fifteen AF specimens stretched at the same loading rate and the same NaCl concentration, indicates a standard deviation of 6.83% with a p-value of 0.0084. A two-way ANOVA without replication is then performed to other AF specimens (n=6) in order to indicate the statistical significance of the regional-dependence, the osmolarity effect and the strain-rate effect. Although the present study is based on a relatively small number of specimens (n=21), the goal is to provide qualitative trends of the chemo-mechanical response in relation to the microstructure, the biochemical environment and the mechanical loading conditions.

2.3.2.2.3. Full-field strain measurements

The displacement fields were computed using the DIC method consisting to compare a deformed image with that of the initial state in order to extract the relative local displacements.

This noninvasive method permits evaluation of behavior without external disturbance and allows capturing the heterogeneous features of soft tissues (Michalek et al., 2009; Baldit et al., 2013; Vergari et al., 2016) while relating them with the macro-behavior. Since early the 1970s (Anuta, 1970), DIC was improved with advances of computer capability and digital cameras. A sequence of images is captured and discretized into small subsets of N×N pixels. Gray level values are then measured for each subset of the undeformed image and looked for in the deformed image to determine relative local displacements. The gray levels of a subset in the reference and deformed configurations, G_1 and G_2, respectively, are given by:

$$G_1(x,y) = G_2(x+u, y+v) \tag{1}$$

in which u and v are the displacement components of the subset center, optimized by minimizing the normalized cross-correlation coefficient r defined by:

$$r = \frac{\sum_{i=1}^{n}\sum_{j=1}^{n} G_1(x_i,y_j)\,G_2(x_i+u, y_j+v)}{\sum_{i=1}^{n}\sum_{j=1}^{n}\sqrt{G_1^2(x_i,y_j)}\sqrt{G_2^2(x_i+u,y_j+v)}} \tag{2}$$

With this finite element-based approach of DIC, displacement field is computed for each subset with keeping continuity between adjacent subsets. This method provides more robust measurements with complex displacement fields (Hild and Roux, 2012).

The local displacement gradient tensor $\mathbf{H}$ is defined by:

$$\mathbf{H} = \begin{pmatrix} \frac{\partial u}{\partial x} & \frac{\partial u}{\partial y} \\ \frac{\partial v}{\partial x} & \frac{\partial v}{\partial y} \end{pmatrix} \tag{3}$$

Then the local Green-Lagrange strain tensor $\mathbf{E}$ is given by:

$$\mathbf{E} = \frac{1}{2}\left(\mathbf{F}\mathbf{F}^T - \mathbf{I}\right) \tag{4}$$

in which $\mathbf{I}$ is the identity tensor and $\mathbf{F} = \mathbf{H} + \mathbf{I}$ is the local deformation gradient tensor.

Images were recorded during experiments by means of a CCD camera Imager E-lite 2M (LaVision GmbH) at a frequency of 3 Hz with resolution of 290 pixels/mm and size of 1628 × 1236 pixels. Images were analyzed with Davis Software 8.0 (StrainMaster, LaVision GmbH). Area of interest was chosen in the central part of the specimen to avoid unlikely cyanoacrylate effect. It was divided into small square subsets in which the displacement vector was determined. The real-time strain field was captured in FP and LP using a right angle prism as schematically shown in Figure 2.3.1. A similar method was previously employed by Roux et al. (2003) and Parsons et al. (2004) for other media. The CCD camera directly captures the front view of the AF specimen corresponding to FP, i.e. plan xy. Through the prism, the CCD camera simultaneously records LP, i.e. xz. The axial stress σ_{xx} is then deduced from the transversal stretches, λ_{yy} and λ_{zz}:

$$\sigma_{xx} = \frac{F}{S_0 \lambda_{yy} \lambda_{zz}} \tag{5}$$

in which F is the actual load and S_0 is the initial cross-section.

The AF tissue being a light medium with a poor natural contrast, DIC requires image processing (Guerin and Elliott, 2006; Baldit et al., 2013) or surface treatment in order to be suitable for measurements. Pins, inserted into the specimen, were also employed (Wagner and Lotz, 2004) but may potentially impact specimen integrity. In this investigation, different surface treatments were tested, and some of them are presented in Figure 2.3.3. Highly contrasted images with adequate surface treatment lead to correlation without images treatment, and ensure no local information loss. Both sides of the AF specimen received different treatments suitable for measurements. A first surface treatment consists to apply directly on the surface specimen a random speckle pattern with airbrush filled with a waterproof black paint (Figure 2.3.3a). It was assured that the speckles were non-overlapped, identical and as small as possible to optimize the spatial resolution. In a second surface treatment, a thin white coat of paint, able to follow

the imposed deformation without breaking is previously applied using an airbrush and the random speckle pattern is then applied with airbrush filled with a waterproof black paint (Figure 2.3.3b). In a third surface treatment, methylene blue was used to enhance the natural contrast (Figure 2.3.3c).

(a) (b) (c)

Figure 2.3.3. Different surface treatments for DIC measurements: random speckle pattern (a) on a natural surface, (b) on a thin white coat of paint, (c) methylene blue.

The surface treatment used for the full-field strain measurements may potentially affect the load. Figure 2.3.4 shows the effect of different surface treatments on the same specimen for successive quasi-static tests after pre-conditioning. The figure shows no significant effect on the overall mechanical response in terms of load-displacement curve. This result also assesses the pre-conditioning in which the mechanical and structural features of the AF specimen remain intact.

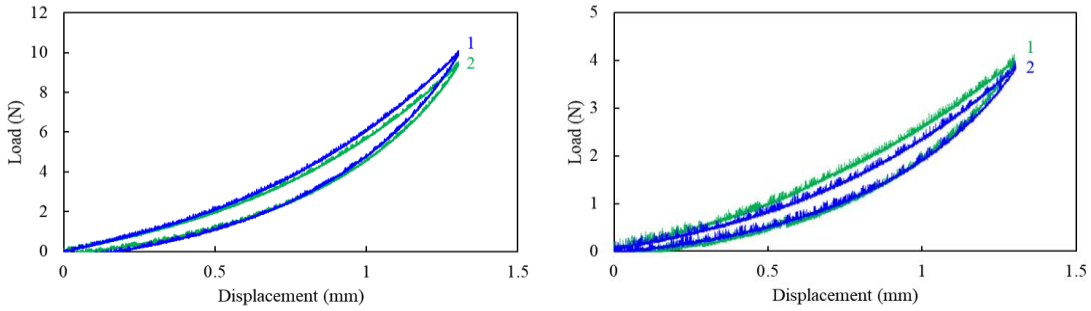

(a) (b)

Figure 2.3.4. Effect of the surface treatment on the AF load-displacement response: (a) effect of the thin white coat of paint (1: with, 2: without), (b) effect of the methylene blue (1: with, 2: without).

2.3.3. Results

2.3.3.1. Local strains

2.3.3.1.1. Error

The optical strain measuring technique introduces two main sources of error. The first one is due to data acquisition, especially the error coming from the surface treatment. Table 2.3.1 provides typical errors, on the local axial and transversal strains, obtained by imposing a rigid body move to the AF specimen, griped at one side and free at the other one. The root mean square error (RMSE) is calculated from the following formula:

$$\mathrm{RMSE} = \sqrt{\frac{1}{2}\left(E_{xx}^2 + E_{yy}^2\right)} \tag{6}$$

in which E_{xx} and E_{yy} are the maximal axial and transversal strains obtained during a rigid body move to the AF specimen.

The error is reasonable for the three surface treatments and the random speckle pattern without white coat of pain was used for practical reasons. The second source of error is due to image correlation procedure itself. Indeed, the noise decreases with the subset size increase, but too large subset sizes lead to loss of local displacements (Parsons et al., 2004). A sensibility study was performed to find an optimal subset size.

Surface treatment	Maximum strains (%)	RMSE (%)
Random speckle pattern on a natural surface	E_{yy} = 0.0185 E_{xx} = -0.193	9.7
Random speckle pattern on a thin white coat of paint	E_{yy} = 0.08 E_{xx} = -0.12	7.2
Methylene blue	E_{yy} = 0.063 E_{xx} = -0.045	3.9

Table 2.3.1. Maximum strains measured in FP under rigid body move and RMSE for different surface treatments.

Figure 2.3.5 presents the strains as a function of time with subset size variation. Correlation windows size is also a key DIC parameter, with larger region of interest, more subsets are followed and with continuity between two neighborhood subsets, false detection probability decreases. In order to avoid glue effect and stress concentration near bounds of the specimen, the region of interest corresponds to 75% of the total specimen with a subset size of 48×48 pixels to reduce noise.

The focal distance in LP being modified due to the use of the prism, it generates randomly distributed noises coming from optical errors which may be reduced by a filtering process. Out-of-plane displacements due to cross-section variation are a systematic source of error, but may be considered not significant under small imposed displacements.

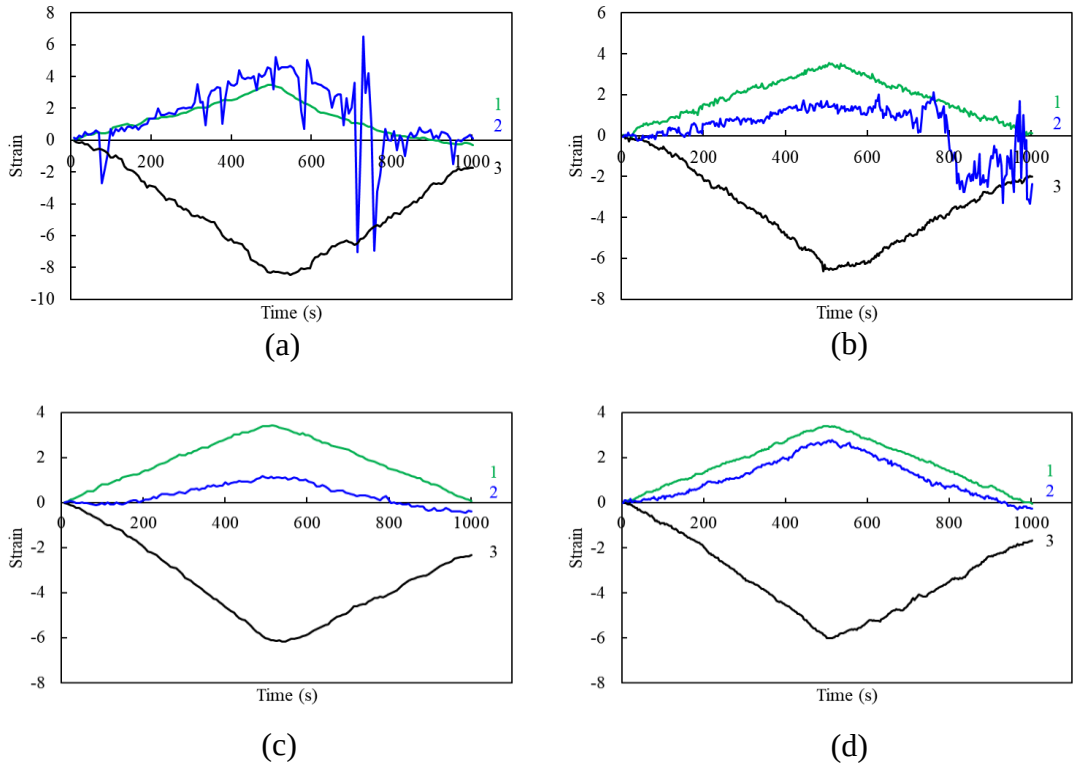

Figure 2.3.5. Strains as a function of time,during a loading-unloading tensile test,for different DIC calculations performed on the same images of 25×9 mm^2 in size: (a) region of interest of 11×3 mm^2 and subsets of 24×24 pixels, (b) region of interest of 24×7 mm^2 and subsets of 24×24 pixels, (c) region of interest of 24×7 mm^2 and subsets of 48×48 pixels, (d) region of interest of 24×7 mm^2 and subsets of 96×96 pixels (1: E_{xx}, 2: E_{zz}, 3: E_{yy} in %).

2.3.3.1.2. Full-field strain contours

The heterogeneity in local strain fields is mainly due to the complex IVD microstructure, consisting in a stratified arrangement of collagen fibers, and by the coupling with the chemical effect during the mechanical loading. As an illustrative example, Figure 6 provides full-field strains in the two plans. Highly localized axial strains in FP are extended along the fiber axis. Despite heterogeneity, the mean axial strain is consistent with the applied macroscopic strain; for 5% applied macroscopic strain, the local axial strains are ranged from 0% to 10%, but the mean value is about 5%. Concerning the transversal strains, an "ordinary" specimen shrinkage in the FP transversal direction leads to negative values.

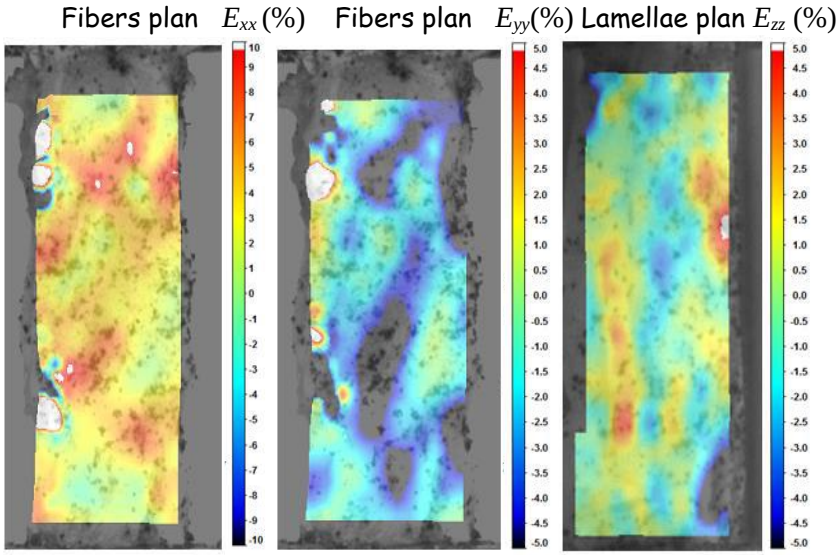

Figure 2.3.6. Full-field strains at 5% applied macroscopic strain.

The mean value of the FP transversal strain is reported in Figure 2.3.7 and shows no significant osmolarity effect. In LP, highly localized transversal strains are extended along the lamellae axis with alternate positive and negative values. The mean value given in Figure 2.3.7 is interestingly positive. Measurements performed directly on LP without prism also confirm these findings. The positivity in LP transversal strains was also evidenced by Baldit et al. (2013) in AF tissues. It can be further observed in Figure 2.3.7 that the LP transversal strain is clearly

dependent on the salt concentration. The higher the NaCl concentration, the smaller the LP transversal strain.

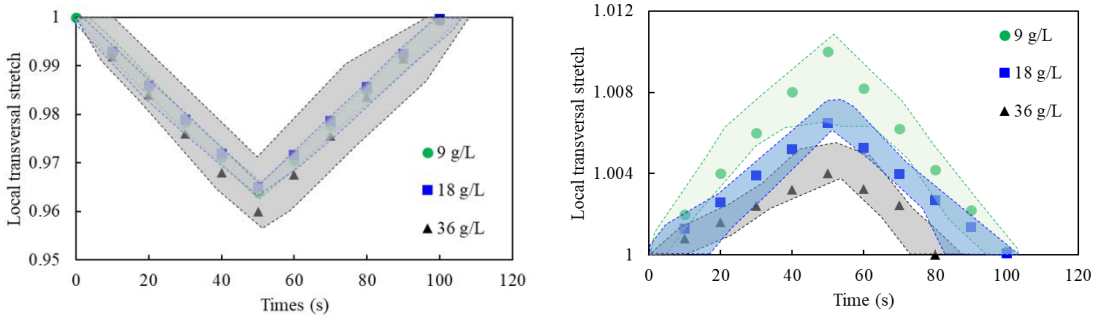

(a) (b)

Figure 2.3.7. Osmolarity effect on the local transversal stretches: (a) FP, (b) LP.

2.3.3.2. Stress-stretch response

The mechanical response of AF is basically defined by the stress-stretch relationship. In order to illustrate the regional variation effect, Figure 2.3.8 presents the VO, VI, and DI stress-stretch responses with a 9 g/L NaCl concentration, considered as the reference configuration of the physiological solution. The regional and strain-rate effects on the response are statistically significant with a p-value of 0.0012 and lesser than 0.001, respectively. The mechanical stiffness is strongly dependent on the distance between the specimen and the nucleus. The stiffening tends to be more important in moving away from the nucleus since the fiber content is greater in the IVD outer part. The elastic stiffness E was calculated from the stress-stretch curves using a simple incompressible isotropic neo-Hookean elastic relationship:

$$\sigma_{xx} = \frac{E}{3}\left(\lambda_{xx}^2 - \frac{1}{\lambda_{xx}}\right) \tag{7}$$

The obtained results are reported in Table 2.3.2. Although the obtained stiffness is in consistence with those reported in the open literature in Table 2.3.3, inter-species differences demand critical analysis (Alini et al., 2008). The regional variation allows establishing the relationship between the AF elastic stiffness and the microstructure. At a fixed strain-rate, by

comparing the outer and inner parts, it is evidenced the content effect of collagen fibers, and by comparing the dorsal and ventral parts, it is evidenced the orientation effect of collagen fibers.

Strain-rate (s^{-1})	Elastic stiffness *E* (MPa) VO	Elastic stiffness *E* (MPa) VI	Elastic stiffness *E* (MPa) DI
10^{-4}	2.78±0.46	0.75±0.12	0.54±0.09
10^{-3}	3.17±0.52	1.01±0.17	0.97±0.16
10^{-2}	3.36±0.56	1.26±0.21	1.21±0.2

Table 2.3.2. Regional effect on the elastic stiffness for a 9 g/L NaCl concentration.

References	Species	Localization	Elastic stiffness *E* (MPa)	Poisson's ratio *v*
Baldit et al.(2013)	Porcine			0.8-1.1
Baldit et al.(2013)	Human			0.5-1.5
O'Connell et al. (2012)	Human	Lumbar	21	2.06
Singha and Singha(2012)	Human	Lumbar	0.88	0.5
O'Connell et al. (2009)	Human	Lumbar	2.7-20.9	2.27
Lewis et al. (2008)	Rabbit	Lumbar	0.66-1.08	0.33-0.47
Guerin and Elliott (2006)	Human	Lumbar	2.5-29.3	4.64
Holzapfel et al. (2005)	Human	Lumbar	3.8-77.6	
Bass et al. (2004)	Human	Lumbar	15.7	
Elliott and Setton (2001)	Human	Lumbar	1.7-2.52	1.8
Ebara et al. (1996)	Human	Lumbar	2.6-40.9	
Acaroglu et al. (1995)			12.7	
Skaggs et al. (1994)	Human	Lumbar	59-136	
Green et al. (1993)		Lumbar	7.2-27.2	

Table 2.3.3. Elastic stiffness and Poisson's ratio reported in the litterature.

The AF tissue stiffens but gets smaller hysteresis area with the strain-rate increase. The maximum axial stress is reported in Figure 2.3.8d as a function of the axial strain-rate, such that a straight-line fit adequately describes the results. It can be observed in the figure that the slope, characterizing the rate-sensitivity, seems to be not sensitive to the region.

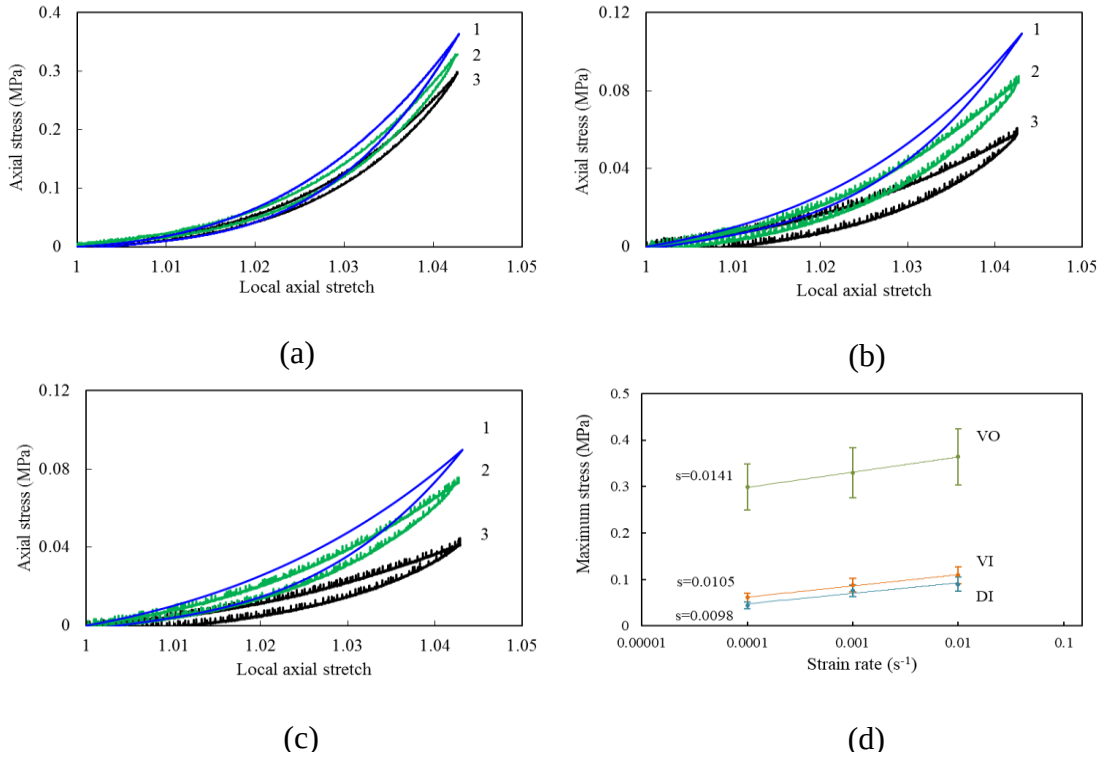

Figure 2.3.8. Strain-rate effect on the (a) VO, (b) VI, (c) DI stress-stretch responses (1: $10^{-2}s^{-1}$, 2: $10^{-3}s^{-1}$, 3: $10^{-4}s^{-1}$) and (d) on the maximum stress.

In order to illustrate the osmolarity effect translated by the chemical environment, Figure 2.3.9 presents the DI stress-stretch response for different saline solution concentrations. The osmolarity and strain-rate effects on the response are statistically significant with a p-value of 0.002 and 0.012, respectively. The mechanical response is strongly dependent on the chemical environment. Indeed, it is observed that the AF tissue stiffens with the salt concentration. The chemical-dependence of the elastic stiffness is reported in Table 2.3.4. The maximum axial stress is reported in Figure 2.3.9d as a function of the NaCl concentration. The slope depends on the osmolarity when the strain-rate decreases with saturated response appearing at the highest osmolarity condition.

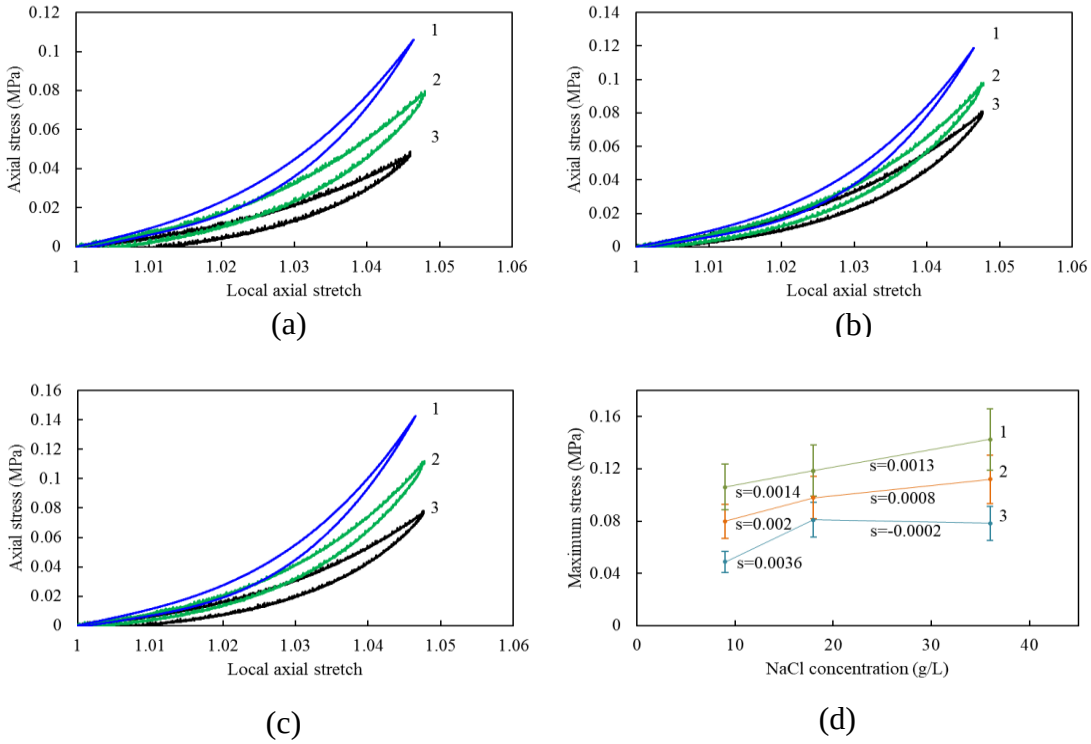

Figure 2.3.9. Strain-rate effect on the DI stress-stretch response for (a) 9 g/L, (b)18 g/L, (c)36 g/L NaCl concentration and (d) on the maximum stress (1: $10^{-2}s^{-1}$, 2: $10^{-3}s^{-1}$, 3: $10^{-4}s^{-1}$).

NaCl concentration (g/L)	Strain-rate (s^{-1})	Elastic stiffness *E* (MPa)
9	10^{-4}	0.55±0.09
	10^{-3}	0.86±0.14
	10^{-2}	1.14±0.19
18	10^{-4}	0.86±0.14
	10^{-3}	0.94±0.16
	10^{-2}	1.16±0.19
36	10^{-4}	0.79±0.13
	10^{-3}	1.05±0.17
	10^{-2}	1.37±0.23

Table 2.3.4. Osmolarity effect on the DI elastic stiffness.

2.3.3.3. Apparent Poisson's ratio

The change in size of AF in a direction perpendicular to the stretching can be basically quantified by the apparent Poisson's ratio. The term "apparent" indicates the fluid flow dependency of this material property. Unlike stiffness, the apparent Poisson's ratio is a two-dimensional property for which the sign and magnitude depend on the plan under consideration,

i.e. FP or LP. Tables 2.3.5 and 2.3.6 report the apparent Poisson's ratios calculated from the full-field strain measurements in FP and in LP:

$$\nu_{xy} = -\frac{E_{yy}}{E_{xx}} \text{ and } \nu_{xz} = -\frac{E_{zz}}{E_{xx}} \quad (8)$$

The apparent Poisson's ratios are clearly out of the classical range, being higher than 0.5 in FP and smaller than 0.0 in LP. The negative Poisson's ratio in LP is necessarily accompanied by a positive Poisson's ratio in FP to ensure a positive volumetric strain.

NaCl concentration (g/L)	Poisson's ratio ν_{xy} FP	Poisson's ratio ν_{xz} LP
9	0.73±0.16	-0.21±0.05
18	0.71±0.15	-0.13±0.03
36	0.81±0.17	-0.08±0.02

Table 2.3.5. Osmolarity effect on the DI apparent Poisson's ratios in FP and in LP.

	Poisson's ratio ν_{xy} FP	Poisson's ratio ν_{xz} LP
VO	1.02±0.22	-0.70±0.15
VI	0.91±0.2	-0.58±0.12
DI	1.02±0.22	-0.58±0.12

Table 2.3.6. Regional effect on the apparent Poisson's ratios in FP and in LP for a 9 g/L NaCl concentration.

The volumetric strain is found higher in VI/VO than in DI. The collagen network seems to cause this difference, since the lamellae thickness is smaller in dorsal part than in ventral part of the IVD. Table 3 reports values existing in the open literature. Unfortunately, studies reporting this property are limited in number, due essentially to the difficulty of measurements and all existing values correspond to a Poisson's ratio in FP (Elliott and Setton, 2001; Guerin and Elliott, 2006; Lewis et al., 2008; O'Connell et al., 2009, 2012; Singha, 2012; Baldit et al., 2013). Although some authors report an apparent FP Poisson's ratio in the classical bounds, the value found in this study is in accordance with others even if there is an important variability caused by age or species. A very low osmolarity sensitivity is found on the apparent FP

Poisson's ratio. Indeed, as shown in Figure 2.3.7, a very small increase of the FP transversal strain is observed with the increase in NaCl concentration which may be related to the collagen fiber reorientation and the induced local stresses. AF presents swelling response in LP related to an auxetic feature (negative Poisson's ratio) which was never quantified on AF in the literature, but also observed on other biological media like skin (Veronda and Westmann, 1970; Lees et al., 1991), arteries (Timmins et al., 2010) and tendons (Gatt et al., 2015). This exciting finding would allow a better understanding of what the nature is able to do since a negative Poisson's ratio is not common in most everyday materials.

2.3.4. Discussion

An accurate method was developed in the aim to evaluate the osmo-inelastic coupling in AF in relation with the material microstructure. Our results show that the hysteretic response and the rate-dependency of the AF tissue are two inelastic features strongly coupled to the osmotic effect due to chemical environment in which the physiological fluid reacts with the soft tissue. By comparing the outer (VO) and inner (VI and DI) responses (Figure 2.3.8), it seems that the hysteresis is not dependent on the fiber content suggesting that this inelastic effect mainly originates from the extracellular matrix rearrangements. Fiber-fiber and fiber-matrix interactions are also usual effects (Ambard and Cherblanc, 2009; O'Connell et al., 2012), but difficult to decouple. In addition, the non-dependence of the region on the rate-sensitivity (Figure 2.3.8d) suggests that the molecular reorganization of the extracellular matrix is probably the main source of rate-dependency. The stiffening with the osmolarity (Figure 2.3.9) points out the coupling in which mechanical and chemical stresses opposite. More the ionic content is important in the solution, less the tissue swells to reach a chemo-mechanical equilibrium and more the stress is important. An increase in osmolarity goes along with an increase in extracellular matrix density. The saturated response manifested by the slope decrease appearing

at low strain-rate and high osmolarity condition (Figure 2.3.9d) may be explained by a more easily reached equilibrium since ionic exchanges are promoted (Vogel and Pioletti, 2012; Vergroesen et al., 2018).

The transversal strain in LP is found positive and dependent on the NaCl concentration as shown in Figure 2.3.7. This observation is to relate to the trend of the soft tissue to contract during the loading in order to keep its chemo-mechanical equilibrium. Before to reach this state, ionic components in solution are expulsed and chemical unbalance is created in the extracellular matrix. The ionic disorder increases with the NaCl concentration. The internal chemical stress tends thus to oppose to the external strain and fluid flows out of the specimen. The osmotic effect is more important in LP than FP. In LP, the negative apparent Poisson's ratio suggests inter-lamellae fluid exchanges. Indeed, although the LP transversal strain is positive in average (Figure 2.3.7), the distribution exhibits alternate positive and negative values as illustrated in Figure 2.3.6. The large thickness in LP induces inter-lamellae interactions (Adams and Green, 1993; Guerin and Elliott, 2006; Adam et al., 1995) and inter-lamellae fluid exchanges. The latter is believed to be the source of the LP auxetic response. The osmotic-dependency of the swelling points out the chemo-mechanical coupling. The inter-lamellae zones seem to play a key role in the underlying physical mechanisms. They are described as an extracellular matrix without organized collagen fibers and may be responsible for a large amount of the inelastic effects (Tavakoli and Costi, 2018), which are altered by changes in PGs density induced by changes in osmolarity. The fluid flow during the AF stretching is thus a consequence of differences in stress between lamellae and inter-lamellae zones. This statement could be verified with transversal strain measurements during long-time relaxation experiments in relation with the surrounding chemical environment.

It is beyond the scope of this work to provide a clear picture on how the different chemo-mechanical features interact in the IVD function. Graded increasing of elastic stiffness, reveals

very accurate AF working. Indeed, higher elastic stiffness of outer part (VO) preserves integrity of the structure and limits deformation of tissue whereas lower elastic stiffness of inner part (VI/DI) permits better softening of stresses from nucleus. Our results show also that the inelastic effects in AF originate from both extracellular matrix and fluid flow, and are combined to a LP auxetic effect. The presence of auxeticity and inelasticity result in a better IVD functionality by optimally managing the axial loads transmitted by the spinal column.

2.3.5. Partial conclusions

This study has been conducted to determine the intrinsic behavior of the bovine AF by considering osmotic and inelastic effects at the same time. The effects of microstructure (trough the IVD locations), biochemical environment and strain-rate have been considered. The osmo-inelastic mechanisms have been revealed by analyzing these effects on both the macro-stress and the full-field transversal strains. The hysteresis area and the rate-sensitivity have been found independent on the collagen fibers content/orientation, suggesting the preponderant role of the PGs macromolecules rearrangements on the inelastic effects. The latter statement has been confirmed by the evident osmotic-dependency of the rate-sensitivity since an increase in osmolarity goes along with an increase in PGs density. The inter-lamellae fluid exchanges have been suggested by the strong chemical dependence of the LP auxetic response.

2.3.6. References

Acaroglu, E.R., Iatridis, J.C., Setton, L.A., Foster, R.J., Mow, V.C., Weidenbaum, M., 1995. Degeneration and aging affect the tensile behavior of human lumbar anulus fibrosus. Spine 20, 2690-2701.

Adam, C., Rouch, P., Skalli, W., 2015. Inter-lamellar shear resistance confers compressive stiffness in the intervertebral disc: an image-based modelling study on the bovine caudal disc. Journal of Biomechanics 48, 4303-4308.

Adams, M.A., Green, T.P., 1993. Tensile properties of the annulus fibrosus. I. The contribution of fibre-matrix interactions to tensile stiffness and strength. European Spine Journal 2, 203-208.

Alini, M., Eisenstein, S.M., Ito, K., Little, C., Kettler, A.A., Masuda, K., Melrose, J., Ralphs, J., Stokes, I., Wilke, H.J., 2008. Are animal models useful for studying human disc disorders/degeneration? European Spine Journal 17, 2-19.

Ambard, D., Cherblanc, F., 2009. Mechanical behavior of annulus fibrosus: a microstructural model of fibers reorientation. Annals of Biomedical Engineering 37, 2256-2265.

Andarawis-Puri, N., Sereysky, J.B., Jepsen, K.J., Flatow, E.L., 2012. The relationships between cyclic fatigue loading, changes in initial mechanical properties, and the in vivo temporal mechanical response of the rat patellar tendon. Journal of Biomechanics 45, 59-65.

Anuta, P.E., 1970. Spatial registration of multispectral and multitemporal digital imagery using fast fourier transform techniques. IEEE Transactions on Geoscience Electronics 8, 353-368.

Baldit, A., Ambard, D., Cherblanc, F., Royer, P., 2014. Experimental analysis of the transverse mechanical behaviour of annulus fibrosus tissue. Biomechanics and Modeling in Mechanobiology 13,643-652.

Bass, E.C., Ashford, F.A., Segal, M.R., Lotz, J.C., 2004. Biaxial testing of human annulus fibrosus and its implications for a constitutive formulation. Annals of Biomedical Engineering 32, 1231-1242.

Bezci, S.E., Nandy, A., O'Connell, G.D., 2015. Effect of hydration on healthy intervertebral disk mechanical stiffness. Journal of Biomechanical Engineering 137, 101007.

Bruehlmann, S.B., Hulme, P.A., Duncan, N.A., 2004. In situ intercellular mechanics of the bovine outer annulus fibrosus subjected to biaxial strains. Journal of Biomechanics 37, 223-231.

Costi, J.J., Hearn, T.C., Fazzalari, N.L., 2002. The effect of hydration on the stiffness of intervertebral discs in an ovine model. Clinical Biomechanics 17, 446-455.

Drost, M.R., Willems, P., Snijders, H., Huyghe, J.M., Janssen, J.D., Huson, A., 1995. Confined compression of canine annulus fibrosus under chemical and mechanical loading. Journal of Biomechanical Engineering 117, 390-396.

Ebara, S., Iatridis, J.C., Setton, L.A., Foster, R.J., Mow, V.C., Weidenbaum, M., 1996. Tensile properties of nondegenerate human lumbar anulus fibrosus. Spine 21, 452-461.

Elliott, D.M., Setton, L.A., 2001. Anisotropic and inhomogeneous tensile behavior of the human annulus fibrosus: experimental measurement and material model predictions. Journal of Biomechanical Engineering 123, 256-263.

Emanuel, K.S., van der Veen, A.J., Rustenburg, C.M.E., Smit, T.H., Kingma, I., 2018. Osmosis and viscoelasticity both contribute to time-dependent behaviour of the intervertebral disc under compressive load: a caprine in vitro study. Journal of Biomechanics 70, 10-15.

Eyre, D.R., 1979. Biochemistry of the intervertebral disc. International Review of Connective Tissue Research 8, 227-291.

Gatt, R., Wood, M.V., Gatt, A., Zarb, F., Formosa, C., Azzopardi, K.M., Casha, A., Agius, T.P., Schembri-Wismayer, P., Attard, L., Chockalingam, N., Grima, J.N., 2015. Negative Poisson's ratios in tendons: an unexpected mechanical response. Acta Biomaterialia 24, 201-208.

Green, T.P., Adams, M.A., Dolan, P., 1993. Tensile properties of the annulus fibrosus. II. Ultimate tensile strength and fatigue life. European Spine Journal 2, 209-214.

Guerin, H.A.L., Elliott, D.M., 2006. Degeneration affects the fiber reorientation of human annulus fibrosus under tensile load. Journal of Biomechanics 39, 1410-1418.

Hild, F., Roux, S., 2012. Comparison of local and global approaches to Digital Image Correlation. Experimental Mechanics 52, 1503-1519.

Holzapfel, G.A., Schulze-Bauer, C.A.J., Feigl, G., Regitnig, P., 2005. Single lamellar mechanics of the human lumbar anulus fibrosus. Biomechanics and Modeling in Mechanobiology 3, 125-140.

Huyghe, J.M., Drost, M.R., 2004. Uniaxial tensile testing of canine annulus fibrosus tissue under changing salt concentrations. Biorheology 41, 255-261.
Iatridis, J.C., MacLean, J.J., Ryan, D.A., 2005. Mechanical damage to the intervertebral disc annulus fibrosus subjected to tensile loading. Journal of Biomechanics 38, 557-565.
Inoue, H., Takeda, T., 1975. Three-dimensional observation of collagen framework of lumbar intervertebral discs. Acta Orthopaedica 46, 949-956.
Johannessen, W., Vresilovic, E.J., Wright, A.C., Elliott, D.M., 2004. Intervertebral disc mechanics are restored following cyclic loading and unloaded recovery. Annals of Biomedical Engineering 32, 70-76.
Kemper, A.R., McNally, C., Duma, S.M., 2007. The influence of strain rate on the compressive stiffness properties of human lumbar intervertebral discs. Biomedical Sciences Instrumentation 43, 176-181.
Lees, C., Vincent, J.F., Hillerton, J.E., 1991. Poisson's ratio in skin. Bio-Medical Materials and Engineering 1, 19-23.
Lewis, N.T., Hussain, M.A., Mao, J.J., 2008. Investigation of nano-mechanical properties of annulus fibrosus using atomic force microscopy. Micron 39, 1008-1019.
Mengoni, M., Luxmoore, B.J., Wijayathunga, V.N., Jones, A.C., Broom, N.D., Wilcox, R.K., 2015. Derivation of inter-lamellar behaviour of the intervertebral disc annulus. Journal of the Mechanical Behavior of Biomedical Materials 48, 164-172.
Michalek, A.J., Buckley, M.R., Bonassar, L.J., Cohen, I., Iatridis, J.C., 2009. Measurement of local strains in intervertebral disc anulus fibrosus tissue under dynamic shear: contributions of matrix fiber orientation and elastin content. Journal of Biomechanics 42, 2279-2285.
Nachemson, A., Morris, J.M., 1964. In vivo measurements of intradiscal pressure: discometry, a method for the determination of pressure in the lower lumbar discs. The Journal of Bone and Joint Surgery 46, 1077-1092.
Newell, N., Grigoriadis, G., Christou, A., Carpanen, D., Masouros, S.D., 2016. Material properties of bovine intervertebral discs across strain rates. Journal of the Mechanical Behavior of Biomedical Materials 65, 824-830.
Newell, N., Little, J.P., Christou, A., Adams, M.A., Adam, C.J., Masouros, S.D., 2017. Biomechanics of the human intervertebral disc: a review of testing techniques and results. Journal of the Mechanical Behavior of Biomedical Materials 69, 420-434.
O'Connell, G.D., Guerin, H.L., Elliott, D.M., 2009. Theoretical and uniaxial experimental evaluation of human annulus fibrosus degeneration. Journal of Biomechanical Engineering 131, 1-7.
O'Connell, G.D., Sen, S., Elliott, D.M., 2012. Human annulus fibrosus material properties from biaxial testing and constitutive modeling are altered with degeneration. Biomechanics and Modeling in Mechanobiology 11, 493-503.
Parsons, E., Boyce, M.C., Parks, D.M., 2004. An experimental investigation of the large-strain tensile behavior of neat and rubber-toughened polycarbonate. Polymer 45, 2665-2684.
Qasim, M., Natarajan, R.N., An, H.S., Andersson, G.B.J., 2014. Damage accumulation location under cyclic loading in the lumbar disc shifts from inner annulus lamellae to peripheral annulus with increasing disc degeneration. Journal of Biomechanics 47, 24-31.
Race, A., Broom, N.D., Robertson, P., 2000. Effect of loading rate and hydration on the mechanical properties of the disc. Spine 25, 662-669.
Roux, D.C., Cooper-White, J.J., McKinley, G.H., Tirtaatmadja, V., 2003. Drop impact of newtonian and elastic fluids. Physics of Fluids 15, S12-S12.
Singha, K., Singha, M., 2012. Biomechanism profile of intervertebral disc's (IVD): strategies to successful tissue engineering for spinal healing by reinforced composite structure. Journal of Tissue Science & Engineering 3, 1000118.

Skaggs, D.L., Weidenbaum, M., Iatridis, J.C., Ratcliffe, A., Mow, V.C., 1994. Regional variation in tensile properties and biochemical composition of the human lumbar anulus fibrosus. Spine 19, 1310-1319.

Tavakoli, J., Costi, J.J., 2018. New findings confirm the viscoelastic behaviour of the inter-lamellar matrix of the disc annulus fibrosus in radial and circumferential directions of loading. Acta Biomaterialia 71, 411-419.

Timmins, L.H., Wu, Q., Yeh, A.T., Moore, J.E., Greenwald, S.E., 2010. Structural inhomogeneity and fiber orientation in the inner arterial media. American Journal of Physiology - Heart and Circulatory Physiology 298, 1537-1545.

Vergari, C., Mansfield, J., Meakin, J.R., Winlove, P.C., 2016. Lamellar and fibre bundle mechanics of the annulus fibrosus in bovine intervertebral disc. Acta Biomaterialia 37, 14-20.

Vergroesen, P.P.A., Emanuel, K.S., Peeters, M., Kingma, I., 2018. Are axial intervertebral disc biomechanics determined by osmosis? Journal of Biomechanics 70, 4-9.

Veronda, D.R., Westmann, R.A., 1970. Mechanical characterization of skin-Finite deformations. Journal of Biomechanics 3, 111-124.

Vogel, A., Pioletti, D.P., 2012. Damping properties of the nucleus pulposus. Clinical Biomechanics 27, 861-865.

Wagner, D.R., Lotz, J.C., 2004. Theoretical model and experimental results for the nonlinear elastic behavior of human annulus fibrosus. Journal of Orthopedic Research 22, 901-909.

Chapter 2: Experimental characterization

Part 4: Poisson's ratio in annulus fibrosus and osmo-inelastic coupling[4]

Abstract

The annulus fibrosus (AF) is a highly complex layered structure in which the inelastic features of the tangled extracellular matrix interact with the surrounding physiological fluid by osmotic effect. In this last part of the Chapter 2, the time-dependent transversal behavior in the two plans of AF (fibers and lamellae plans) is reported by means of an accurate optical strain measuring technique based upon digital image correlation. AF specimens of rectangular cross-section, extracted from bovine cervical discs, are tested under quasi-static and relaxation loading with variation in osmolarity and strain-rate conditions. Analysis of variance highlights osmo-inelastic effects on the elastic stiffness and the apparent Poisson's ratios, with p-value<0.05. Under quasi-static loading, the apparent Poisson's ratio is found higher than 0.5 in fibers plan and negative in lamellae plan. This material property evolves towards classical bounds with relaxation time. The strong dependence of the auxetic behavior on time and chemical environment provides valuable insights about internal fluid exchanges. An interpretation of the osmo-inelastic mechanism is proposed in which mechanical-based and chemical-based fluid-flow interact until chemo-mechanical equilibrium.

Keywords: Annulus fibrosus; Digital image correlation; Poisson's ratio; Auxetic; Osmo-inelastic coupling.

[4] This Part of this chapter is based on the following paper: Amil Derrouiche, Fahmi Zaïri, Fahed Zaïri, Poisson's ratio in annulus fibrosus and osmo-inelastic coupling, *submitted*.

2.4.1. Partial introduction

The intervertebral disc (IVD) is a complex fibrocartilage connecting our vertebrae from cervical to lumbar parts. This soft tissue allows body movements when our vertebral column is subjected to bend or twist. It is composed by gelatinous core, i.e. nucleus pulposus (NP), retained by concentric reinforced layers, i.e. annulus fibrosus (AF). At the microstructural scale, tangled proteoglycans (PGs) macromolecules form an extracellular matrix (ECM) attracting mobile ions and physiological fluid by osmotic effect. In each lamella of AF, oriented collagen fibers increase in content from inner part to outer part, and change in orientation from dorsal part to ventral part (Inoue and Takeda, 1975; Eyre, 1979; Guerin and Elliott, 2006). The AF mechanical properties are thus regional dependent (Skaggs et al., 1994; Ebara et al., 1996; Holzapfel et al., 2005; Michalek et al., 2009). Collagen fibers give high stiffness to the AF in order to contain NP swelling under vertebra-induced compression during our movements. An understanding of interactions between different constituents in relation with the environment is of major importance in the description of the tissue.

As other cartilages, the IVD hydration influences the response by reaction between mobile ions in the physiological fluid and ECM fixed charges. The fluid is a major contributor to the AF behavior, by varying according to external mechanical loads and internal osmotic pressure and by ensuring in-vivo nutrients supply. Indeed, under mechanical loading, the fluid, flowed out, leads to chemical imbalances that generate fluid inflow (Drost et al., 1995; Schmidt et al., 2016). The IVD exhibits a time-dependent mechanical response, governed by the changes in fluid content and the inelastic effects (Race et al., 2000; Holzapfel et al., 2005; Kemper et al., 2007; Ambard and Cherblanc, 2009; Newell et al., 2016, 2017; Tavakoli and Costi, 2018). Since the microstructural organization of collagen fibers is not uniform, strain fields are highly heterogeneous (Moo et al., 2018) and local tracking is required in order to understand the AF response. Chemo-mechanical couplings in the soft tissues are now well accepted (Emanuel et

al., 2018; Vergroesen et al., 2018) but not fully understood, especially in relation with local strain field.

Interlamellar zones in AF play a fundamental role in the coupling (Michalek et al., 2009; Adam et al., 2015; Mengoni et al., 2015; Vergari et al., 2016; Tavakoli and Costi, 2018). In this regard, the quantitative determination of Poisson's ratio in AF specimens composed by multiple lamellae would allow a plausible explication of the implication of interlamellar zones in internal fluid exchanges. This material property, describing the transversal behavior of axially stretched specimens, is between 0 and 0.5 for almost existing materials. Dependent on the observed direction, an out-of-bonds Poisson's ratio was usually observed in the fibers plan (FP) of AF specimens with scattered values between 0.3 and 4.64 (Elliott and Setton, 2001; Guerin and Elliott, 2006; Lewis et al., 2008; O'Connell et al., 2009; O'Connell et al., 2012; Singha and Singha, 2012; Baldit et al., 2014). In the lamellae plan (LP), AF exhibits an auxetic (negative Poisson's ratio) behavior (Baldit et al., 2014). The auxeticity is not common in most everyday materials, but negative values of this material property were also reported for other biological tissues such as cat skin (Veronda and Westmann, 1970), cow teat skin (Lees et al., 1991), human cancellous bone (Williams and Lewis, 1982), bovine arteries (Timmins et al., 2010) and human, pig and sheep Achilles tendon (Gatt et al., 2015).

In this last part of the Chapter 2, full-field transversal strains are determined simultaneously in LP and in FP of AF specimens of rectangular cross-section subjected to quasi-static and relaxation loading. The response is carefully evaluated in relation to the collagen fibers content, the osmolarity and the strain-rate. The Poisson's ratio, obtained in short and long-time experiments, is presented as an indicator of osmo-inelastic coupling in the aim to provide valuable insights into the underlying physical mechanisms.

2.4.2. Materials and methods

2.4.2.1. Specimen preparation

Fifteen AF samples were extracted from cervical bovine spine within two days after death. AF ventro-inner (VI) and ventro-outer (VO) parts were carefully separated from IVD using surgical tool along circumferential direction of IVD. VI and VO parts were then separated to have specimens of rectangular cross-section of approximately 25 × 10 × 10 mm^3. Bovine was selected in reason of its size, facilitating local strain measurements. Moreover, interspecies variability is lower for animals than humans, due to lifestyle but inter-species differences demand critical analysis (Alini et al., 2008). After excision, AF specimens were immerged in 9 g/L saline solution during 100 minutes in order to re-establish hydration due to low humidity of storage room in abattoir (Costi et al., 2002). The extracted AF specimens were stored at 4°C at maximum two days before testing. Fresh specimens were used to avoid any storage effects in terms of temperature and duration. Gripping AF specimen is a difficult task for the mechanical tests due to softness of the tissue and potential failure of the bone with grips pressure. In accordance with the literature, the AF specimen was glued to aluminum plates using cyanoacrylate and then mounted on the testing machine (Bruehlmann et al., 2004; O'Connell et al., 2011; Baldit et al., 2014). The cyanoacrylate influence may be neglected due to higher stiffness than AF tissue.

2.4.2.2. Methods

The tests were carried out at room temperature on the electro-pulse mechanical machine (Instron-5500) with 1 kN load cell. Quasi-static and relaxation tests were performed under axial, i.e. circumferential in IVD, controlled-displacement to characterize both the evolution in stress and the evolution in transversal strains while the specimen is constantly immerged in a saline

solution with various concentrations. The applied circumferential strain represents the AF response exposed to the NP swelling (Nachemson and Morris, 1964).

Prior to each experiment, a three-step preconditioning is applied to ensure repeatability of the mechanical response. After a first step of 30 min of mechanical rest, the AF specimens were preconditioned by 10 cycles with an axial strain amplitude of 1% at a rate of $10^{-3}s^{-1}$ in order to stimulate chemical equilibrium and fluid transfers. Then, the specimens were carefully preloaded at 0.1 N before testing and stretched at an axial strain of 7% at a rate of 10^{-3} s^{-1}. The Mullins effect removing improves the repeatability of the response and ensures the specimen adherence with the metal plates. The results reported in this investigation follow the protocol illustrated in Figure 2.4.1.

Two kinds of experiments were performed to characterize the AF mechanical behavior in relation with the osmo-inelastic coupling. The first one consists in a quasi-static tensile loading-unloading test at a maximum axial strain of 5% (Figure 2.4.1a). The second one consists in a relaxation test in which the axial strain was ramped at a prescribed level and maintained constant during a holding time sufficient to reach the stabilization in load (Figure 2.4.1b).

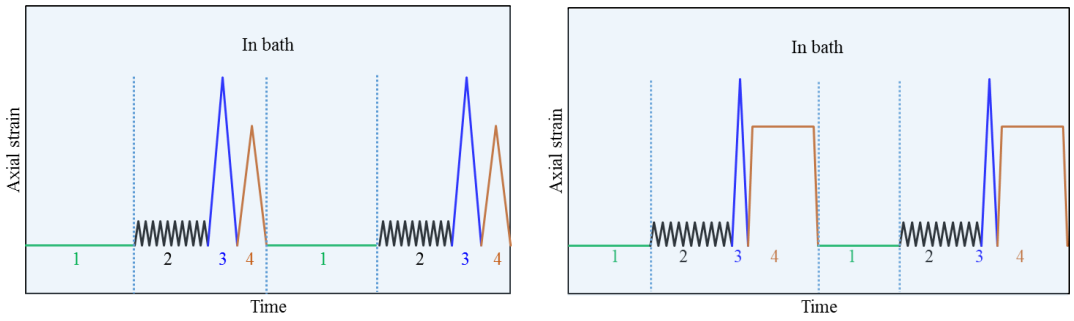

(a) (b)

Figure 2.4.1. Experimental design for two successive tests: (a) quasi-static test and (b) relaxation test (1: mechanical rest, 2: successive low-strain tensions, 3: Mullins effect removing, 4: test).

The strain-rate sensibility was investigated by applying successively the following axial strain-rates: 2×10^{-5} s^{-1}, 2×10^{-4} s^{-1} and 2×10^{-3} s^{-1}. For each strain-rate, experiments were repeated with

increasing of NaCl concentrations from 0 g/L hypo-osmotic solution, 9 g/L iso-osmotic solution and 18 g/L hyper osmotic-solution in order to highlight the chemo-mechanical coupling. The effect of collagen fibers content was examined by comparing VO and VI specimens according to well-documented regional variation in IVD (Inoue and Takeda, 1975; Eyre, 1979; Guerin and Elliott, 2006).

Between two successive experiments, the specimen was completely unloaded to dissipate residual strains. Before each test, the three-step preconditioning is carefully performed on the AF specimento promote chemical equilibrium after changes in NaCl concentration. As an example, Figure 2.4.2 presents the result of two tests showing the repeatability of the visco-elastic response of the AF tissue. The total recovering capability is verified even for thousand preconditioning cycles within physiological loads (Johannessen et al., 2004).

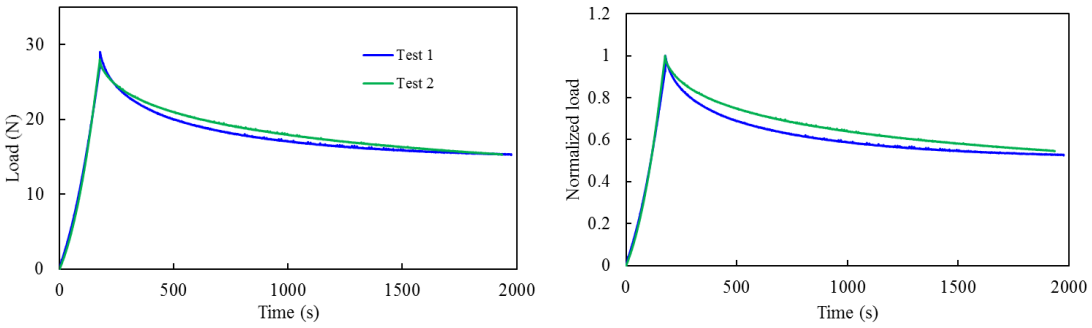

(a) (b)

Figure 2.4.2. Two successive relaxation tests performed on the same AF specimen: (a) load and (b) normalized load as a function of time.

2.4.2.3. Statistical analysis

Validity of the present contribution and errors bars on the load was determined by statistical analysis in order to take into account the inevitable inter-specimen variability, even if this dispersion is lower for animal specimen than human specimen. Fifteen specimens were stretched at the same strain-rate and NaCl concentration and, the results were analyzed by one-way analysis of variance (ANOVA). A p-value < 0.05 was considered to be statistically

significant. Standard deviation at a 95 % confidence was estimated about 6.83% with a p-value of 0.0084 indicating statistical significance of the study. The data presented in each figure in the results section represent the mechanical response of one AF specimen. A two-way ANOVA without replication is then performed in order to indicate the statistical significance of the osmo-inelastic effects. Although the present study is based on a relatively small number of specimens (n=21), the goal is to provide qualitative trends of the chemo-mechanical response in relation to the microstructure, the biochemical environment and the mechanical loading conditions.

2.4.2.4. Full-field strain measurements

A digital image correlation (DIC) system constituted by a charged couple device (CCD) camera (Imager E-lite) interfaced with a computer for image digitizing and analyzing (Davis software developed by Lavision) was used to calculate a two-dimensional (2D) field of in-plane displacements. The lens axis of the CCD camera was kept perpendicular to the front face of the AF specimen to capture the 2D full-field displacements in FP. The 2D full-field displacements in LP were obtained via a right-angle prism placed besides the AF specimen. A schematic overview of the experimental set-up is shown in Figure 2.4.3. The strategy was earlier used by Roux et al. (2003) and Parsons et al. (2004) for other materials. DIC measurements consist in correlating the gray levels of each deformed specimen image to their counterpart of the undeformed specimen image. To obtain randomized gray levels distributions, an artificial random speckle pattern was applied on both sides of each AF specimen with airbrush filled with India ink. It was assured that the speckles were non-overlapped, identical and as small as possible to optimize the spatial resolution.

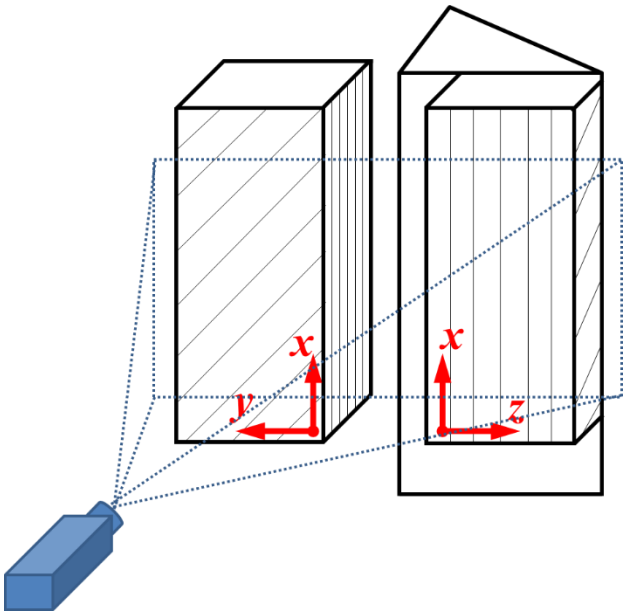

Figure 2.4.3. Schematic view of AF specimen with simultaneous local displacement measurements in fibers plan (xy) and in lamellae plan (xz) using a right angle prism.

The deformed specimen images were recorded at a frequency of 3 Hz with resolution of 290 pixels/mm and size of 1628 × 1236 pixels. The zone of interest (ZOI) of each image was divided into small square subsets of size 48×48 pixels. The in-plane displacement vector was determined in the centre point of each subset. Area of interest was chosen in the central part of the specimen to avoid unlikely cyanoacrylate effect. It was divided into small square subsets in which the displacement vector was determined. A root mean square error of 9.7% from the correlation process is estimated by imposing a rigid body move to AF specimen, griped at one side and free at the other one.

From the full-field strains averaged in the ZOI, the actual specimen cross-section was estimated. Then, the Poisson's ratios ν_{xy} and ν_{xz} were calculated from the ratio between the transversal strain, in FP and LP, respectively, and the axial strain. The elastic stiffness E was determined by fitting a simple neo-Hookean elastic relationship to the tensile response in terms of axial

stress as a function of axial strain. The stress was determined as the ratio of the actual load recorded by the load-cell and the actual specimen cross-section.

2.4.3. Results

2.4.3.1. Quasi-static response

Figures 2.4.4 and 2.4.5 present the AF stress-stretch response for the two locations in IVD, i.e. VI and VO. The effects of the microstructure, the biochemical environment and the strain-rate on the hysteretic response can be observed. The regional variation allows establishing the relationship between the AF mechanical response and the collagen fibers content. Tables 2.4.1 and 2.4.2 provide the elastic stiffness and the Poisson's ratios.

NaCl concentration (g/L)	Strain-rate (s^{-1})	Elastic stiffness *E* (MPa) VI	Elastic stiffness *E* (MPa) VO
0	2×10^{-3}	2.95±0.5	5.85±0.99
	2×10^{-4}	2.44±0.41	5.56±0.95
	2×10^{-5}	2.18±0.37	4.76±0.81
9	2×10^{-3}	5.05±0.86	6.47±1.1
	2×10^{-4}	4.28±0.73	6.16±1.05
	2×10^{-5}	3.54±0.6	5.14±0.87
18	2×10^{-3}	7.73±1.31	7.28±1.24
	2×10^{-4}	5.68±0.97	6.9±1.17
	2×10^{-5}	4.78±0.81	5.78±0.98

Table 2.4.1. Osmolarity effect on the elastic stiffness obtained from quasi-static tests.

The statistical significance of the strain-rate and osmolarity effects are estimated on the material properties in order to highlight the osmo-inelastic coupling. Both effects are statistically significant on the elastic stiffness for VI specimen with a p-value of 0.05 and 0.0045, respectively. These effects are more evidenced for the VO specimen with $p<0.001$ for both effects.

NaCl concentration (g/L)	Strain-rate (s^{-1})	Poisson's ratio VI		Poisson's ratio VO	
		ν_{xy} FP	ν_{xz} LP	ν_{xy} FP	ν_{xz} LP
0	2×10^{-3}	0.887±0.19	-0.468±0.1	1.097±0.24	-0.295±0.06
	2×10^{-4}	0.74±0.16	-0.574±0.12	0.83±0.18	-0.432±0.09
	2×10^{-5}	0.736±0.16	-0.73±0.16	0.87±0.19	-0.55±0.12
9	2×10^{-3}	0.92±0.2	-0.2±0.04	1.12±0.24	-0.156±0.03
	2×10^{-4}	0.74±0.16	-0.387±0.08	1.01±0.22	-0.347±0.07
	2×10^{-5}	0.76±0.16	-0.449±0.1	0.89±0.19	-0.512±0.11
18	2×10^{-3}	0.963±0.21	-0.146±0.03	1.07±0.23	-0.093±0.02
	2×10^{-4}	0.811±0.17	-0.29±0.06	1.06±0.23	-0.215±0.05
	2×10^{-5}	0.78±0.17	-0.36±0.08	0.92±0.2	-0.465±0.1

Table 2.4.2. Osmolarity effect on the Poisson's ratios obtained from quasi-static tests.

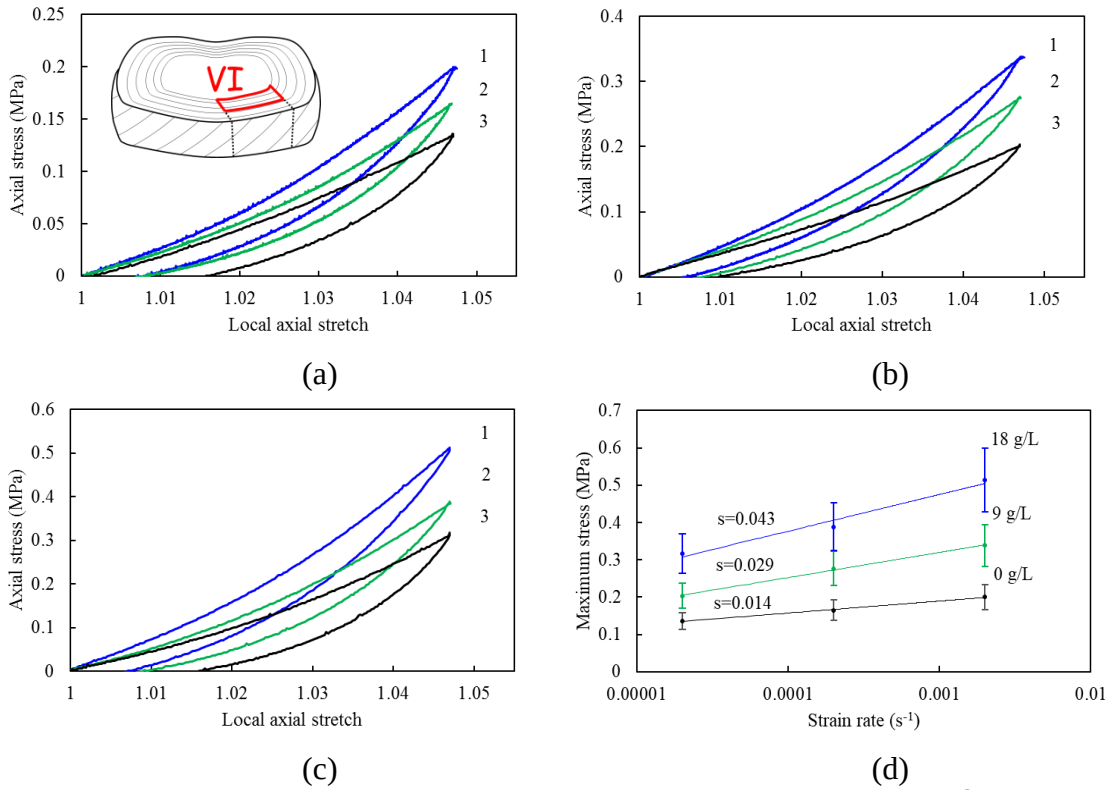

Figure 2.4.4. VI stress-stretch responses at three different strain-rates (1: $2\times10^{-3}s^{-1}$, 2: $2\times10^{-4}s^{-1}$, 3: $2\times10^{-5}s^{-1}$) for (a) 0 g/L, (b) 9 g/L, (c) 18 g/L NaCl concentration, and (d) maximum stress as a function of strain-rate.

The AF tissue stiffening with the salt concentration shows the strong osmotic dependency of the mechanical response. The AF elastic stiffness variation can be also seen on the maximum stress variation represented in Figures 2.4.4d and 2.4.5d. The osmolarity dependence of the rate

sensitivity, characterized by the slope, is more prounounced in VI than in VO, suggesting that high fibers content could hide the osmotic contribution.

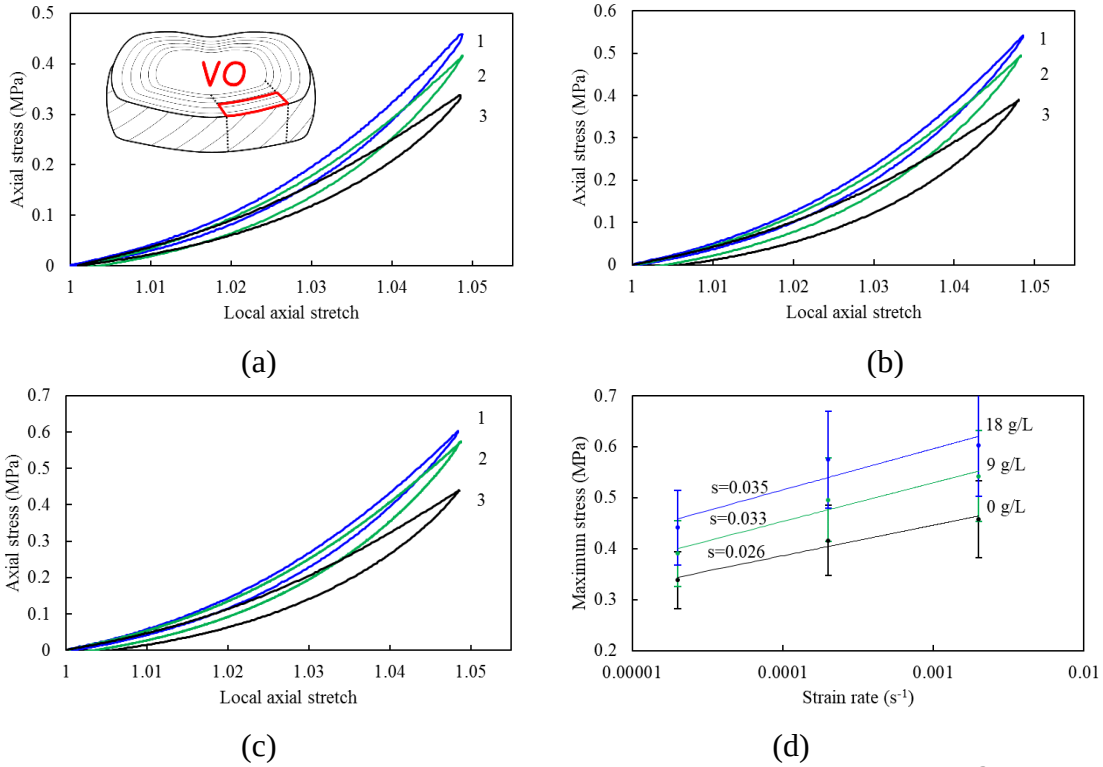

Figure 2.4.5. VO stress-stretch responses at three different strain-rates (1: $2\times10^{-3}s^{-1}$, 2: $2\times10^{-4}s^{-1}$, 3: $2\times10^{-5}s^{-1}$) for (a) 0 g/L, (b) 9 g/L, (c) 18 g/L NaCl concentration, and (d) maximum stress as a function of strain-rate.

The transversal behavior is described by the apparent Poisson's ratios. The term "apparent" is employed in order to point out the fluid flow dependency of this two-dimensional material property, out of the classical bounds: higher than 0.5 in FP and negative in LP. The swelling in LP is accompanied by large shrinkage in FP resulting in overall to a positive volumetric variation. The apparent Poisson's ratio seems reach an equilibrated value in FP when the strain-rate decrease with relative osmolarity dependence in VI (p-value=0.01 and p-value<0.001 for strain-rate and osmolarity effects, respectively). In VO, the strain-rate and osmolarity depedency are not statistically significant in FP (p-value>0.05), confirming that the collagen fibers contribution is preponderant in the mechanical response. In LP, the interesting swelling presents strong variation with strain-rate and osmolarity in both VO and VI (p-value<0.01). The

collagen reinforcement contribution is still evidenced with lower Poisson's ratio values in VO. In order to better understand the AF chemical-dependency, suggesting ionic transport effect, it is now proposed to investigate the AF time-dependency of the chemo-mechanical coupling through relaxation tests under well controlled-environment. In particular, the auxetic response being associated to the fluid transfer, relaxation measurements allow to identify the underlying mechanisms related to mechanical and chemical stresses.

2.4.3.2. Relaxation response

Results of chemo-relaxation tests are presented in Figure 2.4.6 in terms of load evolution. The load seems to evolve towards an end, if the hold time is sufficiently long, corresponding to a stabilized relaxed-load. The normalized load is found markedly depend on the strain-rate (Figure 2.4.6a). The decrease with the strain-rate suggests a strong chemo-mechanical coupling of the AF tissue. Indeed, the fluid transfer seems to be the main source of the chemo-relaxation response. The strain level significantly affects the maximum load and the relaxed-load. Nevertheless, the normalized load is found independent on the strain level (Figure 2.4.6b), suggesting a proportional effect of the applied stretch on the fluid exchange. The external solution concentration has a strong effect on the chemo-relaxation response of the AF tissue (Figure 2.4.6c). By favoring the fluid transfer, the osmolarity has for effect to increase the AF stiffness at the macro-scale and the local stresses. The equilibrium response clearly depends on the environment. With higher local stresses previous to the relaxation, the chemical imbalances are higher and the relaxed-load becomes lower with more fluid exchange.

The transversal behavior can provide some additional insights on the structural changes during the chemo-relaxation. A typical result is provided in Figure 2.4.7a. As a consequence of the applied axial stretching, the LP and FP transversal strains increase. The transversal strains represent structural changes due to fluid content evolution. In FP, the tightening reaches about

a 3% transversal strain for a 3.5% axial strain. In the meantime, the AF swells at about a 1.5% transversal strain in LP. More interestingly, during the relaxation period, an opposite evolution is observed for both transversal strains until to reach a stabilized value due to the chemo-mechanical equilibrium. The equilibrium transversal strain is equal to about 1.7% in FP and close to zero in LP.

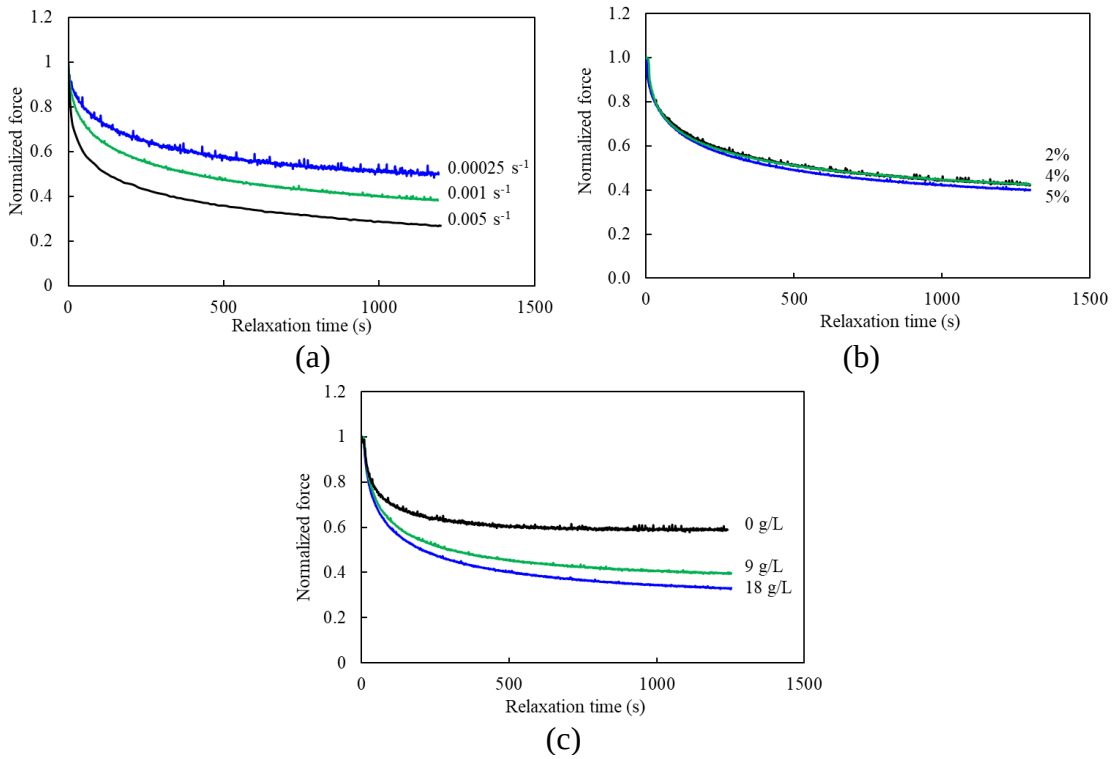

Figure 2.4.6. Evolution under relaxation of load with (a) strain-rate, (b) strain level and (c) osmolarity effects.

Apparent Poisson's ratio may be considered as an indicator of the AF local response in relation with internal changes. As a consequence of the opposite evolution in transversal strains between stretching and relaxation, the apparent Poisson's ratios change during the chemo-relaxation process as shown in Figure 2.4.7b. The apparent Poisson's ratio decreases in FP and increases in LP, to reach stabilized-values in a more classical range, about 0.5 in FP and 0.02 in LP.

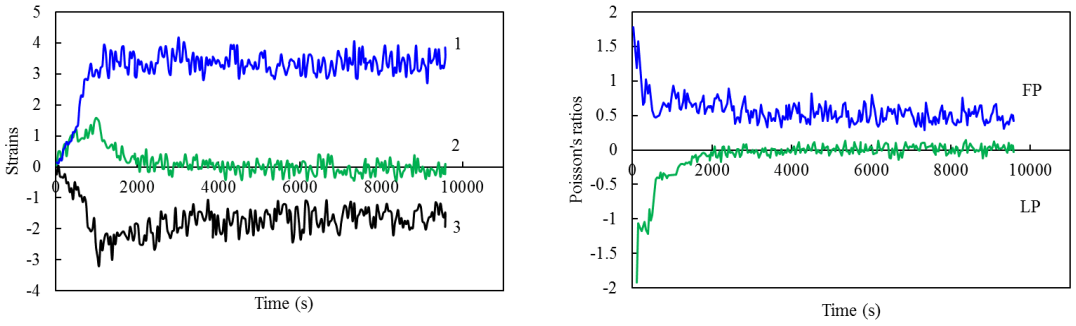

(a) (b)

Figure 2.4.7. Evolution under relaxation of (a) local strains (1: axial strain, 2: LP transversal strain, 3: FP transversal strain) and (b) apparent Poisson's ratios.

The osmo-inelastic effects on the apparent Poisson's ratio are given in Figures 8 and 9. The stabilized values are provided in Tables 2.4.3 and 2.4.4. In FP, the increase in osmolarity leads to decrease the apparent Poisson's ratio and to increase the relaxation time (Figure 2.4.8). When the response is relaxed, the value becomes in the classical range of usual Poisson's ratios. The LP auxetic response vanishes with a high osmolarity dependency of the relaxed-value and the relaxation time. The strain-rate has a strong effect on the relaxation time both in LP and in FP (Figure 2.4.9). The relaxed-value is nearly not affected by the strain-rate in LP and weakly affected in FP.

NaCl concentration (g/L)	Poisson's ratio v_{xy} FP	Poisson's ratio v_{xz} LP
0	0.56±0.12	0.002±0.0004
9	0.51±0.11	0.14±0.03
18	0.51†±0.11	0.31†±0.07

Table 2.4.3. Osmolarity effect on the VI stabilized Poisson's ratios obtained from relaxation tests for a strain-rate of 10^{-3} s^{-1} (†not stabilized).

Strain-rate (s^{-1})	Poisson's ratio v_{xy} FP	Poisson's ratio v_{zx} LP
10^{-3}	0.51±0.11	0.14±0.03
2.5×10^{-4}	0.54±0.12	0.08±0.02
1.25×10^{-4}	0.56±0.12	0.11±0.02

Table 2.4.4. Strain-rate effect on the VI stabilized Poisson's ratios obtained from relaxation tests for a 9 g/L NaCl concentration.

2.4.4. Discussion

Our experimental observations provide valuable insights into the chemo-mechanical coupling and the origin of the time-dependency. The underlying mechanisms involve both ECM rearrangement and ionic transfer by fluid exchange. We evidence that the AF tissue exhibits different transversal behaviors in its two plans, namely FP and LP. An antagonist variation is found during relaxation, suggesting a fluid exchange between FP and LP. The apparent Poisson's ratio is a two-dimensional material property taken as indicator of the chemo-mechanical coupling in the aim to better understand the capability of the AF tissue to maintain its internal chemical balance under external mechanical loading.

Under a quasi-static loading, the volume variation, due to Poisson's ratio effect, is found regional-dependent and higher in VI than in VO (Table 2.4.2). The collagen network seems to cause this difference, since its contribution avoids internal changes. The volume variation is a function of ionic content in solution to equilibrate chemical and mechanical parts of the response. Indeed, the volume variation decreases with NaCl concentration. That may be explained by the fact that in a hyper-osmotic environment, AF needs to swell lesser to catch mobile ions in solution.

The hyper-osmotic effect is also responsible of a microstructure tightening inducing a smaller fluid volume in the tissue. If the environment becomes hypo-osmotic, the AF swelling is higher in order to catch more ions and to reach the chemo-mechanical equilibrium. This time-dependency of the chemo-mechanical response is caused by the fluid transfer between FP and LP. The mechanical stress during the stretching contributes to the fluid flow inducing a chemical stress which provokes the fluid recovering during the relaxation until equilibrium, in which chemical and mechanical stresses become equilibrated. The transferred fluid content increases with the increase in strain level. Indeed, the chemical unbalance is directly related to the fluid exchange. By increasing the prescribed axial strain, at a given strain-rate, a higher

ionic content in the tissue is required to reach the chemo-mechanical equilibrium and the observable relaxed state at the macro-scale.

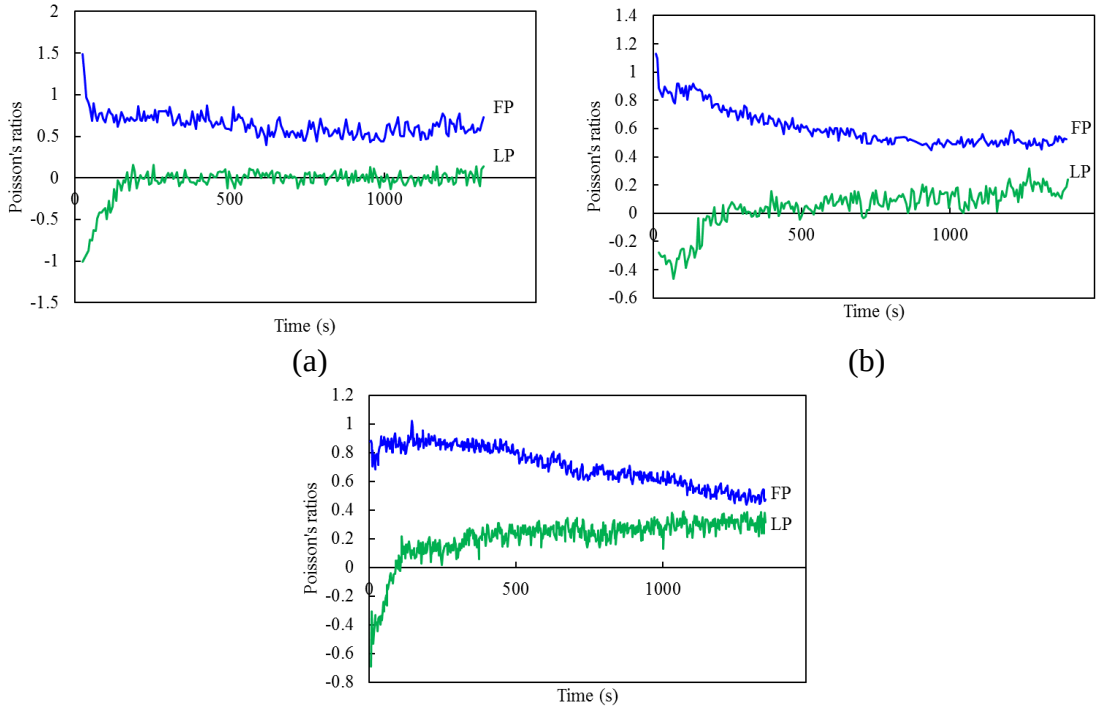

Figure 2.4.8. Evolution under relaxation of apparent Poisson's ratios for (a) 0 g/L, (b) 9 g/L and (c) 18 g/L NaCl concentration, strain-rate of 10^{-3} s^{-1}.

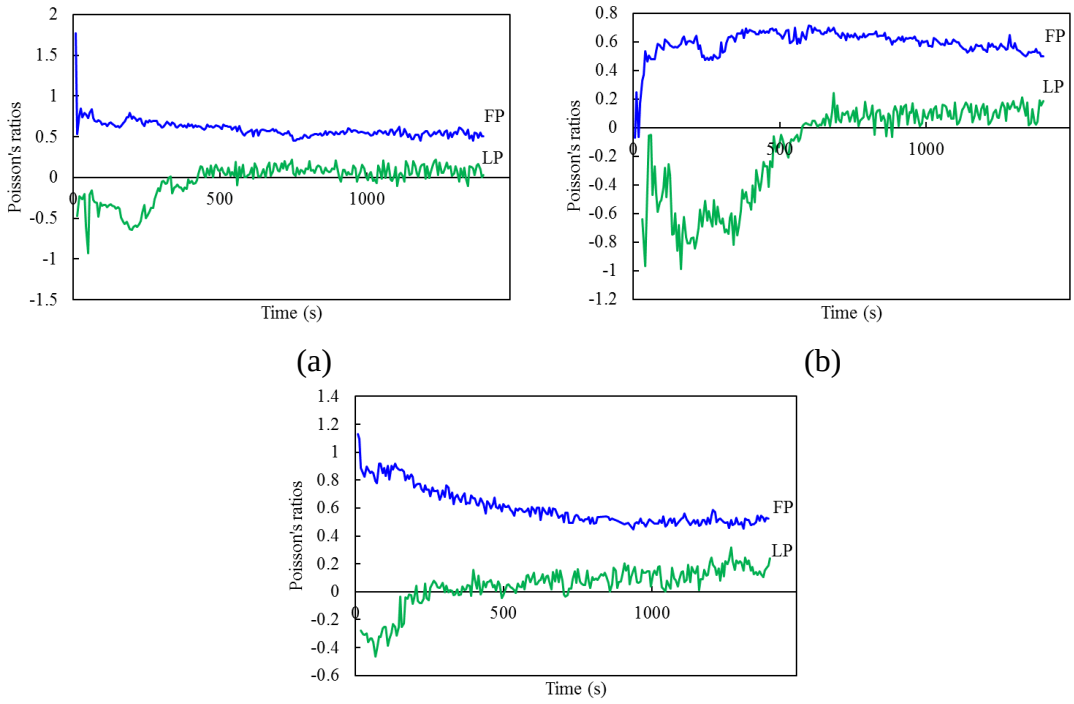

Figure 2.4.9. Evolution under relaxation of apparent Poisson's ratios for (a) 2.5×10^{-4} s^{-1}, (b) 1.25×10^{-4} s^{-1} and (c) 10^{-3} s^{-1}, 9 g/L NaCl concentration.

The osmo-relaxation in AF tissue is a reversible process dependent on fluid exchange. Other reversible factors may participate to the stress relaxation in the AF tissue such as the PGs reorganization (Sverdlik and Lanir, 2002). The stabilized relaxed-load is reached more rapidly at a zero NaCl concentration since a limiting fluid transfer is involved. Higher NaCl concentrations act on the fluid transfer inside the tissue. As a consequence, the degree, to which the AF tissue is relaxed, increases with the osmolarity (Figure 2.4.8). The hold time needed to reach the stabilized relaxed-load increases with the osmolarity. The equilibrium response clearly depends on the environment since PGs macromolecules become closer under hyper-osmotic environment in order to reduce the fluid content and to establish the chemical equilibrium. The microstructure state may be then affected by the chemical stress created with increase in mobile ionic components. The chemo-induced microstructure rearrangement is then responsible of local mechanical stresses that induce more fluid flowed out. With higher local stresses previous to the relaxation, the chemical imbalances are higher and the relaxed-load becomes lower with more fluid exchange.

Fluid transfer inside the tissue is an explanation of the chemo-relaxation response of the AF during the maintaining of the axial stretch. The quantity of flowed fluid is dependent on the rate at which the maintained axial stretch is reached. Indeed, the fluid flow is more important when the strain-rate increases. During the stretching, the local strains or stresses are heterogeneous and dependent on the applied strain-rate. Higher the strain-rate is, higher the local stresses are. At high strain-rate, the highly localized stresses favor the fluid transfer towards zones with lesser stresses. The fluid content in the tissue decreases with the intensity of the local stresses and with the strain-rate. The relaxation response is then dependent on the fluid exchange during the previous stretching rate (Figure 2.4.9). Since a higher amount of fluid is transferred due to local stresses during the initial stretching when the strain-rate increases, the chemical unbalance is higher. Therefore, during the relaxation, a higher transferred fluid content is necessary to

reach the chemo-mechanical equilibrium of the tissue. That leads to the observable increase of the relaxation rate at the macro-scale (Figure 2.4.6).

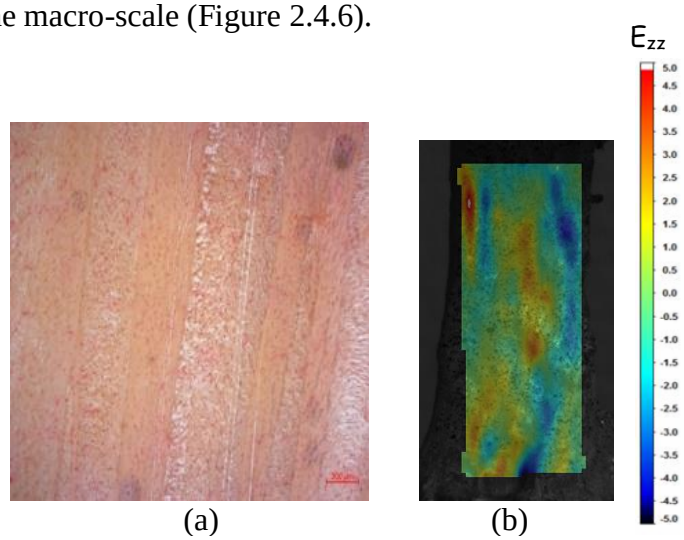

(a) (b)

Figure 2.4.10. Lamellae and inter-lamellae zones in LP: (a) microscopy (section stained using safranin-O) and (b) DIC.

Recall that the lamellae of AF are reinforced with oriented collagen fibers and are inter-spaced with a ground substance without collagen fibers between them. This feature is observable in the section observed through a binocular microscope in Figure 2.4.10a. Although the role of the inter-lamellae zone is not fully known (Pezowicz et al., 2006; Tavakoli et al., 2016), it is believed that it contributes to the fluid exchange. A LP transversal strain plot is given in Figure 2.4.10b and shows that swelled zones are alternated with contracted zones.

The swelling in FP and the tightening in LP suggest a transfer mechanism between the two plans during the relaxation. Lower local stresses in LP may explain the fluid transport towards this plan and the chemical stresses induce the partial return of a fluid content. Figure 2.4.11 gives our interpretation in the form of a schematic view. Fluid flow out creates ionic imbalance and chemical stress. The mechanical strains/stresses are higher in FP and water flows out towards ground substance in which the stress state is lower. The tightening in FP due to flow out and the swelling in LP is observed due to this difference in local mechanical stresses. The difference in chemical state forces a part of fluid to come back to its equilibrium state and

apparent Poisson's ratios to reach usual bounds. In equilibrium, the osmotic pressure is equilibrated by the mechanical state (Maroudas, 1976).

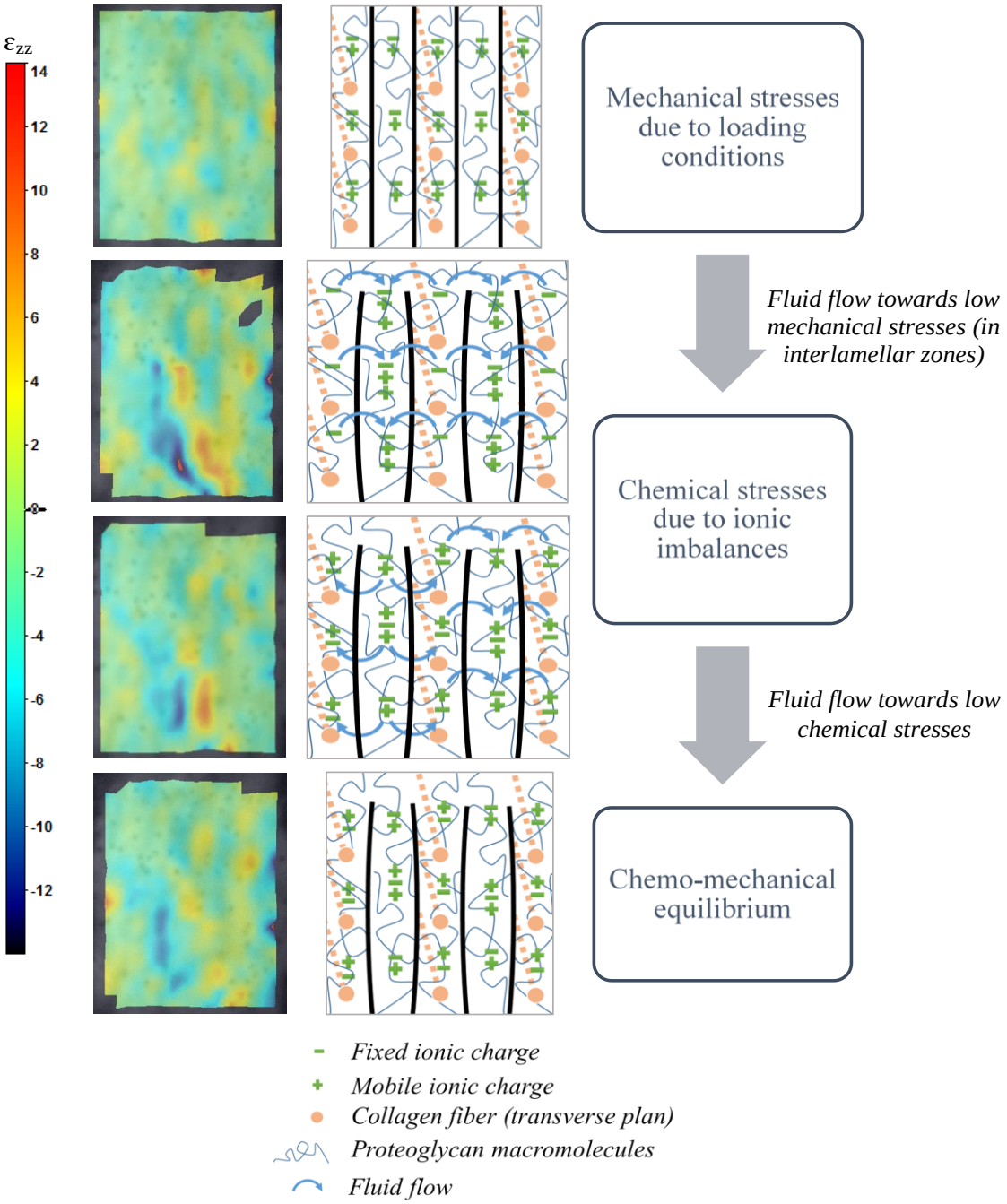

Figure 2.4.11. Chemo-mechanical mechanisms in LP.

2.4.5. Partial conclusions

This last part of the Chapter 2 is a first observation of the establishment of chemo-mechanical equilibrium via an optical strain measuring technique. The determination of the transversal response of AF allowed a better understanding of what the nature is able to do to optimize the IVD functionality by involving auxeticity, inelasticity and osmolarity effects. The time and chemical-dependency of the auxetic behavior in AF lamellae plan highlights the osmo-inelastic coupling. The chemo-mechanical equilibrium, altered by osmolarity and strain-rate, is a process involving local changes in fluid content until a balance between chemical and mechanical states. Further works are needed to validate this behavior to human AF especially in relation with aging and degeneration. Also, the experimental observations provided in this work stimulate the need to formulate an osmo-inelastic modeling of AF which would offer a clearer multi-scale understanding of the IVD function. This aspect constitutes an important issue treated in the next chapter.

2.4.6. References

Adam, C., Rouch, P., Skalli, W., 2015. Inter-lamellar shear resistance confers compressive stiffness in the intervertebral disc: an image-based modelling study on the bovine caudal disc. Journal of Biomechanics 48, 4303-4308.

Alini, M., Eisenstein, S.M., Ito, K., Little, C., Kettler, A.A., Masuda, K., Melrose, J., Ralphs, J., Stokes, I., Wilke, H.J., 2008. Are animal models useful for studying human disc disorders/degeneration? European Spine Journal 17, 2-19.

Ambard, D., Cherblanc, F., 2009. Mechanical behavior of annulus fibrosus: a microstructural model of fibers reorientation. Annals of Biomedical Engineering 37, 2256-2265.

Baldit, A., Ambard, D., Cherblanc, F., Royer, P., 2014. Experimental analysis of the transverse mechanical behaviour of annulus fibrosus tissue. Biomechanics and Modeling in Mechanobiology 13,643-652.

Bruehlmann, S.B., Hulme, P.A., Duncan, N.A., 2004. In situ intercellular mechanics of the bovine outer annulus fibrosus subjected to biaxial strains. Journal of Biomechanics 37, 223-231.

Costi, J.J., Hearn, T.C., Fazzalari, N.L., 2002. The effect of hydration on the stiffness of intervertebral discs in an ovine model. Clinical Biomechanics 17, 446-455.

Drost, M.R., Willems, P., Snijders, H., Huyghe, J.M., Janssen, J.D., Huson, A., 1995. Confined compression of canine annulus fibrosus under chemical and mechanical loading. Journal of Biomechanical Engineering 117, 390-396.

Ebara, S., Iatridis, J.C., Setton, L.A., Foster, R.J., Mow, V.C., Weidenbaum, M., 1996. Tensile properties of nondegenerate human lumbar anulus fibrosus. Spine 21, 452-461.

Elliott, D.M., Setton, L.A., 2001. Anisotropic and inhomogeneous tensile behavior of the human annulus fibrosus: experimental measurement and material model predictions. Journal of Biomechanical Engineering 123, 256-263.

Emanuel, K.S., van der Veen, A.J., Rustenburg, C.M.E., Smit, T.H., Kingma, I., 2018. Osmosis and viscoelasticity both contribute to time-dependent behaviour of the intervertebral disc under compressive load: a caprine in vitro study. Journal of Biomechanics 70, 10-15.

Eyre, D.R., 1979. Biochemistry of the intervertebral disc. International Review of Connective Tissue Research 8, 227-291.

Gatt, R., Wood, M.V., Gatt, A., Zarb, F., Formosa, C., Azzopardi, K.M., Casha, A., Agius, T.P., Schembri-Wismayer, P., Attard, L., Chockalingam, N., Grima, J.N., 2015. Negative Poisson's ratios in tendons: an unexpected mechanical response. Acta Biomaterialia 24, 201-208.

Guerin, H.A.L., Elliott, D.M., 2006. Degeneration affects the fiber reorientation of human annulus fibrosus under tensile load. Journal of Biomechanics 39, 1410-1418.

Holzapfel, G.A., Schulze-Bauer, C.A.J., Feigl, G., Regitnig, P., 2005. Single lamellar mechanics of the human lumbar anulus fibrosus. Biomechanics and Modeling in Mechanobiology 3, 125-140.

Inoue, H., Takeda, T., 1975. Three-dimensional observation of collagen framework of lumbar intervertebral discs. Acta Orthopaedica 46, 949-956.

Johannessen, W., Vresilovic, E.J., Wright, A.C., Elliott, D.M., 2004. Intervertebral disc mechanics are restored following cyclic loading and unloaded recovery. Annals of Biomedical Engineering 32, 70-76.

Kemper, A.R., McNally, C., Duma, S.M., 2007. The influence of strain rate on the compressive stiffness properties of human lumbar intervertebral discs. Biomedical Sciences Instrumentation 43, 176-181.

Lees, C., Vincent, J.F., Hillerton, J.E., 1991. Poisson's ratio in skin. Bio-Medical Materials and Engineering 1, 19-23.

Lewis, N.T., Hussain, M.A., Mao, J.J., 2008. Investigation of nano-mechanical properties of annulus fibrosus using atomic force microscopy. Micron 39, 1008-1019.

Maroudas, A., 1976. Balance between swelling pressure and collagen tension in normal and degenerate cartilage. Nature 260, 808-809.

Mengoni, M., Luxmoore, B.J., Wijayathunga, V.N., Jones, A.C., Broom, N.D., Wilcox, R.K., 2015. Derivation of inter-lamellar behaviour of the intervertebral disc annulus. Journal of the Mechanical Behavior of Biomedical Materials 48, 164-172.

Michalek, A.J., Buckley, M.R., Bonassar, L.J., Cohen, I., Iatridis, J.C., 2009. Measurement of local strains in intervertebral disc anulus fibrosus tissue under dynamic shear: contributions of matrix fiber orientation and elastin content. Journal of Biomechanics 42, 2279-2285.

Moo, E.K., Sibole, S.C., Han, S.K., Herzog, W., 2018. Three-dimensional micro-scale strain mapping in living biological soft tissues. Acta Biomaterialia 70, 260-269.

Nachemson, A., Morris, J.M., 1964. In vivo measurements of intradiscal pressure: discometry, a method for the determination of pressure in the lower lumbar discs. The Journal of Bone and Joint Surgery 46, 1077-1092.

Newell, N., Grigoriadis, G., Christou, A., Carpanen, D., Masouros, S.D., 2016. Material properties of bovine intervertebral discs across strain rates. Journal of the Mechanical Behavior of Biomedical Materials 65, 824-830.

Newell, N., Little, J.P., Christou, A., Adams, M.A., Adam, C.J., Masouros, S.D., 2017. Biomechanics of the human intervertebral disc: a review of testing techniques and results. Journal of the Mechanical Behavior of Biomedical Materials 69, 420-434.

O'Connell, G.D., Guerin, H.L., Elliott, D.M., 2009. Theoretical and uniaxial experimental evaluation of human annulus fibrosus degeneration. Journal of Biomechanical Engineering 131, 1-7.

O'Connell, G.D., Sen, S., Elliott, D.M., 2012. Human annulus fibrosus material properties from biaxial testing and constitutive modeling are altered with degeneration. Biomechanics and Modeling in Mechanobiology 11, 493-503.

Parsons, E., Boyce, M.C., Parks, D.M., 2004. An experimental investigation of the large-strain tensile behavior of neat and rubber-toughened polycarbonate. Polymer 45, 2665-2684.

Pezowicz, C.A., Robertson, P.A., Broom, N.D., 2006. The structural basis of interlamellar cohesion in the intervertebral disc wall. Journal of Anatomy 208, 317-330.

Race, A., Broom, N.D., Robertson, P., 2000. Effect of loading rate and hydration on the mechanical properties of the disc. Spine 25, 662-669.

Roux, D.C., Cooper-White, J.J., McKinley, G.H., Tirtaatmadja, V., 2003. Drop impact of newtonian and elastic fluids. Physics of Fluids 15, S12-S12.

Schmidt, H., Reitmaier, S., Graichen, F., Shirazi-Adl, A., 2016. Review of the fluid flow within intervertebral discs - How could in vitro measurements replicate in vivo? Journal of Biomechanics 49, 3133-3146.

Singha, K., Singha, M., 2012. Biomechanism profile of intervertebral disc's (IVD): strategies to successful tissue engineering for spinal healing by reinforced composite structure. Journal of Tissue Science & Engineering 3, 1000118.

Skaggs, D.L., Weidenbaum, M., Iatridis, J.C., Ratcliffe, A., Mow, V.C., 1994. Regional variation in tensile properties and biochemical composition of the human lumbar anulus fibrosus. Spine 19, 1310-1319.

Sverdlik, A., Lanir, Y., 2002. Time-dependent mechanical behavior of sheep digital tendons, including the effects of preconditioning. Journal of Biomechanical Engineering 124, 78-84.

Tavakoli, J., Elliott, D.M., Costi, J.J., 2016. Structure and mechanical function of the inter-lamellar matrix of the annulus fibrosus in the disc. Journal of Orthopedic Research 34, 1307-1315.

Tavakoli, J., Costi, J.J., 2018. New findings confirm the viscoelastic behaviour of the inter-lamellar matrix of the disc annulus fibrosus in radial and circumferential directions of loading. Acta Biomaterialia 71, 411-419.

Timmins, L.H., Wu, Q., Yeh, A.T., Moore, J.E., Greenwald, S.E., 2010. Structural inhomogeneity and fiber orientation in the inner arterial media. American Journal of Physiology - Heart and Circulatory Physiology 298, 1537-1545.

Vergari, C., Mansfield, J., Meakin, J.R., Winlove, P.C., 2016. Lamellar and fibre bundle mechanics of the annulus fibrosus in bovine intervertebral disc. Acta Biomaterialia 37, 14-20.

Vergroesen, P.P.A., Emanuel, K.S., Peeters, M., Kingma, I., 2018. Are axial intervertebral disc biomechanics determined by osmosis? Journal of Biomechanics 70, 4-9.

Veronda, D.R., Westmann, R.A., 1970. Mechanical characterization of skin-Finite deformations. Journal of Biomechanics 3, 111-124.

Williams, J.L., Lewis, J.L., 1982. Properties and an anisotropic model of cancellous bone from the proximal tibial epiphysis. Journal of Biomechanical Engineering 104, 50-56.

Chapter 3: Constitutive modeling and simulation

Part 1: A chemo-mechanical constitutive model for osmo-inelastic effects in the annulus fibrosus[5]

Abstract

The annulus fibrosus (AF) exhibits complex osmo-inelastic effects responsible for unusual transversal behavior with a Poisson's ratio higher than 0.5 in fibers plan and negative in lamellae plan. In this part of the Chapter 3, we present a new chemo-mechanical approach for the prediction of the AF intrinsic osmo-inelastic response in relation with the microstructure of the layered reinforced soft tissue, the biochemical environment and the mechanical loading conditions. The constitutive model introduces the coupling between the deformation-induced inelastic stress in the tangled extracellular matrix and the stress-free swelling due to internal fluid content variation by osmosis. The proposed formulation is implemented into a finite element code and numerical simulations on AF specimens, including explicitly lamellae and interlamellar zones, are presented to illustrate the capability of the approach. The simulated results compared favorably with experimental observations, in terms of stress-stretch curve and transversal behavior with variation in osmolarity and strain-rate conditions, obtained by monitoring the full-field strain in AF specimens using digital image correlation method. The stress/strain patterns in the AF model simulation provide valuable insights about the role of the interlamellar zone in the osmo-inelastic mechanisms.

Keywords: Annulus fibrosus; Constitutive modeling; Osmo-inelastic coupling; Transversal behavior; Finite element analysis.

[5] This Part of this chapter is based on the following paper: Amil Derrouiche, Fahmi Zaïri, Fahed Zaïri, A chemo-mechanical constitutive model for osmo-inelastic effects in the annulus fibrosus, *submitted*.

3.1.1. Partial introduction

The response of the annulus fibrosus (AF) presents a set of complex history-dependent effects related to its microstructure and local fluid exchange. The AF is constituted by proteoglycans (PGs) macromolecules and regularly-oriented collagen fibers (Inoue and Takeda, 1975; Eyre, 1979; Guerin and Elliott, 2006), immerged in a physiological solution of water and ions (Maroudas, 1976; Drost et al., 1995; Schmidt et al., 2016). It is generally described as an anisotropic fiber-reinforced deformable solid, the collagen network ensuring the mechanical resistance. Radial and circumferential variations in content and orientation of collagen fibers imply a regional variation in tissue mechanical response (Skaggs et al., 1994; Ebara et al., 1996; Holzapfel et al., 2005; Michalek et al., 2009). The chemo-mechanical constitutive response of soft tissues is intrinsically linked to the osmolarity. The osmotic effect, coming from negatively charged extracellular matrix (ECM), induces modifications in PGs macromolecules organization resulting in modifications in the AF mechanical response. In addition, the modulation of the PGs density induces an evolution of the osmotic effect. A strong coupling exists therefore between chemical and mechanical features.

Over the years, various constitutive models were proposed to relate the microstructure to the nonlinear macro-response in which fiber content and orientation are explicitly taken into account. The soft tissue is considered either as a purely elastic medium (Shirazi-Adl et al. 1986; Weiss et al., 1996; Eberlein et al., 2004; Wagner and Lotz, 2004; Guo et al., 2006; Peng et al., 2006) or a viscoelastic medium (Wang et al., 1997; Holzapfel et al., 2000). Alternatively, to consider the interstitial fluid, other authors proposed constitutive models based on a fluid-solid representation of the soft tissue, i.e. a porous medium including an interstitial fluid (Mow et al., 1980; Simon et al., 1985; Argoubi and Shirazi-Adl, 1996; Iatridis et al., 1998; Ayotte et al., 2000; Klisch and Lotz, 2000). The chemo-mechanical coupling was incorporated by adding the

ionic population as a supplementary phase in a fluid-solid representation (Lanir, 1987; Lai et al., 1991; Frijns et al. 1997; Ehlers et al., 2008). By distinguishing anions and cations, the effects of fixed and mobile charges were also taken into account (Gu et al., 1998; Iatridis et al., 2003; Galbusera et al., 2011).

There is a considerable qualitative understanding of the chemical factors that govern the response of soft tissues. However, the coupling between osmotic effects and inelastic effects is far to be fully understood yet in AF (Emanuel et al., 2018; Vergroesen et al., 2018). The osmo-inelastic coupling in AF involves very complex muti-scale phenomena. At the micro-scale, the PGs macromolecules rearrangement induces inelastic effects and are strongly affected by the variation of fluid content by osmotic effect. Establishing predictive models for the osmo-inelastic response of AF remain a challenging task. At a higher scale, the concentric lamellar structure has a complex organization in which the zone between fiber reinforced lamellae (interlamellar zone) plays an important role in the IVD biomechanics (Pezowicz et al., 2006; Yu et al., 2005, 2007; Schollum et al., 2009). A literature survey shows that there exists very few contributions dealing with the constitutive modeling of IVD biomechanics taking into account the interlamellar interactions in spite of their significance (Guerin and Elliott, 2007; Nerurkar et al., 2011; Labus et al., 2014; Adam et al., 2015). A rigorous modeling of the time-dependent behavior requires to take into account the effects of the biochemical environment and the actual microstructure of the reinforced soft tissue at different scales.

The aim of this part of the Chapter 3 is to provide a quantitative prediction of the osmo-inelastic coupling in AF in relation with heterogeneous and anisotropic features. The proposed chemo-mechanical constitutive model is a new approach in the description of the soft tissue able to reproduce the osmo-induced volumetric changes in relation with microstructure, biochemical environment and inelastic effects in terms of strain-rate dependency and hysteresis. The present

formulation is implemented into a finite element program and numerical simulations on AF specimens, including explicitly lamellae and interlamellar zones, are conducted using the implemented constitutive model. The validity of our approach is examined by comparing the numerical simulations with experimental observations, in terms of macro-stress and transversal response, obtained using full-field strain measurements by digital image correlation (DIC) method. The comparison with experiments is performed for different saline concentrations and strain-rates. The simulation model is then used to appreciate the local fields in the aim to bring a better understanding of the interlamellar zone role in the IVD working, in relation with the biochemical environment and the mechanical loading conditions.

Section 2 presents the main elements of the model formulation. Section 3 is devoted to the numerical application using the implemented model and the comparison with experimental observations. Concluding remarks are finally given in Section 4.

3.1.2. Model formulation

The following notation is used throughout the text. Tensors and vectors are denoted by normal boldfaced letters and italicized boldfaced letters, respectively, while scalars and individual components of vectors and tensors are denoted by normal italicized letters. The superposed dot designates the time derivative.

3.1.2.1. Constitutive equations

The AF is constituted by negatively charged ECM, superimposed collagen fibers and mobile charges as illustrated in Figure 3.1.1. ECM consists of randomly distributed PGs molecules. These molecules are very large with glycosaminoglycan chains that have ionic imbalances. This particularity is common for soft tissues and gives chemical properties. These negative charges are fixed within ECM and attract mobile cations dissolved in the surrounding physiological

fluid to maintain electroneutrality by osmotic effect. The latter interactions are primarily responsible for the chemo-mechanical coupling, that is essential for understanding IVD functionality. ECM and collagen fibers are supposed to participate to deformation via the Taylor assumption, i.e. they act in parallel. In the present model, the origin of the history-dependent phenomena at the macro-scale are attributed to the PGs rearrangement and to the osmo-induced volumetric changes.

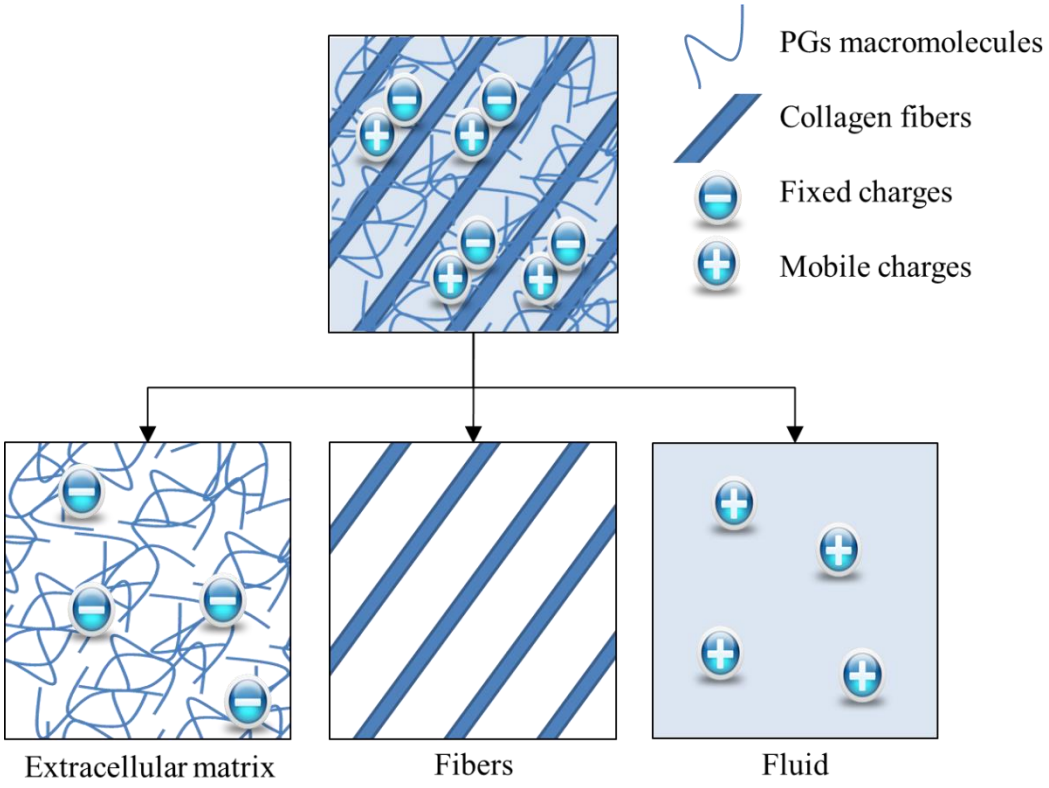

Figure 3.1.1. Decomposition of AF into negatively charged PGs macromolecules, superimposed collagen fibers and mobile charges. The reaction of PGs with mobile charges of physiological fluid results in the osmo-induced volumetric changes.

3.1.2.1.1. Kinematics

According to continuum mechanics, the deformation gradient is defined as: $\mathbf{F} = \nabla_X \boldsymbol{\varphi}$, $\boldsymbol{x} = \boldsymbol{\varphi}(\boldsymbol{X}, t)$ being the position vector in the current configuration Ω and $\boldsymbol{X}$ the position vector in the reference configuration Ω_0 of a given material point. The concept of the deformation

gradient decomposition (Lee, 1969; Holzapfel and Simo, 1996) is used to consider the chemical dilatation effects and the inelastic effects. It is based on a conceptual sequence of configurations as illustrated in Figure 3.1.2 in which we consider two intermediate configurations: the chemical stress-free configuration Ω_{chem} and the relaxed configuration Ω_{relax}.

The chemo-mechanical response can be described as the multiplicative decomposition of the deformation gradient $\mathbf{F}$ into a chemical part $\mathbf{F}_{chem}$ and a mechanical part $\mathbf{F}_{mech}$:

$$\mathbf{F} = \mathbf{F}_{chem}\mathbf{F}_{mech} \tag{1}$$

in which $\mathbf{F}_{chem}$ is the stress-free swelling due to internal fluid content variation and $\mathbf{F}_{mech}$ is the deformation-induced stress.

The mechanical deformation is assumed isochoric, i.e. the determinant J_{mech} of the mechanical deformation gradient tensor $\mathbf{F}_{mech}$ is:

$$J_{mech} = \det\left(\mathbf{F}_{mech}\right) = 1 \tag{2}$$

The chemical part $\mathbf{F}_{chem}$ is expressed by:

$$\mathbf{F}_{chem} = J_{chem}^{1/3}\mathbf{I} \tag{3}$$

where $\mathbf{I}$ is the unit tensor and $J_{chem} = \det\left(\mathbf{F}_{chem}\right) > 0$ denotes the determinant of the chemical deformation gradient tensor $\mathbf{F}_{chem}$. The mechanical incompressibility imposes that $\det\left(\mathbf{F}\right) = J_{chem}$.

The mechanical deformation gradient $\mathbf{F}_{mech}$ is multiplicatively decomposed into an elastic part $\mathbf{F}_e$ and an inelastic (viscous) part $\mathbf{F}_v$ as:

$$\mathbf{F}_{mech} = \mathbf{F}_e\mathbf{F}_v \tag{4}$$

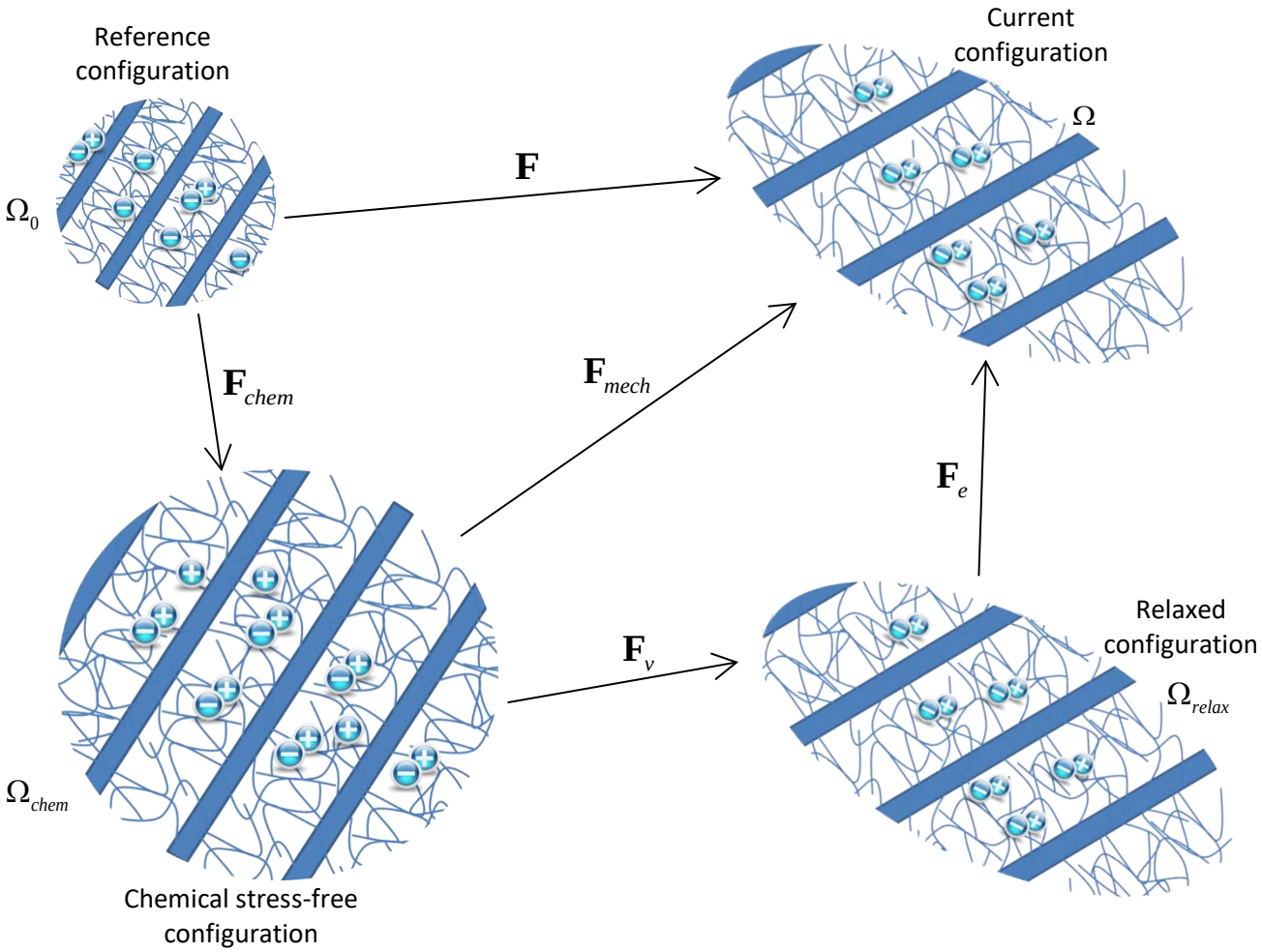

Figure 3.1.2. Multiplicative decomposition of the deformation gradient.

The gradient tensor $\mathbf{L} = \nabla_x \boldsymbol{v}$ of the spatial velocity $\boldsymbol{v} = \partial \boldsymbol{\varphi} / \partial t$ can be decomposedinto a chemical part $\mathbf{L}_{chem}$ and a mechanical part $\mathbf{L}_{mech}$ in an additive manner as:

$$\mathbf{L} = \underbrace{\dot{\mathbf{F}}_{mech}\mathbf{F}_{mech}^{-1}}_{\mathbf{L}_{mech}} + \underbrace{\mathbf{F}_{mech}\dot{\mathbf{F}}_{chem}\mathbf{F}_{chem}^{-1}\mathbf{F}_{mech}^{-1}}_{\mathbf{L}_{chem}} \tag{5}$$

in which the chemical velocity gradient tensor $\mathbf{L}_{chem}$ is given by:

$$\mathbf{L}_{chem} = \frac{\dot{J}_{chem}}{3J_{chem}}\mathbf{I} \tag{6}$$

The mechanical velocity gradient tensor $\mathbf{L}_{mech}$ can be further decomposed into an elastic part $\mathbf{L}_e$ and an inelastic part $\mathbf{L}_v$ as:

$$\mathbf{L}_{mech} = \underbrace{\dot{\mathbf{F}}_e \mathbf{F}_e^{-1}}_{\mathbf{L}_e} + \underbrace{\mathbf{F}_e \dot{\mathbf{F}}_v \mathbf{F}_v^{-1} \mathbf{F}_e^{-1}}_{\mathbf{L}_v} \tag{7}$$

The inelastic velocity gradient tensor $\mathbf{L}_v$ consists of a symmetric inelastic rate tensor $\mathbf{D}_v$ and an antisymmetric inelastic spin tensor $\mathbf{W}_v$:

$$\mathbf{L}_v == \underbrace{\frac{1}{2}\left(\mathbf{L}_v + \mathbf{L}_v^{\mathrm{T}}\right)}_{\mathbf{D}_v} + \underbrace{\frac{1}{2}\left(\mathbf{L}_v - \mathbf{L}_v^{\mathrm{T}}\right)}_{\mathbf{W}_v} \tag{8}$$

in which the superscript T indicates the transpose quantity.

A common assumption is to consider, with no loss in generality, the irrotationality of the inelastic flow (Gurtin and Anand, 2005). The inelastic spin rate $\mathbf{W}_v$ drops out and $\mathbf{L}_v = \mathbf{D}_v$.

The above equations for the kinematics are general and the constitutive equations for the PGs macromolecules and the collagen fibers will define the specificity of the chemo-mechanical approach for the prediction of the AF intrinsic response.

3.1.2.1.2. Osmo-inelastic effects

The PGs macromolecules may be described by hyperelastic laws derived from free energy functions. In the present approach, the free energy function ψ_{PGs} of PGs is additively split into a mechanical (isochoric) part ψ_{mech} and a chemical (volumetric) part ψ_{chem}:

$$\psi_{PGs} = \psi_{mech} + \psi_{chem} \tag{9}$$

A purely elastic contribution ψ_e and an inelastic contribution ψ_v interact to represent the viscoelasticity of PGs macromolecular network. These two contributions are added to form the mechanical part ψ_{mech}:

$$\psi_{mech} = \psi_e + \psi_v \tag{10}$$

The Gent strain energy function is used to represent the purely elastic part ψ_e (Gent, 1996):

$$\psi_e = -\frac{\mu I_{1\lim}}{2}\ln\left(1-\frac{I_{1e}-3}{I_{1\lim}}\right) \tag{11}$$

where μ is the shear modulus, $I_{1\lim}$ is a parameter related to the limiting extensibility of PGs macromolecular network and $I_{1e} = \text{trace}\mathbf{B}_e$ is the elastic first stretch invariant, $\mathbf{B}_e = \mathbf{F}_e\mathbf{F}_e^T$ being the elastic left Cauchy-Green strain tensor.

The inelastic contribution ψ_v is given by a Neo-Hookean formulation:

$$\psi_v = C_v\left(I_{1v}-3\right) \tag{12}$$

where C_v is a parameter and $I_{1v} = \text{trace}\mathbf{B}_v$ is the inelastic first stretch invariant, $\mathbf{B}_v = \mathbf{F}_v\mathbf{F}_v^T$ being the inelastic left Cauchy-Green strain tensor.

The chemical part ψ_{chem} is associated with the osmo-induced volumetric changes (Miehe, 1995):

$$\psi_{chem} = \frac{1}{4}k\left(J_{chem}^2 - 1 - 2\ln J_{chem}\right) \tag{13}$$

in which k is the bulk modulus.

The chemo-mechanical equilibrium is reached when a balance exists between the external mechanical loading and the volumetric tissue deformation induced by the internal fluid content. A chemical disorder is expected under a mechanical stress due to internal fluid content variation, which in turn induces a variation in the mechanical response. In that sense, a strong chemo-mechanical coupling exists. We propose to express the determinant J_{chem} as a function of the internal fluid content:

$$J_{chem} = \left(\alpha\left(n_{f_{ref}} + n_{f_m} - 2n_{f_s}\right) f\left(c_{ext}\right)\right)^{3/2} \tag{14}$$

where α is a parameter, $n_{f_{ref}}$ is the reference fluid content in the saturated tissue, n_{f_s} is the fluid content during the swelling, n_{f_m} is the fluid content during the mechanical loading and $f\left(c_{ext}\right)$ is a function of the external ionic concentration c_{ext}:

$$f\left(c_{ext}\right) = s_1 + s_2 \exp\left(-s_3 c_{ext}\right) \tag{15}$$

in which s_1, s_2 and s_3 are parameters.

The following equations are proposed for the evolution of the internal fluid content during the swelling n_{f_s} and during the mechanical loading n_{f_m}:

$$\dot{n}_{f_s} = \beta_s \left(1 - \frac{n_{f_s}}{n_{f_{ref}}}\right) \text{ and } \dot{n}_{f_m} = \beta_m \left(1 - \frac{n_{f_m}}{n_{f_{\lim}}}\right) \tag{16}$$

in which β_s and β_m are parameters, and $n_{f_{\lim}}$ is the limiting fluid content taken equal to 0.99.

The external ionic concentration c_{ext} is always in equilibrium and is given by:

$$c_{ext} = \frac{n_{f_m}}{n_{f_{\lim}}} c_{sol} \tag{17}$$

where c_{sol} is the ionic concentration of the surrounding biochemical environment.

As an expression of chemo-mechanical interactions the fixed charged density c_F of PGs macromolecules depends on the volumetric tissue deformation J_{chem} and is expressed as (Lanir, 1987; Schroeder et al., 2007):

$$c_F = \frac{n_{f_{ref}} c_{F_{ref}}}{n_{f_{ref}} - 1 + J_{chem}} \tag{18}$$

in which $c_{F_{ref}}$ is the reference fixed charged density in the saturated tissue.

The chemical equilibrium is assumed to be instantaneous with the surrounding biochemical environment. The electro-neutrality in the tissue is supposed to be always maintained between

mobile ions, c^+ and c^-, and fixed charges c_F: $c^+ = c^- + c_F$. The chemo-mechanical coupling induced by the fluid flow is created by differences between internal osmotic pressure $\pi_{int} = \phi_{int} RT\left(c^+ + c^-\right)$ and external osmotic pressure $\pi_{ext} = \phi_{ext} RT\left(c_{ext}^+ + c_{ext}^+\right) = 2\phi_{ext} RTc_{ext}$ in the condition of saturated tissue, in which ϕ_{int} and ϕ_{ext} are osmotic coefficients, R is the universal gas constant and T is the absolute temperature.

The concentrations of mobile cations and anions, c^+ and c^-, are (Huyghe and Janssen, 1997):

$$c^{\pm} = \frac{\pm c_F + \sqrt{c_F^2 + 4\dfrac{\left(\gamma_{ext}^{\pm}\right)^2}{\left(\gamma_{int}^{\pm}\right)^2} c_{ext}^2}}{2} \tag{19}$$

where $\gamma_{int}^{\pm}$ and $\gamma_{ext}^{\pm}$ are the activity coefficients.

Finally, the osmotic pressure in equilibrium becomes (Schroeder et al., 2007):

$$\Delta\pi = \phi_{int} RT\left(\sqrt{c_F^2 + 4\frac{\left(\gamma_{ext}^{\pm}\right)^2}{\left(\gamma_{int}^{\pm}\right)^2} c_{ext}^2}\right) - 2\phi_{ext} RTc_{ext} \tag{20}$$

The bulk modulus k in Eq. (13) may be evaluated from the osmotic pressure:

$$\Delta\pi = k\left(J_{chem} - 1\right) \tag{21}$$

The mechanical-based Cauchy stress $\boldsymbol{\sigma}_{mech} = \boldsymbol{\sigma}_e + \boldsymbol{\sigma}_v$ and the chemical-based Cauchy stress $\boldsymbol{\sigma}_{chem}$ are obtained from the differentiation of the free energy functions with respect to the corresponding deformations:

$$\boldsymbol{\sigma}_e = 2\mathbf{F}_{mech}\frac{\partial\psi_e}{\partial\mathbf{C}_{mech}}\mathbf{F}_{mech}^T,\ \boldsymbol{\sigma}_v = 2\mathbf{F}_e\frac{\partial\psi_v}{\partial\mathbf{C}_e}\mathbf{F}_e^T \text{ and } \boldsymbol{\sigma}_{chem} = \frac{\partial\psi_{chem}}{\partial J_{chem}}\mathbf{I} \tag{22}$$

in which $\mathbf{C}_{mech} = \mathbf{F}_{mech}^T\mathbf{F}_{mech}$ and $\mathbf{C}_e = \mathbf{F}_e^T\mathbf{F}_e$ are the mechanical and elastic right Cauchy-Green strain tensors.

The terms $\boldsymbol{\sigma}_e$ and $\boldsymbol{\sigma}_v$ are two traceless tensors, i.e. $\text{trace}(\boldsymbol{\sigma}_e)=\text{trace}(\boldsymbol{\sigma}_v)=0$, due to mechanical incompressibility and $\boldsymbol{\sigma}_{chem}=p\mathbf{I}$ with the hydrostatic pressure $p=\text{trace}(\boldsymbol{\sigma})/3$.

The evolution law for the inelastic rate tensor, used to compute the inelastic part of the deformation gradient, has the following form:

$$\mathbf{D}_v=\dot{\gamma}_v\frac{\boldsymbol{\sigma}'_v}{\sqrt{2}\tau_v} \tag{23}$$

in which $\dot{\gamma}_v$ is the accumulated inelastic strain rate and τ_v is the effective inelastic shear stress defined, respectively, as:

$$\dot{\gamma}_v=\sqrt{\text{trace}(\mathbf{D}_v\mathbf{D}_v)}\ \text{and}\ \tau_v=\sqrt{\frac{1}{2}\text{trace}(\boldsymbol{\sigma}'_v\boldsymbol{\sigma}'_v)} \tag{24}$$

the term $\boldsymbol{\sigma}'_v=\boldsymbol{\sigma}_v-1/3\,\text{trace}(\boldsymbol{\sigma}_v)\mathbf{I}$ being the deviatoric part of the inelastic Cauchy stress tensor $\boldsymbol{\sigma}_v$.

The accumulated inelastic strain rate takes the form of the Bergstrom-Boyce power law (Bergstrom and Boyce, 1998):

$$\dot{\gamma}_v=d\frac{1}{\left(\sqrt{I_{1v}/3}-1\right)^m}\tau_v \tag{25}$$

where d and m are parameters governing the rate of relaxation needed to reach the mechanical equilibrium state.

Numerical stability of Eq. (25) due to singularity at the beginning of the loading process is ensured by adding a perturbation coefficient κ to $\sqrt{I_{1v}/3}$ (κ=0.01 is taken throughout our simulations).

3.1.2.1.3. Collagen fibers contribution

The AF has a layered structure with an increase in collagen fiber content from inner to outer parts of IVD, and change in collagen fiber orientation from dorsal to ventral parts (Inoue and Takeda, 1975; Eyre, 1979; Guerin and Elliott, 2006). The theory of fiber-reinforced composites may be used to relate the AF microstructure to the mechanical behavior (Holzapfel et al., 2000). The free energy function ψ_f of collagen fibers is given by (Cantournet et al., 2007):

$$\psi_f = A_1\left(\lambda_f^2 - 1\right) + A_2\left(\lambda_f^2 - 1\right)^2 - 2A_1 \ln\left(\lambda_I^{x^2}\lambda_{II}^{y^2}\lambda_{III}^{z^2}\right) \tag{26}$$

where A_1 and A_2 are parameters, λ_I, λ_{II} and λ_{III} are the stretches along the principal axes of collagen fibers:

$$\lambda_I = \sqrt{\boldsymbol{e}_1\mathbf{C}\boldsymbol{e}_1},\ \lambda_{II} = \sqrt{\boldsymbol{e}_2\mathbf{C}\boldsymbol{e}_2} \text{ and } \lambda_{III} = \sqrt{\boldsymbol{e}_3\mathbf{C}\boldsymbol{e}_3} \tag{27}$$

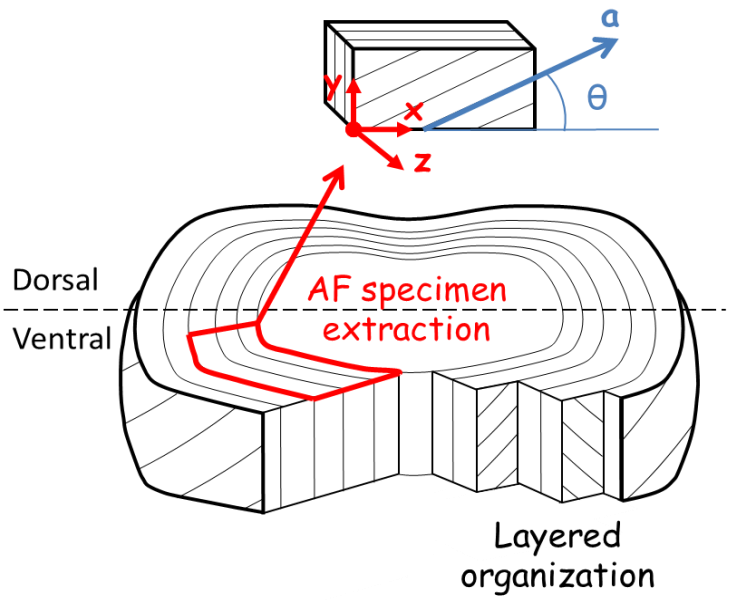

Figure 3.1.3. Layered structure of IVD and orientation of collagen fibers in the AF specimen.

and λ_f represents the stretch of collagen fibers according to the direction given by the unit vector $\boldsymbol{a}$ represented in Figure 3.1.3:

$$\lambda_f = \sqrt{\boldsymbol{a}\mathbf{C}\boldsymbol{a}},\ \boldsymbol{a} = x\boldsymbol{e}_1 + y\boldsymbol{e}_2 + z\boldsymbol{e}_3 \tag{28}$$

According to the decomposition of AF in Figure 3.1.1, the ECM and the collagen fibers are assumed to occur concurrently and without interaction. Also, the interfaces are assumed perfect and the inter-fiber interactions are not considered. The total free energy function of AF is determined using the rule of mixture:

$$\psi = \left(1-v_f\right)\psi_{PGs} + v_f\psi_f \tag{29}$$

where v_f is the collagen fiber content.

The chemo-mechanical constitutive model, described in the previous section, has been implemented into the finite element code MSC.Marc to simulate the osmo-inelastic effects in AF. This subroutine allows definition of the strain energy function (MSC.Marc, 2015) taking into account the material compressibility behavior. The main calculation steps are summarized in the flowchart of Figure 3.1.4.

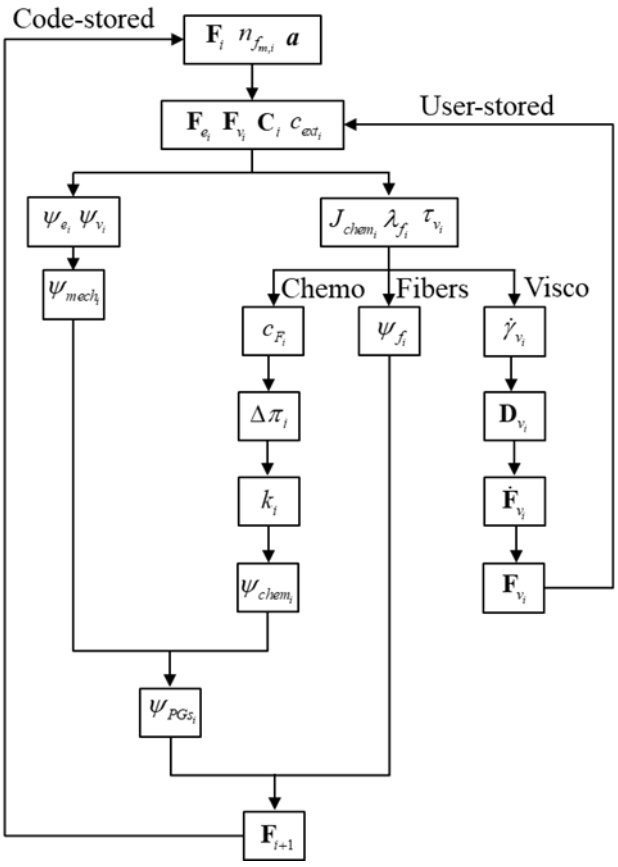

Figure 3.1.4. Flowchart of the chemo-mechanical algorithm.

3.1.3. Finite element computations and comparison with experiments

To verify our approach, tests on AF specimens were simulated using the implemented constitutive model and compared to experimental observations.

3.1.3.1. Experimental database

3.1.3.1.1. Materials and methods

Experimentally, rectangular circumferentially-oriented specimens with a regular cross-section of approximately 25 × 10 × 10 mm^3 were extracted from the ventro-lateral region (Figure 3) of bovine AF within two days after animal death. The AF specimens, stored at 4°C at maximum two days, were glued to aluminum plates using cyanoacrylate and then mounted on the testing machine (electro-pulse Instron-5500).

An accurate optical strain measuring technique, based upon DIC, was used to in-situ determine the full-field strain both in the fibers plan (FP) and in the lamellae plan (LP) of the AF specimen. The efficiency of this optical full-field technique to characterize the transversal behavior of AF specimens in LP has been demonstrated, as far as we know, only by Baldit et al. (2013). This is a very attractive technique because of its accuracy and its spatial resolution performances for strain gradient measurement. Images of the AF specimen surface were recorded throughout the test at regular intervals (acquisition rate of 3 Hz) via an Imager E-lite CCD camera and digitized in 1628 × 1236 pixels, with a resolution of 290 pixels/mm. Figure 5 shows the configuration of the AF specimen for strain measurements. The lens axis of the CCD camera of DIC system is kept perpendicular to the FP of the AF specimen, i.e. plan xy. The CCD camera simultaneously records the LP of the AF specimen using a right angle prism, i.e. plan xz. The DIC calculations, performed using Davis software developed by Lavision, consist to correlate the gray levels of each deformed image to the gray levels of the reference image. A random speckle pattern was

applied to two plans of the AF specimen with airbrush filled with India ink in order to get randomized gray levels distributions. The speckle diameter was as uniform and small as possible to ensure a good spatial resolution. The zone of interest (ZOI) was divided into small square subsets of size 48×18 pixels in which the axial and transversal in-plane displacement vectors were calculated. The full-field data were then processed to obtain the (average) axial and transversal strain history in the ZOI. Two different tests[6] were carried out at room temperature while the specimen is constantly immerged in a saline solution with various concentrations c_{sol} :

- Free swelling response: The AF specimen is griped on the testing machine at one side while keeping the other one free. The temporal changes in the local axial stretch, λ_{xx}, and the local transversal stretches, λ_{yy} and λ_{zz}, were recorded during the swelling of the AF specimen. Once the local stretches known, the local volume variation was then determined from the following expression: $V/V_0 = \lambda_{xx}\lambda_{yy}\lambda_{zz}$.
- Stress-stretch and transversal responses: Loading-unloading tensile tests were performed to characterize both the evolution in stress and the evolution in transversal strains. The AF specimen was stretched up to a prescribed stretch and unloaded, the loading and unloading paths being performed at the same absolute axial strain-rate. The two experimental parameters, load F and local transversal stretches, acquired in real time were used to evaluate the axial macro-stress σ_{xx} at the specimen scale: $\sigma_{xx} = F/\left(S_0\lambda_{yy}\lambda_{zz}\right)$ in which S_0 is the initial cross-section. In order to re-establish

[6] The errors bars were calculated on the axial stress and the strains. Standard deviation of 6.83% on the axial stress was estimated at a 95% confidence on fifteen AF specimens loaded in tension. A root mean square error of 9.7% from the correlation process was estimated on the strains by imposing a rigid body move to AF specimens, griped at one side and free at the other one.

hydration of the AF specimen, it was immerged in a 9 g/L saline solution during 100 minutes before testing (Costi et al., 2002).

3.1.3.1.2. Experimental observations

Prior to the comparison of the model simulations with the experimental data, a brief description of experimental observations is provided to address the influence of osmolarity and strain-rate. Figure 3.1.5 presents the free swelling response of the AF specimen. Due to a period of storage of the AF specimen in a low humidity chamber in abattoir, the fluid content begins to increase until a stabilized state in which chemical and mechanical contributions on the internal stresses are equilibrated.

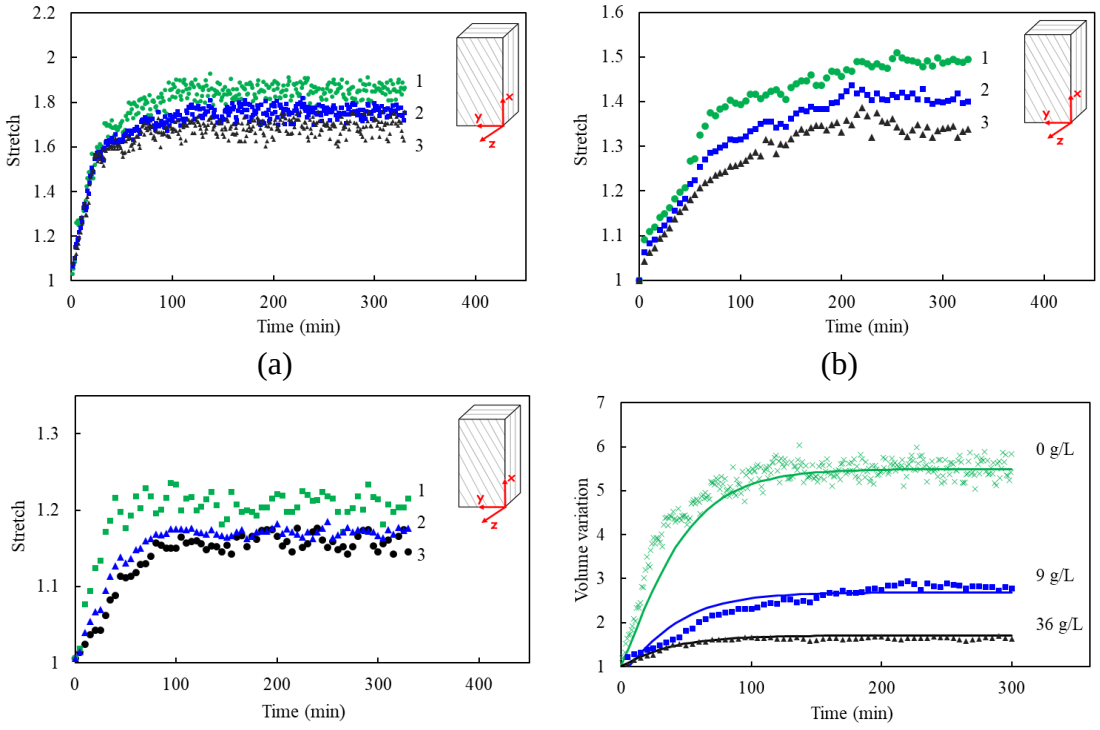

Figure 3.1.5. Free swelling response for different saline concentrations: (a) 0 g/L, (b) 9 g/L, (c) 36 g/L (1: λ_{xx}, 2: λ_{zz}, 3: λ_{yy}), (d) comparison with simulation results (solid line).

The free swelling response is found anisotropic. Since the chemo-mechanical equilibrium depends on the mobile ions in solution, the volume variation is affected by the osmolarity but not the time needed to reach the equilibrium state. The swelling decrease with the increase in osmolarity is due to a decrease in water exchange.

Figure 3.1.6 presents the stress-stretch response in which a strong osmo-inelastic dependency is evidenced. The experimental data are presented as dashed lines and symbols with standard deviation error bars in both axes. The AF stiffness is strongly altered by the strain-rate but also by the osmolarity illustrating structural changes. The dissipative capability of the AF tissue is characterized by the stress difference between loading and unloading paths.

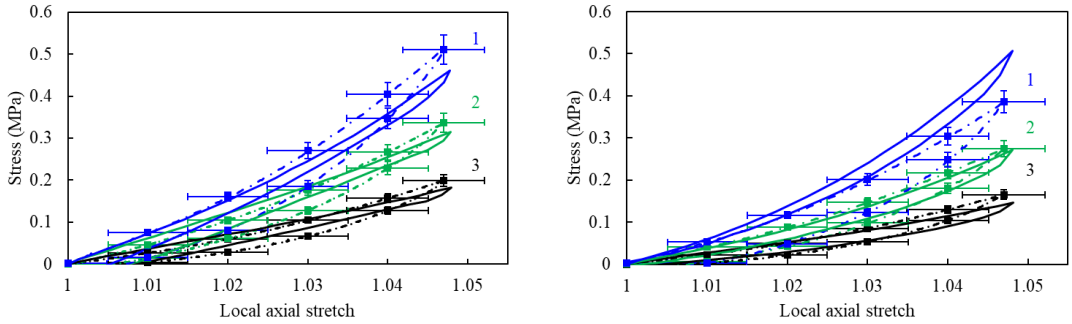

(a) (b)

Figure 3.1.6. Experimental (dashed line) and simulated (solid line) loading-unloading stress-stretch response for different saline concentrations (1: 18 g/L, 2: 9 g/L, 3: 0 g/L) and strain-rates: (a) 2×10^{-3} s^{-1}, (b) 2×10^{-4} s^{-1}.

Figure 3.1.7 provides the transversal strain history obtained by averaging the local transversal strains in FP and in LP. The experimental data are presented as symbols with standard deviation error zones. These results illustrate the strong anisotropic behavior of the AF tissue. An important shrinking is found in FP without dependence on osmolarity. A swelling response (i.e. auxetic) is observed in LP with a strong dependence on osmolarity and strain-rate. These inverse behaviors suggest a fluid exchange from FP towards LP during the mechanical loading.

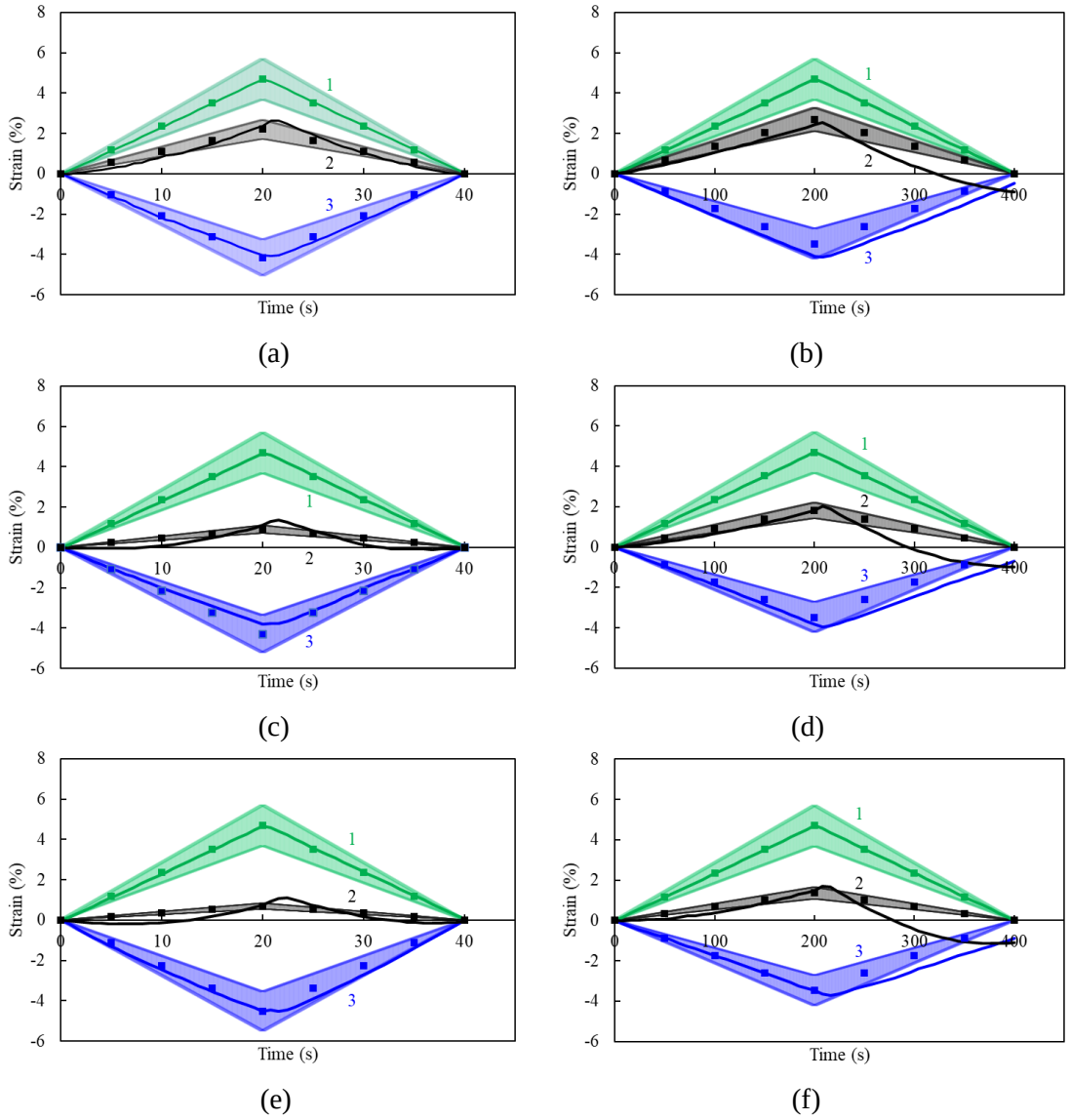

Figure 3.1.7. Experimental (symbols) and simulated (solid line) axial and transversal strains (1: E_{xx}, 2: E_{zz}, 3: E_{yy}) for different saline concentrations and strain-rates: (a) 0 g/L and 2×10^{-3} s^{-1}, (b) 0 g/L and 2×10^{-4} s^{-1}, (c) 9 g/L and 2×10^{-3} s^{-1}, (d) 9 g/L and 2×10^{-4} s^{-1}, (e) 18 g/L and 2×10^{-3} s^{-1}, (f) 18 g/L and 2×10^{-4} s^{-1}.

We shall now compare the proposed constitutive model with these experimental observations.

3.1.3.2. Simulations and parameter identification

The numerical analysis of the AF specimen was carried out under three-dimensional conditions using the finite element method. The model simulation includes fiber reinforced lamella zones separated by interlamellar zones. Figure 3.1.8 shows the three-dimensional finite element mesh

of the AF specimen using 8-node meshing elements, isoparametric and arbitrarily hexahedrics. Due to the symmetry, only a representative volume of the AF specimen was modeled. The same boundary conditions regarding the experimental tests were simulated.

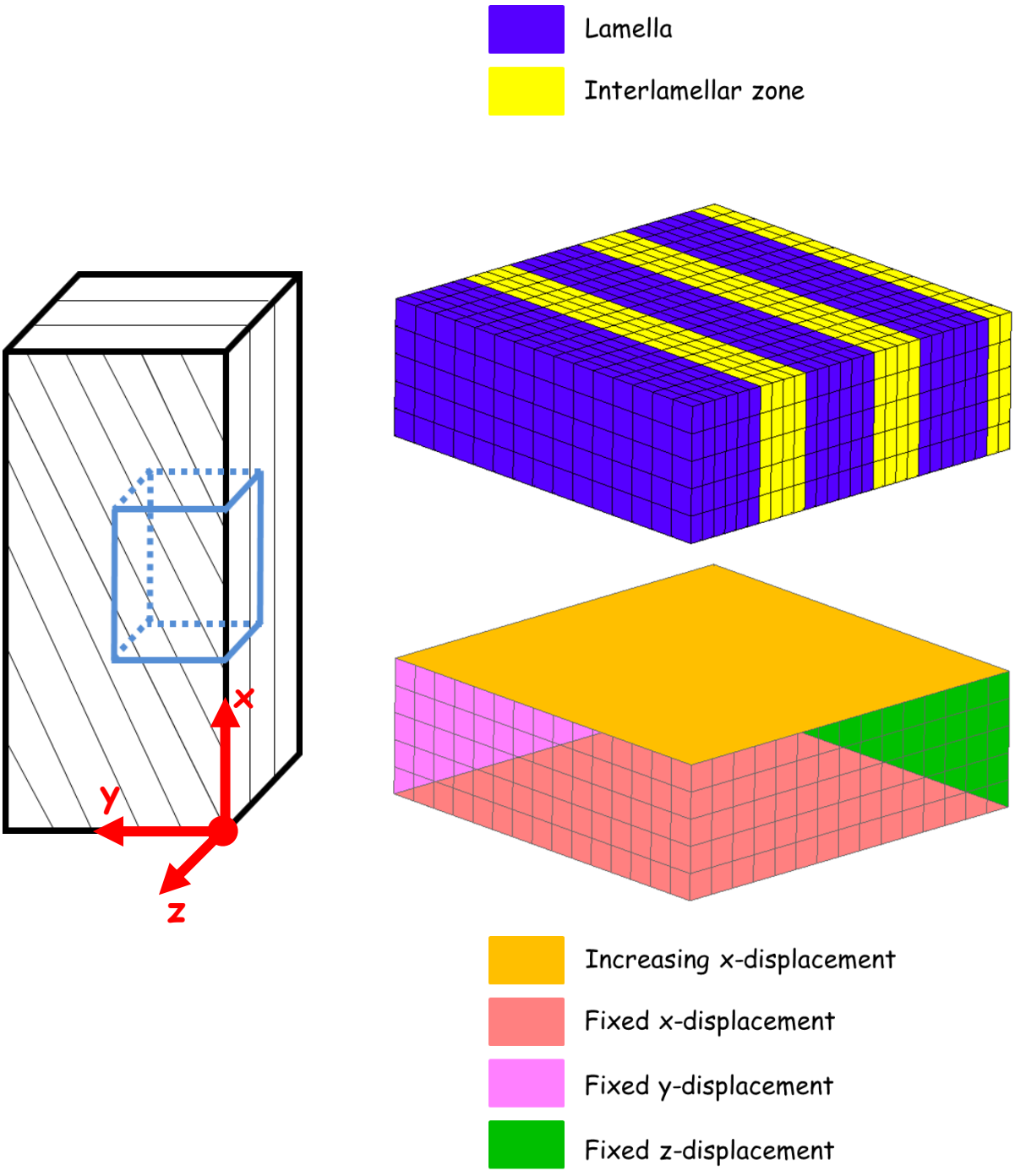

Figure 3.1.8. AF specimen and boundary conditions.

The constitutive model includes the following input constants:

- Five parameters related to the PGs macromolecules: μ, $I_{1\lim}$, C_v, d and m
- Two parameters related to the collagen fibers: A_1 and A_2
- Eight parameters related to the osmo-induced volumetric contribution: $n_{f_{ref}}$, β_m, β_s, s_1, s_2, s_3, k and α.

Taking the orientation and content in collagen fibers, $\theta = 67°$ and v_f =0.05, in the lamellae, the parameters were the outcome of a standard optimization procedure that provides the best fit of the experimental macro-response and transversal response by means of trial and error. Unless explicitly stated, the following parameter values are used in the lamellae and the interlamellar zones:

- PGs macromolecules:
  $\mu = 5.2c_{sol}^2 + 0.78c_{sol} + 0.23$ MPa
  $I_{1\lim} = 3$
  $C_v = 0.52$ MPa
  $d = 0.01$ MPa^{-1}s^{-1}
  $m = 0.001$
- Collagen fibers (lamella):
  $A_1 = 10$ MPa
  $A_2 = 210$ MPa
- Osmo-induced volumetric contribution:
  $n_{f_{ref}} = 0.78$
  $\beta_m = -0.0004$ s^{-1} (lamella)
  $\beta_m = -0.00097$ s^{-1} (interlamellar zone)
  $\beta_s = -0.0005$ s^{-1}
  $s_1 = 0.24$
  $s_2 = 0.74$
  $s_3 = -6949$ mol l^{-1}
  $k = 1000$ MPa
  $\alpha = 7623\exp(0.068c_{sol})\dot{\varepsilon} + 0.26$ (lamella)
  $\alpha = 8665\exp(0.085c_{sol})\dot{\varepsilon} - 0.07$ (interlamellar zone)

The quantitative comparisons between the model simulations and the measured experimental data are presented in Figures 3.1.5d, 3.1.6 and 3.1.7.

The free swelling process is numerically replicated in Figure 5d. The water intakes in the AF specimen until the reference value $n_{f_{ref}}$ of 0.78. One can observe a very good agreement between measured and simulated results at different saline concentrations. This observation indicates that the constitutive model can accuratelycapturethe chemical response of AF. However, it may be recognized that the model is not able to reproduce the anisotropy of the free swelling shown in Figures 3.1.5a, 3.1.5b and 3.1.5c.

The simulation results are compared in Figures 3.1.6 and 3.1.7 with the experimental data in terms of macro-response and transversal strain history. A global view at these results shows that the general trends provided by the computed results are satisfactory when compared with the experimental measurements. The osmolarity effect on the macro-response is fairly well reproduced whereas a saturation of the strain-rate effect is observed at the highest saline concentration.

At the micro-scale, the tightening of the PGs macromolecules with osmolarity is described by the dependence of the shear modulus μ with the concentration c_{sol}. At the stratified scale, the lamellae and the interlamellar zones in LP induce a strong anisotropy in the transversal behavior of the AF specimen. The latter was used to calculate the Poisson's ratio ν_{xy} in FP and ν_{xz} in LP. This two-dimensional material property is defined as the ratio between the transversal strain in the corresponding plan and the axial strain. The results are reported in Table 3.1.1. The close agreement between computed results and test findingsvalidates the capability of our approach to predict the chemo-mechanical response of AF.

NaCl concentration (g/L)	Strain-rate (s^{-1})	Poisson's ratio Experiments		Poisson's ratio Simulation	
		ν_{xy} FP	ν_{xz} LP	ν_{xy} FP	ν_{xz} LP
0	2×10^{-3}	0.887±0.19	-0.468±0.1	0.89	-0.43
	2×10^{-4}	0.74±0.16	-0.574±0.12	0.88	-0.49
9	2×10^{-3}	0.92±0.2	-0.2±0.04	0.84	-0.14
	2×10^{-4}	0.74±0.16	-0.387±0.08	0.81	-0.34
18	2×10^{-3}	0.963±0.21	-0.146±0.03	1.00	-0.06
	2×10^{-4}	0.811±0.17	-0.29±0.06	0.75	-0.25

Table 3.1.1. Experimental and simulated Poisson's ratios for different saline concentrations and strain-rates.

3.1.3.3. Numerical local fields

The question, which arises, is how the local stresses/strains are distributed in the AF specimen. Figures 3.1.9, 3.1.10, 3.1.11 and 3.1.12 present the predicted distributions for different saline concentrations and strain-rates.

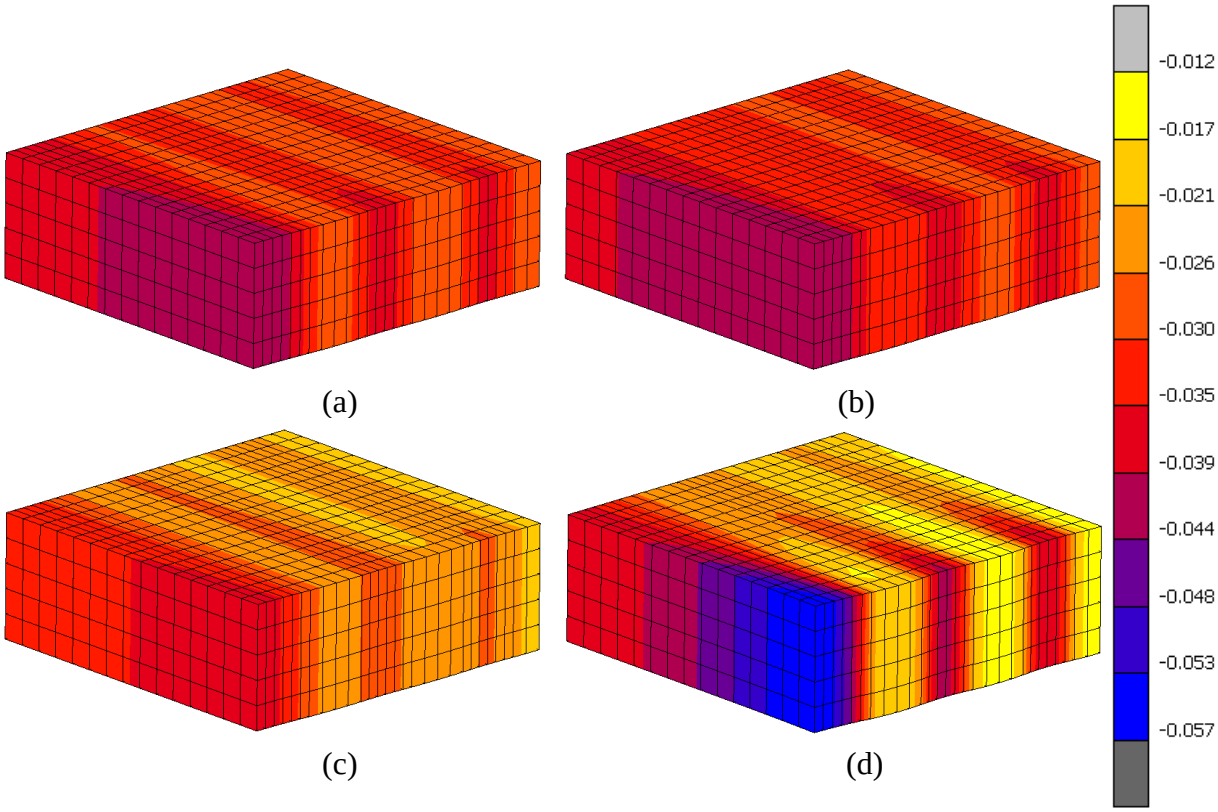

Figure 3.1.9. Distribution of the transversal strain E_{yy} in the AF specimen for different saline concentrations and strain-rates: (a) 0 g/L and 2×10^{-3} s^{-1}, (b) 0 g/L and 2×10^{-4} s^{-1}, (c) 18 g/L and 2×10^{-3} s^{-1}, (d) 18 g/L and 2×10^{-4} s^{-1}.

The local transversal strain E_{yy} in Figure 9 exhibits a strong dependence on the osmolarity and a strain-rate effect mainly under the hyper-osmotic condition. The strain field becomes heterogeneous with the osmolarity and the local values increase with the time (i.e. a decrease in strain-rate). The observed shrinkage is explained by the level of strains observed in FP.

The transversal strain E_{zz} in Figure 3.1.10 is moderately affected by the time and the osmolarity. The averaged swelling observed by DIC in LP is perceptible with alternate negative transversal strains in the lamellae and positive transversal strains in the interlamellar zones.

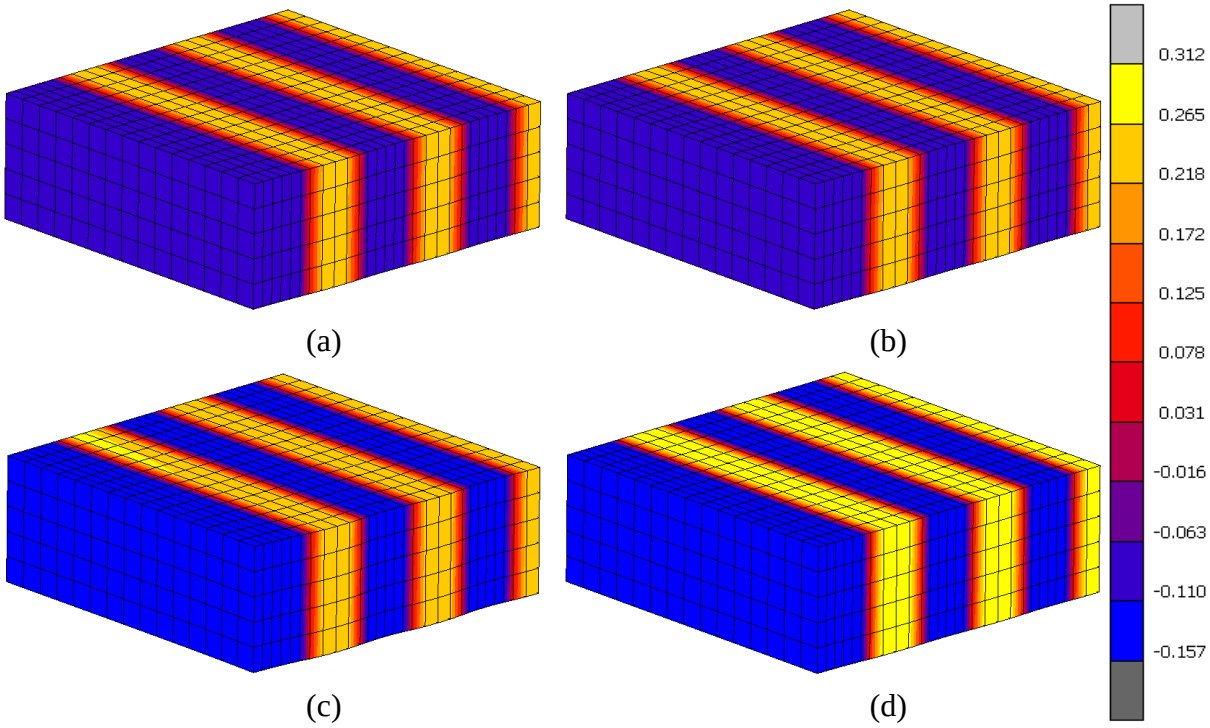

Figure 3.1.10. Distribution of the transversal strain E_{zz} in the AF specimen for different saline concentrations and strain-rates: (a) 0 g/L and 2×10^{-3} s^{-1}, (b) 0 g/L and 2×10^{-4} s^{-1}, (c) 18 g/L and 2×10^{-3} s^{-1}, (d) 18 g/L and 2×10^{-4} s^{-1}.

In Figure 3.1.11, the osmo-inelastic effect on the local axial stress σ_{xx} is obvious. However, the heterogeneity increases mostly with the osmolarity. Interesting negative values are found in the

interlamellar zones showing the effect of local swelling while the stress increases strongly in the lamellae.

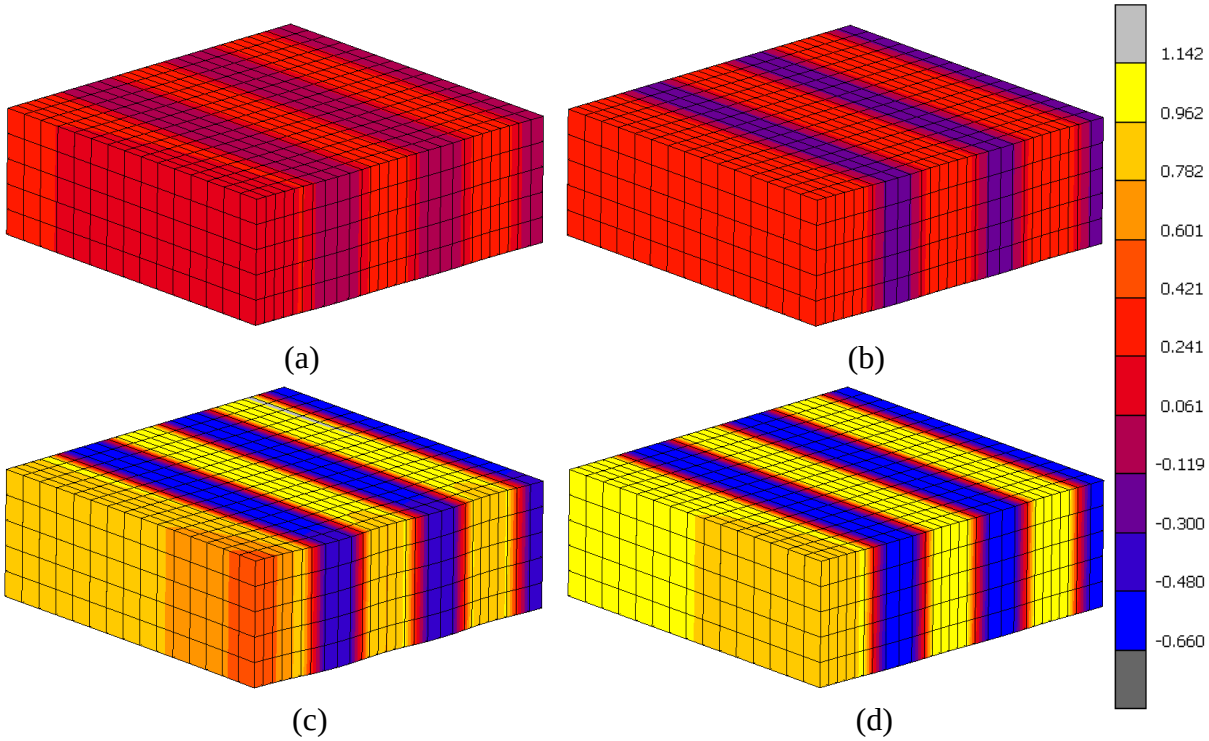

Figure 3.1.11. Distribution of the axial stress σ_{xx} in the AF specimen for different saline concentrations and strain-rates: (a) 0 g/L and 2×10^{-3} s^{-1}, (b) 0 g/L and 2×10^{-4} s^{-1}, (c) 18 g/L and 2×10^{-3} s^{-1}, (d) 18 g/L and 2×10^{-4} s^{-1}.

The increase in osmolarity induces a stronger contrast between lamellae and interlamellar zones, inducing a shear stress σ_{yx} in the interlamellar zones as illustrated in Figure 3.1.12. This component plays an important role in the AF failure (Costi et al., 2007). Direct measurements of stresses in the spine unit evidence that the shear stresses are higher than the perpendicular stresses. This behavior is also verified experimentally at the AF lamellae scale by optical tomographic elastography (Han et al., 2016). The measured shear strain is found higher in the interlamellar zones than in the lamellae, which confirms that this region may be more susceptible to damage. The layered structure of the AF enhances the chemo-mechanical

coupling by improving the internal fluid exchange, but this configuration induces heterogeneity of strain field at all levels of scale.

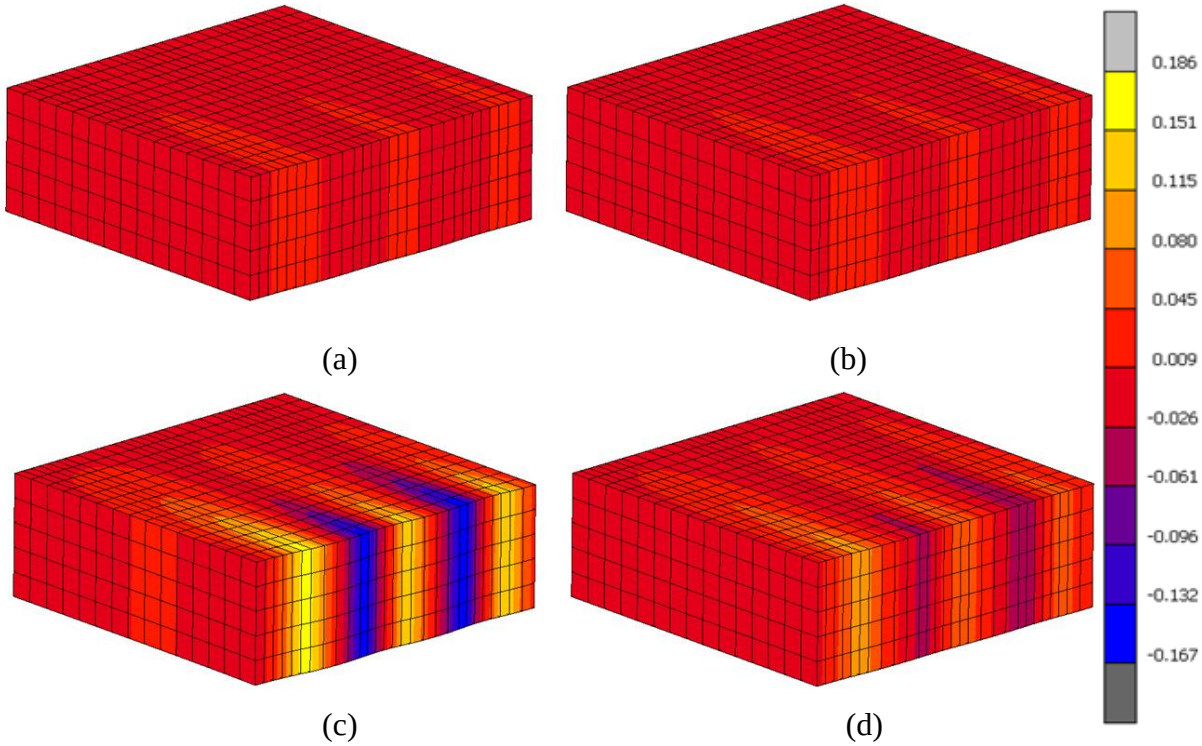

Figure 3.1.12. Distribution of the shear stress σ_{yz} in the AF specimen for different saline concentrations and strain-rates: (a) 0 g/L and 2×10^{-3} s^{-1}, (b) 0 g/L and 2×10^{-4} s^{-1}, (c) 18 g/L and 2×10^{-3} s^{-1}, (d) 18 g/L and 2×10^{-4} s^{-1}.

3.1.4. Partial conclusions

A chemo-mechanical approach was adopted for the osmo-inelastic prediction of AF response in connection to the microstructure. A fairly good agreement was obtained between the model results and the experimental data in terms of stress-stretch and transversal behaviors of AF specimens locally determined by DIC method. The constitutive model, implemented into a finite element code, provides a useful tool for stress/strain patterns estimate in AF. The capability of the model to simulate the transversal strain fields on AF specimens, especially the auxeticity, was shown.

Although uniaxial tensile deformation provides important indications concerning the osmo-inelastic mechanisms, it would be also interesting to consider the time-dependent transversal response under relaxation loading. It remains an important issue for further studies.

3.1.5. References

Adam, C., Rouch, P., Skalli, W., 2015. Inter-lamellar shear resistance confers compressive stiffness in the intervertebral disc: An image-based modelling study on the bovine caudal disc. Journal of Biomechanics 48, 4303-4308.

Argoubi, M., Shirazi-Adl, A., 1996. Poroelastic creep response analysis of a lumbar motion segment in compression. Journal of Biomechanics 29, 1331-1339.

Ayotte, D.C., Ito, K., Perren, S.M., Tepic, S., 2000. Direction-dependent constriction flow in a poroelastic solid: The intervertebral disc valve. Journal of Biomechanical Engineering 122, 587-593.

Baldit, A., Ambard, D., Cherblanc, F., Royer, P., 2014. Experimental analysis of the transverse mechanical behaviour of annulus fibrosus tissue. Biomechanics and Modeling in Mechanobiology 13,643-652.

Bergstrom, J.S., Boyce, M.C., 1998. Constitutive modeling of the large strain time-dependent behavior of elastomers. Journal of the Mechanics and Physics of Solids 46, 931-954.

Cantournet, S., Boyce, M.C., Tsou, A.H., 2007. Micromechanics and macromechanics of carbon nanotube-enhanced elastomers. Journal of the Mechanics and Physics of Solids 55, 1321-1339.

Costi, J.J., Hearn, T.C., Fazzalari, N.L., 2002. The effect of hydration on the stiffness of intervertebral discs in an ovine model. Clinical Biomechanics 17, 446-455.

Costi, J.J., Stokes, I.A., Gardner-Morse, M., Laible, J.P., Scoffone, H.M., Iatridis, J.C., 2007. Direct measurement of intervertebral disc maximum shear strain in six degrees of freedom: Motions that place disc tissue at risk of injury. Journal of Biomechanics 40, 2457-2466.

Drost, M.R., Willems, P., Snijders, H., Huyghe, J.M., Janssen, J.D., Huson, A., 1995. Confined compression of canine annulus fibrosus under chemical and mechanical loading. Journal of Biomechanical Engineering 117, 390-396.

Ebara, S., Iatridis, J.C., Setton, L.A., Foster, R.J., Mow, V.C., Weidenbaum, M., 1996. Tensile properties of nondegenerate human lumbar anulus fibrosus. Spine 21, 452-461.

Eberlein, R., Holzapfel, G.A., Schulze-Bauer, C.A.J., 2001. An anisotropic model for annulus tissue and enhanced finite element analyses of intact lumbar disc bodies. Computer Methods in Biomechanics and Biomedical Engineering 4, 209-229.

Ehlers, W., Karajan, N., Markert, B., 2009. An extended biphasic model for charged hydrated tissues with application to the intervertebral disc. Biomechanics and Modeling in Mechanobiology 8, 233-251.

Emanuel, K.S., van der Veen, A.J., Rustenburg, C.M.E., Smit, T.H., Kingma, I., 2018. Osmosis and viscoelasticity both contribute to time-dependent behaviour of the intervertebral disc under compressive load: A caprine in vitro study. Journal of Biomechanics 70, 10-15.

Eyre, D.R., 1979. Biochemistry of the intervertebral disc. International Review of Connective Tissue Research 8, 227-291.

Frijns, A.J.H., Huyghe, J.M., Janssen, J.D., 1997. A validation of the quadriphasic mixture theory for intervertebral disc tissue. International Journal of Engineering Science 35, 1419-1429.

Galbusera, F., Mietsch, A., Schmidt, H., Wilke, H.J., Neidlinger-Wilke, C., 2013. Effect of intervertebral disc degeneration on disc cell viability: A numerical investigation. Computer Methods in Biomechanics and Biomedical Engineering 16, 328-337.

Gent, A.N., 1996. A new constitutive relation for rubber. Rubber Chemistry and Technology 69, 59-61.

Gu, W.Y., Lai, W.M., Mow, V.C., 1998. A mixture theory for charged-hydrated soft tissues containing multi-electrolytes: Passive transport and swelling behaviors. Journal of Biomechanical Engineering 120, 169-180.

Guerin, H.L., Elliott, D.M., 2006. Degeneration affects the fiber reorientation of human annulus fibrosus under tensile load. Journal of Biomechanics 39, 1410-1418.

Guerin, H.L., Elliott, D.M., 2007. Quantifying the contributions of structure to annulus fibrosus mechanical function using a nonlinear, anisotropic, hyperelastic model. Journal of Orthopaedic Research25, 508-516.

Guo, Z.Y., Peng, X.Q., Moran, B., 2006. A composites-based hyperelastic constitutive model for soft tissue with application to the human annulus fibrosus. Journal of the Mechanics and Physics of Solids 54, 1952-1971.

Gurtin, M.E., Anand, L., 2005. The decomposition $F=F^eF^p$, material symmetry, and plastic irrotationality for solids that are isotropic-viscoplastic or amorphous. International Journal of Plasticity 21, 1686-1719.

Han, S.K., Chen, C.W., Labus, K.M., Puttlitz, C.M., Chen, Y., Hsieh, A.H., 2016. Optical coherence tomographic elastography reveals mesoscale shear strain inhomogeneities in the annulus fibrosus. Spine 41, E770-E777.

Holzapfel, G., Simo, J., 1996. Entropy elasticity of isotropic rubber-like solids at finite strains. Computer Methods in Applied Mechanics and Engineering 132, 17-44.

Holzapfel, G.A., Gasser, T.C., Ogden, R.W., 2000. A new constitutive framework for arterial wall mechanics and a comparative study of material models. Journal of Elasticity and the Physical Science of Solids 61, 1-48.

Holzapfel, G.A., Schulze-Bauer, C.A.J., Feigl, G., Regitnig, P., 2005. Single lamellar mechanics of the human lumbar anulus fibrosus. Biomechanics and Modeling in Mechanobiology 3, 125-140.

Huyghe, J.M., Janssen, J.D., 1997. Quadriphasic mechanics of swelling incompressible porous media. International Journal of Engineering Science 35, 793-802.

Iatridis, J.C., Setton, L.A., Weidenbaum, M., Mow, V.C., 1997. The viscoelastic behavior of the non-degenerate human lumbar nucleus pulposus in shear. Journal of Biomechanics 30, 1005-1013.

Iatridis, J.C., Laible, J.P., Krag, M.H., 2003. Influence of fixed charge density magnitude and distribution on the intervertebral disc: Applications of a poroelastic and chemical electric (PEACE) model. Journal of Biomechanical Engineering 125, 12-24.

Inoue, H., Takeda, T., 1975. Three-dimensional observation of collagen framework of lumbar intervertebral discs. Acta Orthopaedica 46, 949-956.

Klisch, S.M., Lotz, J.C., 2000. A special theory of biphasic mixtures and experimental results for human annulus fibrosus tested in confined compression. Journal of Biomechanical Engineering 122, 180-188.

Labus, K.M., Han, S.K., Hsieh, A.H., Puttlitz, C.M., 2014. A computational model to describe the regional interlamellar shear of the annulus fibrosus. Journal of Biomechanical Engineering 136, 051009.
Lai, W.M., Hou, J.S., Mow, V.C., 1991. A triphasic theory for the swelling and deformation behaviors of articular cartilage. Journal of Biomechanical Engineering 113, 245-258.
Lanir, Y., 1987. Biorheology and fluid flux in swelling tissues. I. Bicomponent theory for small deformations, including concentration effects. Biorheology 24, 173-187.
Lee, E. H., 1969. Elastic-plastic deformation at finite strains. Journal of Applied Mechanics 36, 1-6.
MSC.Marc, 2015. MSC. Marc Volume D: User Subroutines and Special Routines. MSC Software Corporation.
Maroudas, A., 1976. Balance between swelling pressure and collagen tension in normal and degenerate cartilage. Nature 260, 808-809.
Michalek, A.J., Buckley, M.R., Bonassar, L.J., Cohen, I., Iatridis, J.C., 2009. Measurement of local strains in intervertebral disc anulus fibrosus tissue under dynamic shear: Contributions of matrix fiber orientation and elastin content. Journal of Biomechanics 42, 2279-2285.
Miehe, C., 1995. Entropic thermoelasticity at finite strains. Aspects of the formulation and numerical implementation. Computer Methods in Applied Mechanics and Engineering 120, 243-269.
Mow, V.C., Kuei, S.C., Lai, W.M., Armstrong, C.G., 1980. Biphasic creep and stress relaxation of articular cartilage in compression? Theory and experiments. Journal of Biomechanical Engineering 102, 73-84.
Nerurkar, N.L., Mauck, R.L., Elliott, D.M., 2011. Modeling interlamellar interactions in angle-ply biologic laminates for annulus fibrosus tissue engineering. Biomechanics and Modeling in Mechanobiology 10, 973-984.
Peng, X.Q., Guo, Z.Y., Moran, B., 2006. An anisotropic hyperelastic constitutive model with fiber-matrix shear interaction for the human annulus fibrosus. Journal of Applied Mechanics 73, 815-824.
Pezowicz, C.A., Robertson, P.A., Broom, N.D., 2006. The structural basis of interlamellar cohesion in the intervertebral disc wall. Journal of Anatomy 208, 317-330.
Schmidt, H., Reitmaier, S., Graichen, F., Shirazi-Adl, A., 2016. Review of the fluid flow within intervertebral discs - How could in vitro measurements replicate in vivo? Journal of Biomechanics 49, 3133-3146.
Schollum, M.L., Robertson, P.A., Broom, N.D., 2009. A microstructural investigation of intervertebral disc lamellar connectivity: Detailed analysis of the translamellar bridges. Journal of Anatomy 214, 805-816.
Schroeder, Y., Sivan, S., Wilson, W., Merkher, Y., Huyghe, J.M., Maroudas, A., Baaijens, F.P.T., 2007. Are disc pressure, stress, and osmolarity affected by intra- and extrafibrillar fluid exchange? Journal of Orthopaedic Research 25, 1317-1324.
Shirazi-Adl, A., Ahmed, A.M., Shrivastava, S.C., 1986. Mechanical response of a lumbar motion segment in axial torque alone and combined with compression. Spine 11, 914-927.
Simon, B.R., Wu, J.S., Carlton, M.W., Evans, J.H., Kazarian L.E., 1985. Structural models for human spinal motion segments based on a poroelastic view of the intervertebral disk. Journal of Biomechanical Engineering 107, 327-335.
Skaggs, D.L., Weidenbaum, M., Iatridis, J.C., Ratcliffe, A., Mow, V.C., 1994. Regional variation in tensile properties and biochemical composition of the human lumbar anulus fibrosus. Spine 19, 1310-1319.

Vergroesen, P.P.A., Emanuel, K.S., Peeters, M., Kingma, I., 2018. Are axial intervertebral disc biomechanics determined by osmosis? Journal of Biomechanics 70, 4-9.

Wagner, D.R., Lotz, J.C., 2004. Theoretical model and experimental results for the nonlinear elastic behavior of human annulus fibrosus. Journal of Orthopaedic Research 22, 901-909.

Wang, J.L., Parnianpour, M., Shirazi-Adl, A., Engin, A.E., Li S., Patwardhan, A., 1997. Development and validation of a viscoelastic finite element model of an L2/L3 motion segment. Theoretical and Applied Fracture Mechanics 28, 81-93.

Weiss, J.A., Maker, B.N., Govindjee, S., 1996. Finite element implementation of incompressible, transversely isotropic hyperelasticity. Computer Methods in Applied Mechanics and Engineering 135, 107-128.

Yu, J., Fairbank, J.C., Roberts, S., Urban, J.P.G., 2005. The elastic fiber network of the anulus fibrosus of the normal and scoliotic human intervertebral disc. Spine 30, 1815-1820.

Yu, J., Tirlapur, U., Fairbank, J.C., Handford, P., Roberts, S., Winlove, C.P., Cui, Z., Urban, J., 2007. Microfibrils, elastin fibres and collagen fibres in the human intervertebral disc and bovine tail disc. Journal of Anatomy 210, 460-471.

Chapter 3: Constitutive modeling and simulation

Part 2: A finite element model for time-dependent biomechanics of the intervertebral disc[7]

Abstract

A finite element model for time-dependent biomechanics of the spine unit was developed in which the natural regional variation in structure and properties of the real intervertebral disc (IVD) was taken into account. The different IVD sub-regions were described by the chemo-inelastic constitutive equations coupled to solutes diffusion equations. In-vitro experimental tests were reproduced in-silico in order to verify the ability of the finite element model to reproduce the nonlinear motion patterns of a real spine segment. The time-dependent response of the healthy IVD is discussed with respect to the heterogeneous mechanics and solutes patterns within the simulation model.

Keywords: Intervertebral disc; Time-dependent response; Nutrients supply; Finite element analysis.

[7] This Part of this chapter is based on the following paper: Amil Derrouiche, Fahmi Zaïri, Fahed Zaïri, A finite element model for time-dependent biomechanics of the intervertebral disc, *in preparation*.

3.2.1. Partial introduction

The non-fatal diseases grow with the reducing mortality, which concerns an increasing part of the population and leads to new health policies (Vos et al., 2016). There is a correlation between the lifestyle in developed countries and the pain location with high prevalence for the back pain (Breivik et al., 2006; Skoffer and Foldspang, 2008; Vos et al., 2016). The intervertebral disc (IVD) is often concerned especially when the pain becomes chronic and severe. However, a better understanding of the IVD diseases requires an explanation of the healthy working in relation with the time-dependency.

The IVD becomes thinner during the day while its height is restored during the night (de Puky, 1935). This soft tissue exhibits a complex time-dependent mechanical response dependent on lifestyle and age, and presents a degeneration process even in normal conditions (Campana et al., 2011). Multiple plausible explanations have been proposed to explain the origin of the different history-dependent effects: the recovering property of the soft tissue at middle-term and the degeneration at long-term. Internal micro-alteration could cause mechanical response degradation (Natarajan et al., 2007). During the degeneration process of the soft tissue, a loss of proteoglycans (PGs) macromolecules, and thus of fixed charge density, is observed, implying lesser swelling pressure and thus bad nutrient transport (Lyons et al., 1981; Urban and Holm, 1986; Antoniou et al., 1996). Although cells nutrition and degeneration are not directly linked, the process is a vicious circle since a change in composition, induced by bad nutrient transport or high stresses, imply IVD degeneration. The PGs extracellular matrix (ECM) contains an interstitial fluid allowing the nutrition of cells by diffusion to vessels near IVD (Urban et al., 1979; Lai et al., 1991; Gu et al., 1993; Urban et al., 2004). The fixed charge density of ECM contributes to hydration and nutrition of the tissue. Oxygen and glucose are the main nutrients of IVD cells and lactic acid is the main waste that leads to a pH decrease in ECM if it is not

sufficiently evacuated (Horner and Urban, 2001; Urban et al., 2004; Grunhagen et al., 2006; Neidlinger-Wilke et al., 2012; Wills et al., 2016). A good chemical balance with usual pH is strongly dependent on good interstitial fluid diffusion (Urban et al., 2004).

In the aim to better understand the time-dependent behavior of IVD in relation with the above biological effects, the chemo-inelastic equations are coupled to solutes diffusion equations. An accurate three-dimensional finite element model of the human cervical spine is developed using computerized tomography (CT) images. The constitutive modeling of each spinal component is identified using intrinsic experimental data. Numerical simulations are performed in order to predict the biomechanical response under physiological movements and to check the ability of the finite element model to provide a realistic response of the cervical spine segment. The heterogeneous mechanics and solutes patterns in healthy IVD are then analyzed using the developed finite element model.

Section 2 gives the details of the finite element computations. Section 3 presents and discusses the numerical results. Finally, some concluding remarks are given in Section 4.

3.2.2. Finite element computations

3.2.2.1. Model and boundary conditions

An anatomically accurate finite element model of the functional spine unit was constructed in the aim to predict its biomechanical response and the local fields in the soft tissues under complex quasi-static loading conditions.

The three-dimensional model of a human C5-C6 cervical spine was constructed using CT data. The reconstruction procedure of a vertebra using CT images is given in Figure 3.2.1. The three-dimensional visualization was created from CT images using the 3DSlicer software. Each vertebra is then isolated and exported into Catia V5 while preserving the original positions.

After some corrections and smoothing operations, the finite element mesh was performed using Abaqus. According to their stiffness compared to soft tissues, the vertebrae were treated as stiff solids and were meshed using triangular surface elements. The IVD, created by extruding the surfaces of above and below vertebrae, was meshed using tetrahedral elements.

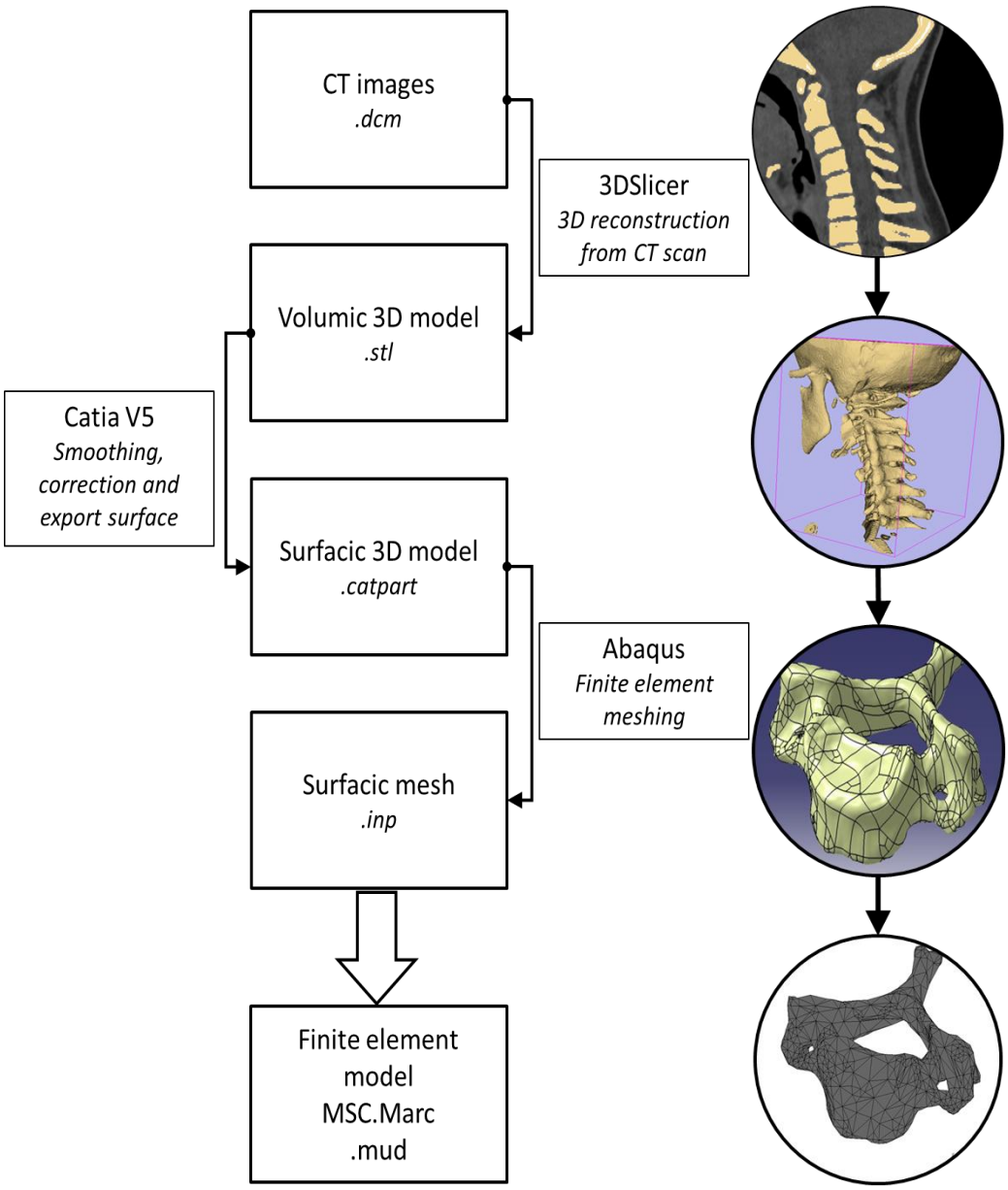

Figure 3.2.1. Reconstruction procedure of vertebrae.

The main ligaments were considered: anterior longitudinal ligament (ALL), posterior longitudinal ligament (PLL), ligamentum flavum (LF), interspinous ligament (ISL) and

capsulary ligament (CL). The location of each ligament was determined according to qualitative anatomical descriptions. Since they are loading only in tension, the ligaments were meshed using truss elements. The vertebrae, the IVD and the ligaments were assembled into the finite element code MSC.Marc in order to obtain the finite element model shown in Figure 3.2.2. The different spinal components were assumed strongly joined.

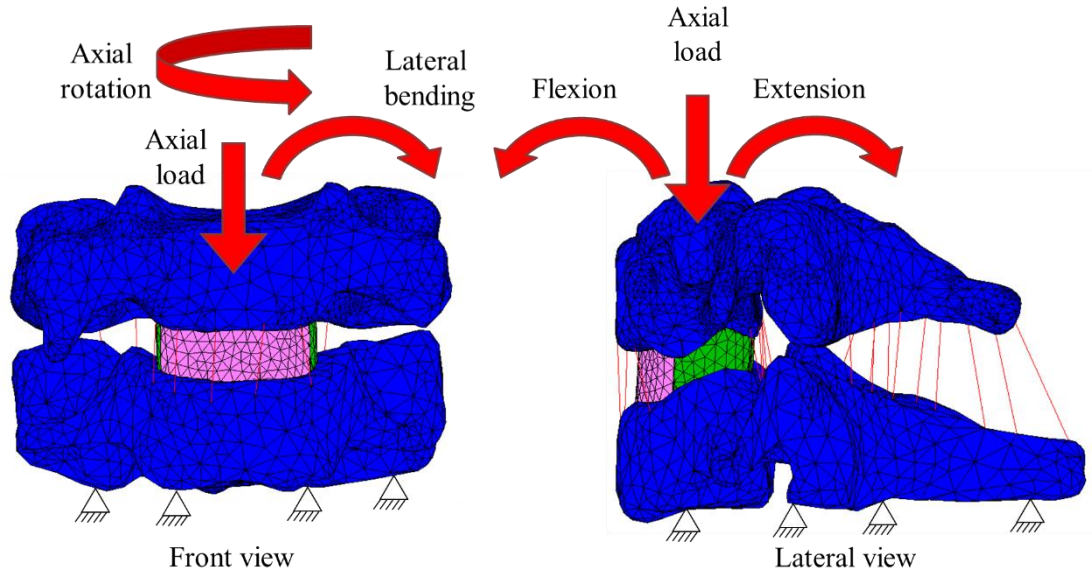

Figure 3.2.2. Mesh and boundary conditions of the spine unit model.

During the finite element simulations, a vertical axial load of 73.6 N was applied on the superior surface of the C5 vertebral body to simulate the weight of the skull and upper segments, and the inferior surface of the C6 vertebral body was constrained. Different neck movements, namely, flexion-extension, lateral bending and axial rotation movements were simulated.

3.2.2.2. Constitutive equations of soft tissues

The regional variation in structure and properties of the IVD was taken into account in the aim to propose the most realistic representation of the natural IVD. The IVD core, i.e. nucleus pulposus (NP), and its shell, i.e. AF, were explicitly modeled as shown in Figure 3 based upon

qualitative anatomical data. The distinct AF sub-regions were taken into account: ventro-outer (VO), ventro-inner (VI), dorso-outer (DO) and dorso-inner (DI). The soft tissues were represented using the constitutive model developed in the previous part. Note that the NP was considered as a PGs ECM without organized collagen fibers.

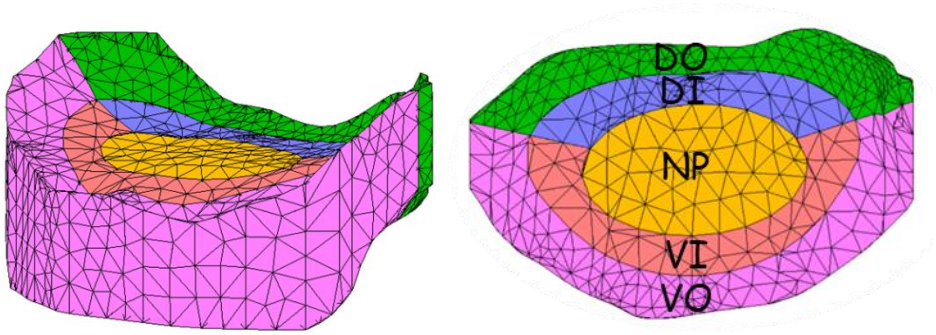

Figure 3.2.3. Mesh of the IVD with different sub-regions.

The inputs, related to structural and mechanical parameters of IVD sub-regions, and required by the constitutive modeling are listed in Table 3.2.1. The model parameters were identified using published experiments on human AF sub-regions loaded in tension (Holzapfel et al., 2005) and human NP loaded in compression (Bertagnoli et al., 2005). The applied strain-rates were 9×10^{-4} s^{-1}, 1.4×10^{-3} s^{-1}, 1.5×10^{-3} s^{-1}, 1.7×10^{-3} s^{-1} and 1.3×10^{-1} s^{-1} for VO, VI, DO, DI and NP, respectively.

Parameters	VO	VI	DO	DI	NP
θ (°)	67	67	42	42	0
v_f	0.125	0.06	0.125	0.06	0
A_1 (MPa)	150	15	3	1	0
A_2 (MPa)	2500	1	250	4	0
μ (MPa)			0.36		0.24
$I_{1\text{lim}}$			3.17		3.69
C_v (MPa)			0.85		
d ($MPa^{-1}s\text{-}^{1}$)			15.25		
m			4.0		
k (MPa)			10		

Table 3.2.1. Structural and material parameters of the IVD sub-regions.

The model results in terms of stress-strain curves are presented in Figure 3.2.4 by comparison to the experimental data. The experimental data are presented as dashed lines while the solid lines represent the model results. The correlation of the model with the experimental data can be considered as acceptable. The ligaments were considered as incompressible isotropic neo-Hookean elastic media. The stiffness and the cross-section area of the ligaments, reported in Table 3.2.2, are taken from (Ha, 2006).

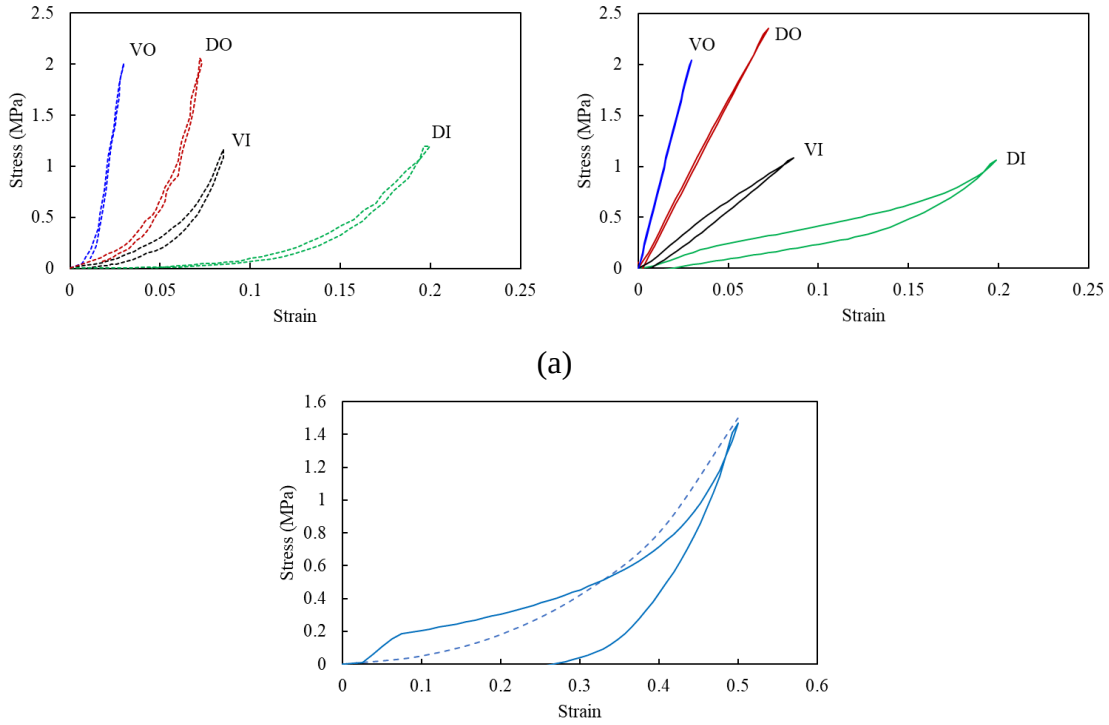

Figure 3.2.4. Experimental (dashed lines) and simulated (continuous lines) stress-strain responses: (a) AF, (b) NP.

Parameters	ALL	PLL	LF	ISL	CL
A (mm^2)	6.1	5.4	50.1	13.1	46.6
C (MPa)	9.08	3.33	0.25	0.25	0.25

Table 3.2.2. Cross-section area and stiffness of the ligaments.

3.2.2.3. Nutrients supply

Chondrocytes and fibroblasts are the two cell populations responsible for the production of PGs and collagen fibers, respectively (Bibby et al., 2001). The nutrients supply governs the cell population in IVD by providing source of energy, e.g. Oxygen and glucose, and evacuate the waste, e.g. lactate. This mechanism is based on diffusion via water exchange induced by mechanical loadings. Understanding the mechano-biological interactions could allow a better understanding of the degeneration process of our spine (Urban et al., 2004; Malandrino et al., 2015; Wills et al., 2016). We propose to couple the constitutive model of IVD with diffusion equations to simulate the effect of the mechanical loading on the mechanism of nutrients supply. The spatially and time-dependent solutes repartition is given by the following transport equation:

$$\frac{\partial \boldsymbol{C}_{solutes}}{\partial t} - \mathbf{D}_{solutes}\,\nabla^2 \boldsymbol{C}_{solutes} = \boldsymbol{R}_{solutes} \tag{1}$$

where $\boldsymbol{C}_{solutes}$ is the solutes concentration, $\mathbf{D}_{solutes}$ is the solutes diffusion coefficient and $\boldsymbol{R}_{solutes}$ is the solutes reaction.

The considered solutes are oxygen, lactate and glucose, Eq. (1) may be re-written as:

$$\frac{\partial}{\partial t}\begin{pmatrix} C_{O_2} \\ C_{lactate} \\ C_{glucose} \end{pmatrix} - \begin{pmatrix} D_{0_2} & 0 & 0 \\ 0 & D_{lactate} & 0 \\ 0 & 0 & D_{glucose} \end{pmatrix} \nabla^2 \begin{pmatrix} C_{O_2} \\ C_{lactate} \\ C_{glucose} \end{pmatrix} = \begin{pmatrix} R_{O_2} \\ R_{lactate} \\ R_{glucose} \end{pmatrix} \tag{2}$$

The solutes diffusion coefficient $\mathbf{D}_{solutes}$ is dependent on the internal water content according to the following equation (Mackie and Meares, 1955):

$$\mathbf{D}_{solutes} = \left(\frac{n_f}{2 - n_f}\right)^2 \mathbf{D}_{solutes}^{water} \tag{3}$$

where n_f is the internal water content of the tissue and $\mathbf{D}_{solutes}^{water}$ is the solutes diffusivity in water. In the present modeling, the chemo-mechanical equilibrium is considered instantaneously reached and the internal fluid exchange in AF is not considered. The water content variation n_f

is assumed to be directly related to the volumetric tissue deformation induced by the mechanical loading. The solutes repartitions are calculated according to the flowchart given in Figure 3.2.5.

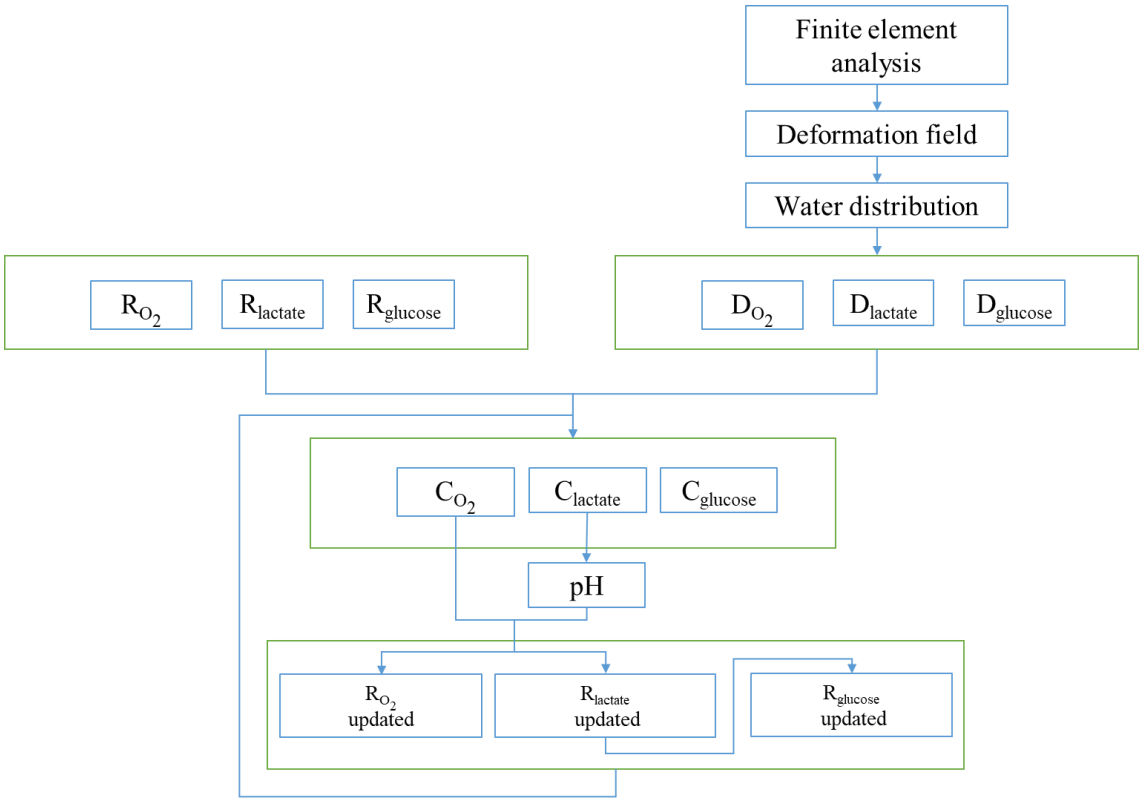

Figure 3.2.5. Coupling between mechanics and nutrients supply.

The oxygen cell consumption R_{O_2}, the lactate production $R_{lactate}$ and the glucose cell consumption $R_{glucose}$ are, respectively, given by (Bibby et al., 2005):

$$R_{O_2} = \frac{7.28 C_{O_2} \left(\mathrm{pH} - 4.95\right)}{1.46 + C_{O_2} + 4.03\left(\mathrm{pH} - 4.95\right)} \tag{4}$$

$$R_{lactate} = \exp\left(-2.47 + 0.93\mathrm{pH} + 0.16 C_{O_2} - 0.0058 C_{O_2}^2\right) \tag{5}$$

$$R_{glucose} = -0.5 R_{lactate} \tag{6}$$

in which the changes in pH induced by the lactate concentration $C_{lactate}$ is given by:

$$\mathrm{pH} = 7.4 - 0.09 C_{lactate} \tag{7}$$

The solutes boundary conditions were applied with $D_{O_2}^{water}$ = 7.6, $D_{lactate}^{water}$ = 0.35, $D_{glucose}^{water}$ = 3.92, C_{O_2} = 5.1 kPa, $C_{lactate}$ = 0.8 nmol/mL and $C_{glucose}$ = 4 nmol/mL at the superior and inferior

surfaces of IVD, and with $D_{O_2}^{water}$ = 9.5, $D_{lactate}^{water}$ = 1.0, $D_{glucose}^{water}$ = 5.6, C_{O_2} = 5.8 kPa, $C_{lactate}$ = 0.9 nmol/mL and $C_{glucose}$ = 5 nmol/mL at the external surfaces of IVD (Malandrino et al., 2015).

3.2.3. Results and discussion

3.2.3.1. Motion range

In this sub-section, the ability of the proposed finite element model to capture the biomechanical behavior of the cervical spine unit is examined by comparing simulations to experimental results. Three physiological movements are studied, namely flexion-extension, lateral bending and axial rotation. All movements of our cervical spine are combinations of these basic ones. Experimental kinematics data are rather rare in the literature (Pelker et al., 1991; Maurel et al., 1997; Goel and Clausen, 1998; Wheeldon et al., 2006). Goel and Clausen (1998) studied the in-vitro biomechanical response of the C5-C6 spine unit under the three physiological movements. Their experimental results are reported in Figure 6 as open symbols with standard deviation error bars. For a sake of comparison, other experimental data extracted from published in-vitro studies are added. The C5-C6 segment behavior in flexion-extension was studied by Pelker et al. (1991) and Wheeldon et al. (2006) until a 2 Nm maximal loading. Maurel et al. (1997) presented the C5-C6 segment twist response until a 1 Nm maximum loading. Differences in age, weight or lifestyle of donators explain the discrepancies of reported results. It is important to note that a notable difference exists between in-vivo and in-vitro studies. In vivo, the healthy IVD completely recovers its height and intradiscal pressure after long diurnal loading. In-vitro, several studies reported losses in the IVD height and intradiscal pressure. Indeed, blood clots near endplates may alter the fluid exudation (Schmidt et al., 2016). The simulation results are compared to the experimental data in Figure 6. The simulations were performed at a loading rate of 1° s^{-1}. A global view at these plots shows that our model provides

an acceptable replicate of the nonlinear response for the different kinematics patterns. The flexion-extension and lateral bending predictions fall within the experimental standard deviation interval. The axial rotation prediction is comprised between the two sets of data. Note that the spine unit movement can be associated to a rotation of the total cervical spine (Anderst et al., 2015). The 3° angle applied on C5 in flexion-extension (Figures 3.2.5a and 3.2.5b) corresponds to 20° rotation of the total cervical spine. In lateral bending (Figure 3.2.5c), 1.5° applied on C5 is equivalent to 17° rotation of the total cervical spine. In axial rotation (Figure 3.2.5d), 2° applied on C5 is equivalent to 40° rotation of the total cervical spine. Indeed, the C1-C3 part of the cervical spine is the main contributor for this movement. These ranges of motion are sufficiently low to avoid possible damage or preponderant response of ligaments.

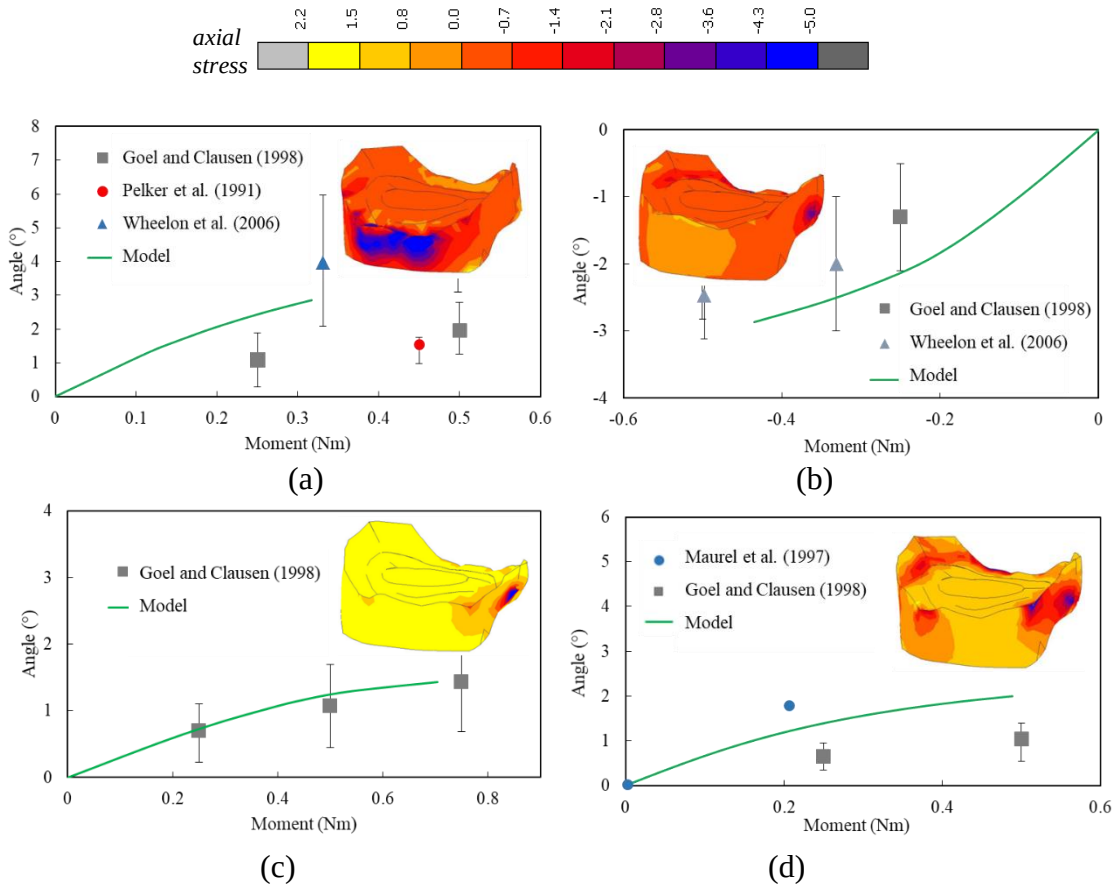

Figure 3.2.6. Experimental (symbols) and simulated (solid line) response of the C5-C6 spine unit under different neck movements: (a) flexion, (b) extension, (c) lateral bending and (d) axial rotation.

The hysteretic response and the frequency dependency are two key features of the spine which can be taken into account by the model. These inelastic effects are essential for good working of the healthy IVD, too fast moves being responsible for trouble arrival. An illustrative example of these inelastic effects is given in Figure 3.2.7. The mechanical dissipation, depicted by the hysteresis loop area during the physiological movement,decreases when the strain rate increases.

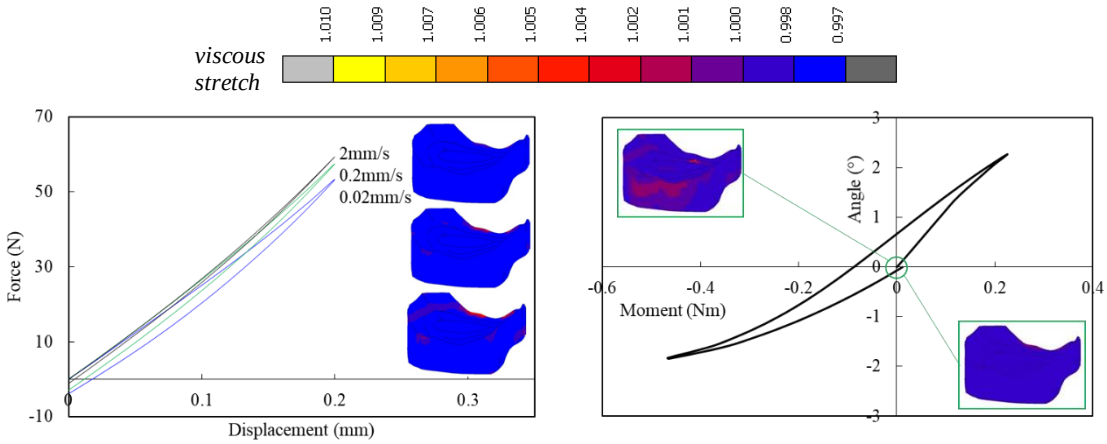

(a) (b)

Figure 3.2.7. Frequency and hysteretic effects: (a) compression, (b) flexion-extension.

3.2.3.2. Local fields

The developed finite element model can be used to predict the local fields within the IVD under complex biomechanical loading conditions. As an illustrative example, Figures 3.2.6 and 3.2.7 give the local axial stress and viscous stretch fields, respectively, during physiological movements. The viscous stretch gives an indication of level and repartition of the local dissipation. The highest dissipation is located in the IVD outer part. The dissipation distribution is similar to the maximum shear strain repartition and may be related to the AF failure (Costi et al., 2007).

The solutes repartition inside the healthy IVD is examined under a specific mechanical loading case. Multiple relaxations under loading-unloading in compression are applied on the finite element model. The displacement, applied on the superior surface of the C5 vertebral body, was ramped to a value of 0.2 mm, maintained constant for a relaxation period, ramped down to zero and then maintained constant for another relaxation period. The same absolute displacement rate of 0.2 mm/h was imposed to the loading and unloading paths. At each relaxation period, the applied displacement was maintained constant during 10 h. The results in terms of load evolution and pH fields inside the IVD are reported in Figure 3.2.8. The pH is uniformly distributed inside the IVD at the first steps of the loading. Due to the lactate production during the mechanical loading, a center-to-surface gradient in pH is predicted. The latter reproduces the avascular nature of the tissue. The decrease in pH is found faster under the loaded state than under the unloaded state. The predicted pH values remain in the range of those of a healthy IVD (about 7.2), an acid pH corresponding to the degenerated case (Bibby et al., 2001). The acidic state has a direct implication in the solute consumption (Bibby et al., 2005). Indeed, cell culture under low oxygen level does not show cellular death whereas the viability is compromised when low pH level is observed. Indeed, the activity of IVD cells is regulated by glucose contribution and pH with a balance between PGs production and breakdown.

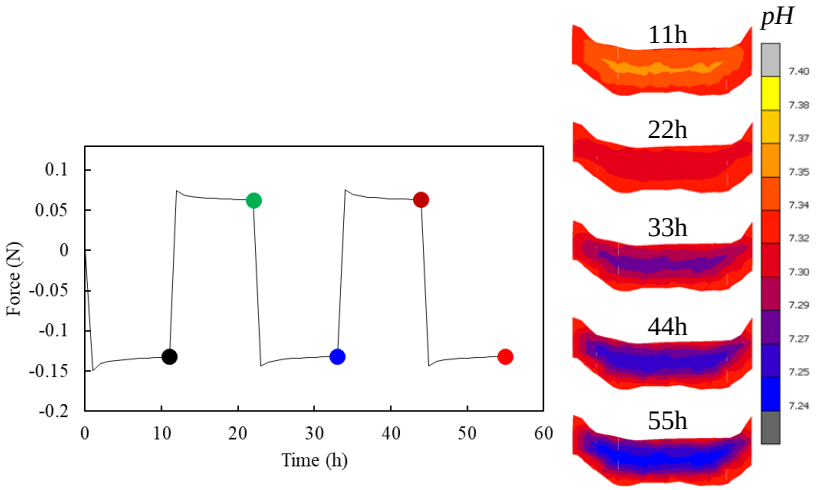

Figure 3.2.8. pH distribution inside IVD during a mechanical loading case corresponding to multiple relaxations under loading-unloading in compression.

A strong coupling exists therefore between biochemical and biomechanical features. The loss of water content and PGs amount is considered as the first sign of IVD degeneration (Buckwalter, 1995). It implies a decrease in osmotic gradient which results in IVD height reduction and alters the spine biomechanical response. Therefore, a modification in the motion range could be considered as an indicator of IVD degeneration (Pearcy and Tibrewal, 1984; Pearcy et al., 1984; Parnianpour et al., 1988; Dvorak et al., 1991). In the case of a degenerated IVD, the delicate coupling between biomechanics, biochemical environment and cell biology is perturbed (Vergroesen et al., 2015). Indeed, the reduction of fluid exchange implies a decrease in nutrients supply and pH. The induced diminution of cellular activity leads to reduction of chemical contribution. The ionic transport is perturbed and the balance between internal chemical contribution and external mechanical contribution is irreversibly modified.

3.2.4. Partial conclusions

An anatomically accurate finite element model of the human cervical spine was developed in which the IVD was described by the chemo-inelastic constitutive equations coupled to solutes diffusion equations. The developed finite element model provides a useful tool for mechanics and solutes patterns estimation in a healthy IVD during physiological movements.

The presented model involves mechanical, chemical and biological couplings. At this step of the model development, the mechano-biological coupling is not strong. The long-time prediction of IVD behavior, with aging, could be taken into account by considering the solutes effect on the chemo-mechanical response via the description of cellular population. This key point is topic of future investigations.

3.2.5. References

Anderst, W.J., Donaldson, W.F., Lee, J.Y., Kang, J.D., 2015. Cervical motion segment contributions to head motion during flexion\extension, lateral bending, and axial rotation. The Spine Journal 15, 2538-2543.

Antoniou, J., Steffen, T., Nelson, F., Winterbottom, N., Hollander, A.P., Poole, R.A., Aebi, M., Alini, M., 1996. The human lumbar intervertebral disc: Evidence for changes in the biosynthesis and denaturation of the extracellular matrix with growth, maturation, ageing, and degeneration. The Journal of Clinical Investigation 15, 996-1003.

Bertagnoli, R., Sabatino, C.T., Edwards, J.T., Gontarz, G.A., Prewett, A., Parsons, J.R., 2005. Mechanical testing of a novel hydrogel nucleus replacement implant. The Spine Journal 5, 672-681.

Bibby, S.R., Jones, D.A., Lee, R.B., Yu, J., Urban, J.P., 2001. The pathophysiology of the intervertebral disc. Joint Bone Spine 68, 537-542.

Bibby, S.R., Jones, D.A., Ripley, R.M., Urban, J.P., 2005. Metabolism of the intervertebral disc: Effects of low levels of oxygen, glucose, and pH on rates of energy metabolism of bovine nucleus pulposus cells. Spine 30, 487-496.

Breivik, H., Collett, B., Ventafridda, V., Cohen, R., Gallacher, D., 2006. Survey of chronic pain in Europe: Prevalence, impact on daily life, and treatment. European Journal of Pain 10, 287-333.

Buckwalter, J.A., 1995. Aging and degeneration of the human intervertebral disc. Spine 20, 1307-1314.

Campana, S., Charpail, E., de Guise, J.A., Rillardon, L., Skalli, W., Mitton, D., 2011. Relationships between viscoelastic properties of lumbar intervertebral disc and degeneration grade assessed by MRI. Journal of the Mechanical Behavior of Biomedical Materials 4, 593-599.

Costi, J.J., Stokes, I.A., Gardner-Morse, M., Laible, J.P., Scoffone, H.M., Iatridis, J.C., 2007. Direct measurement of intervertebral disc maximum shear strain in six degrees of freedom: Motions that place disc tissue at risk of injury. Journal of Biomechanics 40, 2457-2466.

de Puky, P., 1935. The physiological oscillation of the length of the body. Acta Orthopaedica Scandinavica 6, 338-347.

Dvorak, J., Panjabi, M.M., Novotny, J.E., Antinnes, J.A., 1991. In vivo flexion/extension of the normal cervical spine. Journal of Orthopaedic Research 9, 828-834.

Goel, V.K., Clausen, J.D., 1998. Prediction of load sharing among spinal components of a C5-C6 motion segment using the finite element approach. Spine 15, 684-691.

Grunhagen, T., Wilde, G., Soukane, D.M., Shirazi-Adl, S.A., Urban, J.P., 2006. Nutrient supply and intervertebral disc metabolism. The Journal of Bone and Joint Surgery 88, 30-35.

Gu, W.Y., Lai, W.M., Mow, V.C., 1993. Transport of fluid and ions through a porous-permeable charged-hydrated tissue, and streaming potential data on normal bovine articular cartilage. Journal of Biomechanics 26, 709-723.

Ha, S.K., 2006. Finite element modeling of multi-level cervical spinal segments (C3-C6) and biomechanical analysis of an elastomer-type prosthetic disc. Medical Engineering and Physics 28, 534-541.

Holzapfel, G.A., Schulze-Bauer, C.A.J., Feigl, G., Regitnig, P., 2005. Single lamellar mechanics of the human lumbar anulus fibrosus. Biomechanics and Modeling in Mechanobiology 3, 125-140.

Horner, H.A., Urban, J.P., 2001. Effect of nutrient supply on the viability of cells from the nucleus pulposus of the intervertebral disc. Spine 26, 2543-2549.

Lai, W.M., Hou, J.S., Mow, V.C., 1991. A triphasic theory for the swelling and deformation behaviors of articular cartilage. Journal of Biomechanical Engineering 113, 245-258.
Lyons, G., Eisenstein, S.M., Sweet, M.B., 1981. Biochemical changes in intervertebral disc degeneration. Biochimica et Biophysica Acta 673, 443-453.
Mackie, J.S., Meares, P., 1955. The diffusion of electrolytes in a cation-exchange resin membrane. I. Theoretical. Proceedings of the Royal Society of London Series A: Mathematical, Physical and Engineering Sciences 232, 498-509.
Malandrino, A., Jackson, A.R., Huyghe, J.M., Noailly, J., 2015. Poroelastic modeling of the intervertebral disc: A path toward integrated studies of tissue biophysics and organ degeneration. MRS Bulletin 40, 324-332.
Maurel, N., Lavaste, F., Skalli, W., 1997. A three-dimensional parameterized finite element model of the lower cervical spine. Study of the influence of the posterior articular facets. Journal of Biomechanics 30, 921-931.
Natarajan, R.N., Williams, J.R., Lavender, S.A., Andersson, G.B.J., 2007. Poro-elastic finite element model to predict the failure progression in a lumbar disc due to cyclic loading. Computers and Structures 85, 1142-1151.
Neidlinger-Wilke, C., Mietsch, A., Rinkler, C., Wilke, H.J., Ignatius, A., Urban, J., 2012. Interactions of environmental conditions and mechanical loads have influence on matrix turnover by nucleus pulposus cells. Journal of Orthopaedic Research 30, 112-121.
Parnianpour, M., Nordin, M., Kahanovitz, N., Frankel, V., 1988. The triaxial coupling of torque generation of trunk muscles during isometric exertions and the effect of fatiguing isoinertial movements on the motor output and movement patterns. Spine 13, 982-992.
Pearcy, M.J., Tibrewal, S.B., 1984. Axial rotation and lateral bending in the normal lumbar spine measured by three-dimensional radiography. Spine 9, 582-587.
Pearcy, M., Portek, I., Shepherd, J., 1984. Three-dimensional X-ray analysis of normal movement in the lumbar spine. Spine 9, 294-297.
Pelker, R.R., Duranceau, J.S., Panjabi, M.M., 1991. Cervical spine stabilization. A three-dimensional, biomechanical evaluation of rotational stability, strength, and failure mechanisms. Spine 16, 117-122.
Schmidt, H., Reitmaier, S., Graichen, F., Shirazi-Adl, A., 2016. Review of the fluid flow within intervertebral discs - How could in vitro measurements replicate in vivo? Journal of Biomechanics 49, 3133-3146.
Skoffer, B., Foldspang, A., 2008. Physical activity and low-back pain in schoolchildren. European Spine Journal 17, 373-379.
Urban, J.P., Maroudas, A., 1979. The measurement of fixed charged density in the intervertebral disc. Biochimica et Biophysica Acta 586, 166-178.
Urban, J.P., Holm, S.H., 1986. Intervertebral disc nutrition as related to spinal movements and fusion. In Hargens A.R. (eds.) Tissue Nutrition and Viability, Springer, New York, 101-119.
Urban, J.P., Smith, S., Fairbank, J.C., 2004. Nutrition of the intervertebral disc. Spine 29, 2700-2709.
Vergroesen, P.P., Kingma, I., Emanuel, K.S., Hoogendoorn, R.J., Welting, T.J., van Royen, B.J., van Dieen, J.H., Smit, T.H., 2015. Mechanics and biology in intervertebral disc degeneration: A vicious circle. Osteoarthritis and Cartilage 23, 1057-1070.
Vos, T., Allen, C., Arora, M., Barber, R.M., Bhutta, Z.A., Brown, A., et al., 2016. Global, regional, and national incidence, prevalence, and years lived with disability for 310 diseases and injuries, 1990-2015: a systematic analysis for the Global Burden of Disease Study 2015. Lancet 388, 1545-1602.

Wheeldon, J.A., Pintar, F.A., Knowles, S., Yoganandan, N., 2006. Experimental flexion/extension data corridors for validation of finite element models of the young, normal cervical spine. Journal of Biomechanics 39, 375-380.

Wills, C.R., Malandrino, A., van Rijsbergen, M.M., Lacroix, D., Ito, K., Noailly, J., 2016. Simulating the sensitivity of cell nutritive environment to composition changes within the intervertebral disc. Journal of the Mechanics and Physics of Solids 90, 108-123.

Conclusion

The intervertebral disc (IVD) is a complex element of our body with unclear couplings. This PhD dissertation provides an experimental and numerical investigation of IVD and annulus fibrosus (AF) biomechanics. The effect of the surrounding biochemical environment has been studied in relation with mechanical loading conditions in order to simulate the complex in-vivo environment of the tissue.

We have reported our experimental observations in the Chapter 2. An experimental study has been firstly performed on functional spine units (FSUs) in order to determine the chemical sensitivity of the inelastic response under different mechanical loading paths. The torsional stiffness and rate-dependency have been found chemically insensitive whereas an inverse chemical sensitivity was found between tension and compression. The mechanical response has been then observed during multiaxial loading with variation of the osmolarity. It has been found that the axial pre-strain type leads to a significant variation of the chemo-torsional response with a chemical sensitivity significantly higher in compression than in tension. Although it is difficult to know to what extent the time-dependent behavior can be attributed to the microstructural rearrangement and the fluid flow, a plausible interpretation of the inherent chemo-mechanical coupling with the pre-strain dependency has been proposed according to our experimental observations. We have concluded that the modulation of the proteoglycans (PGs) density due to mechanical and chemical loadings is the governing factor of the response by modulation of microstructural interactions and fluid contribution.

The intrinsic mechanical response has been secondly studied at the AF scale via an optical strain measuring technique. The osmo-inelastic mechanisms have been revealed by analyzing these effects on both the macro-stress and the local transversal strains. The effect of microstructure

in relation with the collagen fibers has been observed on the axial and transversal behavior. The hysteresis area and the rate-sensitivity have been found independent on the collagen fibers content/orientation, suggesting the preponderant role of the PGs macromolecules rearrangements on the inelastic effects. The apparent Poisson's ratio has been provided with interesting out-of-bond values. The observed auxetic response highlighted the inter-lamellae fluid exchanges due to the strong chemical dependence of the LP transversal strains. The observation of the establishment of chemo-mechanical equilibrium during relaxation tests provided a better understanding of what the nature is able to do to optimize the IVD functionality by involving auxeticity, inelasticity and osmolarity effects. The AF chemo-mechanical equilibrium, altered by mechanical or chemical loading, is a process involving local changes in fluid content until a balance between chemical and mechanical states.

Based upon these experimental observations, we have formulated a new chemo-mechanical constitutive model that has been implemented into a finite element program. This model is a new approach in the description of healthy soft tissues able to reproduce the osmo-induced volumetric changes in relation with microstructure, water content, inelasticity and mechanical loading conditions. A fairly good agreement has been obtained between the model results and the experimental data in terms of stress-stretch and transversal behaviors of AF specimens. The constitutive model has been also applied to reproduce the FSU biomechanics under complex loading conditions. The developed model has provided a useful tool for local patterns estimate in AF and in IVD.

Research perspectives

This PhD thesis was dedicated to the experimental characterization and the constitutive modeling of healthy IVD in relation with the osmo-inelastic coupling. The inter-lamellar zone appeared as an important component in the IVD response illustrated by the auxetic behavior. On the experimental point of view, a microscopic observation of the lamellae during a mechanical test would allow to validate the proposed mechanism, especially with variation of the chemical environment. The validation of the present experimental observation on human spine is important for future investigations in the aim to provide some considerations about degeneration appearance. On the numerical point of view, although the simulation of the uniaxial tensile deformation provided important indications concerning the osmo-inelastic mechanisms, it would be also interesting to simulate the time-dependent transversal response under relaxation loading. By taking into account induced damage, the degeneration process would be better understood on long-time response. The recent experimental studies about nutrient supply effect on the mechanical response could be simulated in order to improve the mechano-biological coupling, by considering the solutes effect on the chemo-mechanical response via the description of cellular population. The long-time prediction of IVD behavior, with aging, should be taken into account at the mechanical and biological point of view.

Abstract:

The spinal column is a fundamental element of our body, subjected to troubles concerning half of the population with significant impact on quality of life and costs estimated around 3 billion euros per year in France. Although the exact origin of the pain remains unclear, its correlation with the intervertebral disc (IVD) is often found. Understanding the healthy IVD response is required to improve the treatments and to prevent back pain. The IVD is a soft tissue composed by a gelatinous core and concentric layers: nucleus pulposus (NP) and annulus fibrosus (AF). At the microstructural scale, an extracellular matrix (ECM) reacts with mobile ions in the physiological fluid by osmotic effect. Axial loads are transmitted from the NP to the AF by hydrostatic pressure and absorbed thanks to the viscous behavior of the tissue. Indeed, the IVD exhibits a complex inelastic response dependent on the chemical environment. This coupling between osmotic and inelastic effects is far from being fully established. This PhD thesis is focused on the experimental characterization and the constitutive modeling of the osmo-inelastic coupling in healthy IVD. An experimental study is performed on functional spine units extracted from sheep cervical spine. Multiaxial mechanical tests provide some insights on the source of inelastic effects in relation with osmolarity by varying mechanical loading path. The osmo-inelastic features are found higher in compression due to the increase in ECM density leading to higher chemical sensitivity and rate dependency. Experimental observations are then provided on bovine AF in cyclic tension and relaxation. Tested rectangular cross-section specimens, present two different plans with strong anisotropy due to the layered reinforced structure of the AF. Therefore, a method based upon digital image correlation is developed in order to estimate AF local mechanical response that is found hysteretic, rate-dependent and osmolarity-dependent. The AF response presents a regional dependency due to collagen fibers organization with a Poisson's ratio higher than 0.5 in the fibers plan and negative in the lamellae plan. An interpretation of the osmo-inelastic mechanisms is proposed with two sources of inelastic effects, i.e. ECM rearrangements and internal fluid exchange created by osmotic effect. A chemo-mechanical constitutive model taking into account the osmo-inelastic coupling in relation with heterogeneous and anisotropic features is then formulated. This model is a new approach in the description of soft tissues able to reproduce the osmo-induced volumetric changes in relation with osmolarity, water content and mechanical loading conditions. The present formulation is implemented into a finite element (FE) program and used to reproduce the intrinsic response of AF. Observed inelastic effects and fluid contribution are reproduced as described in our experiments. The presented constitutive model is applied to a FE model of C5-C6 unit constructed from computed tomography. Comparisons with experimental data for different neck movements allows us to analyze the local fields in healthy IVD. Some elements towards a better understanding of the mechano-biological coupling in healthy IVD make it possible to envisage the future development of a predictive modeling of the DIV degeneration.

Résumé:

La colonne vertébrale est un élément fondamental de notre corps, sujet à des troubles touchant la moitié de la population avec un impact significatif sur la qualité de la vie et des coûts estimés à environ 3 milliards d'euros par an en France. Bien que l'origine exacte de la douleur reste incertaine, on trouve souvent une corrélation avec le disque intervertébral (DIV). Comprendre la réponse du DIV sain est nécessaire pour améliorer les traitements et prévenir la douleur. Le DIV est un tissu mou composé d'un noyau gélatineux et de lamelles concentriques : le nucleus pulposus (NP) et l'annulus fibrosus (AF). À l'échelle microstructurale, une matrice extracellulaire (MEC) réagit avec les ions mobiles du liquide physiologique par effet osmotique. Les charges axiales sont transmises du NP à l'AF par la pression hydrostatique et absorbées grâce au comportement visqueux du tissu. En effet, le DIV présente une réponse inélastique complexe dépendant de l'environnement chimique. Ce couplage entre les effets osmotiques et inélastiques est loin d'être complètement établi. Cette thèse de doctorat porte sur la caractérisation expérimentale et la modélisation constitutive du couplage osmo-inélastique du DIV sain. Une étude expérimentale est réalisée sur des unités fonctionnelles de rachis extraites de la colonne cervicale du mouton. Les tests mécaniques multiaxiaux fournissent des informations sur la source des effets inélastiques en relation avec l'osmolarité en faisant varier le type de chargement mécanique. Les caractéristiques osmo-inélastiques sont plus élevées en compression en raison de l'augmentation de la densité de la MEC, ce qui entraîne une sensibilité chimique et une dépendance à la vitesse plus élevées. Des observations expérimentales sont ensuite fournies sur l'AF bovin en traction cyclique et en relaxation. Les éprouvettes à section rectangulaire testées présentent deux plans différents avec une anisotropie forte en raison de la structure lamellaire renforcée de l'AF. Par conséquent, une méthode basée sur la corrélation d'images numériques est développée afin d'estimer la réponse mécanique locale de l'AF qui s'avère hystérétique, dépendante de la vitesse et de l'osmolarité. La réponse de l'AF présente une dépendance régionale due à l'organisation des fibres de collagène avec un coefficient de Poisson supérieur à 0,5 dans le plan des fibres et négatif dans le plan des lamelles. Une interprétation des mécanismes osmo-inélastiques est proposée avec deux sources d'effets inélastiques, à savoir les réarrangements de la MEC et l'échange interne de fluide créé par effet osmotique. Un modèle constitutif chemo-mécanique prenant en compte le couplage osmo-inélastique en relation avec les caractéristiques hétérogènes et anisotropes est ensuite formulé. Ce modèle est une nouvelle approche dans la description des tissus mous capables de reproduire les modifications volumétriques en relation avec l'osmolarité, la quantité d'eau et le type de chargement mécanique. Le modèle est implémenté dans un programme éléments finis (EF) et utilisé pour reproduire la réponse intrinsèque de l'AF. Les effets inélastiques observés et la contribution du fluide sont reproduits comme décrit dans nos expériences. Le modèle présenté est ensuite appliqué à une unité C5-C6 reconstruite en éléments finis à partir de coupes tomographiques. Des comparaisons avec des données expérimentales pour différents mouvements du cou nous permettent de valider et d'analyser les champs locaux dans un DIV sain. Certains éléments visant à une meilleure compréhension du couplage mécano-biologique dans un DIV sain permettent d'envisager le développement futur d'une modélisation prédictive de la dégénérescence du DIV.